August 2022

Ph.D. Thesis

BODIPY dyes for mitochondria-targeted cell imaging and photodynamic therapy of cancer cells

Chosun University Graduate School

Department of Chemistry

Badon, Isabel Wen T.

BODIPY dyes for mitochondria-targeted cell imaging and photodynamic therapy of cancer cells

암세포의 미토콘드리아 표적 세포 영상화 및 광역학 치료를 위한 **BODIPY** 염료

August 26, 2022

Chosun University Graduate School

Department of Chemistry

Badon, Isabel Wen T.

BODIPY dyes for mitochondria-targeted cell imaging and photodynamic therapy of cancer cells

Supervisor Prof. Kim Ho-Joong

This thesis is submitted in partial fulfillment of the requirements for the
Doctor of Philosophy in Chemistry.

April 2022

Chosun University Graduate School

Department of Chemistry

Badon, Isabel Wen T.

Confirmation of Doctoral's Thesis

위원장 조선대학교 교수 고 문 주 (인)

위 원 조선대학교 교수 김 호 중 (인)

위 원 조선대학교 교수 임 종 국 (인)

위 원 조선대학교 교수 조 승 주 (인)

위 원 전남대학교 교수 양 시 경 (인)

June 2022

Chosun University Graduate School

TABLE OF CONTENTS

LIST OF PUBLICATIONS

Badon, I. W., Kim, C., Lim, J. M., Duy, M. K., Vales, T. P., Kang, D., Cho, S., Lee, J., Kim, H.J., & Yang, J. (2022). Mitochondrion-Targeting PEGylated BODIPY Dyes for Near-Infrared Cell Imaging and Photodynamic Therapy. *Journal of Materials Chemistry B*, 10(8), 1196-1209.

Mai, D. K., Kim, C., Lee, J., Vales, T. P., Badon, I.W., De, K., Cho, S., Yang, J., & Kim, H.J. (2022). BODIPY nanoparticles functionalized with lactose for cancer-targeted and fluorescence imaging-guided photodynamic therapy. *Scientific reports* 12, no. 1, 1-11.

Vales, T. P., Cho, S., Lee, J., Bui, H. T., Mai, D. K., Badon, I. W., Lim, H., Jeong, W., Kim, J. L., Kim, H. K. & Kim, H. J. (2021). Functionalization of 4, 4-difluoro-4-bora-3a, 4a-diaza-s-indacene (BODIPY)-based photosensitizers with Triphenylphosphonium (TPP) for mitochondria-targeted fluorescence bioimaging and photodynamic therapy. *Journal of Molecular Structure*, 1246, 131284.

Mai, D. K., Kang, B., T. P. Vales, Badon, I.W., Cho, S., Lee, J., Kim, E., and Kim, H.J. (2020). Synthesis and photophysical properties of tumor-targeted water-soluble BODIPY photosensitizers for photodynamic therapy. *Molecules* 25, no. 15: 3340.

LIST OF TABLES

LIST OF FIGURES

LIST OF ABBREVIATIONS

BODIPY	**4,4-difluoro-4-bora-3a,4a-diaza-s-indacene**
HOMO	**Highest occupied molecular orbital**
LUMO	**Lowest occupied molecular orbital**
ROS	**Reactive oxygen species**
DNA	**Deoxyribonucleic acid**
TCA	**Tricarboxylic acid**
PDT	**Photodynamic Therapy**
ISC	**Intersystem crossing**
SOC	**Spin-orbit coupling**
HAE	**Heavy-atom effect**
PEG	**Poly(ethylene) glycol**
TPP	**Triphenylphosphine**
DQA	**dequalinium**
CLSM	**Confocal laser scanning microscopy**
ACQ	**Aggregation-caused quenching**
LED	**Light emitting diode**
NIR	**Near-infrared**
DPBF	**1,3-Diphenylisobenzofuran**
HEMA	**2-Hydroxyethyl methacrylate**
TEM	**Transmission electron microscopy**
DLS	**Dynamic light scattering**

ABSTRACT

BODIPY dyes for mitochondria-targeted cell imaging and photodynamic therapy of cancer cells

Badon, Isabel Wen T.

Advisor: Prof. Kim, Ho-Joong, Ph. D.

Department of Chemistry

Graduate School of Chosun University

A series of BODIPY-derived nanomaterials are synthesized for the development of promising mitochondria-targeting photodynamic agents. Small molecules possess the advantage of size and availability to target areas. BODIPYs AmH2, AmBr2 and AmI2 have cationic trimethylammonium groups on the *meso*-position that allows localization to the negatively charged mitochondria. The halogens (bromine and iodine) featured in the structure makes them ideal as photodynamic agents brought about by the enhanced intersystem crossing (ISC) due to heavy-atom effect. However, they have short absorption wavelength which deters near-infrared (NIR)-activation. NIR light is preferable because it penetrates deeper into tissues and overcomes autofluorescence. PyBHI, PyBMI and PyBBrI are fluorophores with extended π-conjugation resulting to shifts in absorption spectra to the NIR region and with PEG coils for hydrophilicity. The presence of bromine atoms imparts photosensitizing ability without diminishing the fluorescence imaging ability of the dyes. Lastly, the polymerized BN-H2 and BN-Br2 incorporate the fluorophore/photodynamic agent in a nanogel for an efficient delivery and lessened off-target effects of the dyes. The nanogel consists of N-isopropylacrylamide (NIPAM), 2-hydroxyethyl methacrylate(HEMA), and two fluorophores nitrobenzoxadiazole (NBD) and BODIPY for a dual-chromatic fluorescence imaging ability.

ABSTRACT

암세포의 미토콘드리아 표적 세포 영상화 및 광역학 치료를 위한 BODIPY 염료

Badon, Isabel Wen T.

Advisor: Prof. Kim, Ho-Joong, Ph. D.

Department of Chemistry

Graduate School of Chosun University

미토콘드리아를 표적으로 하는 유망한 광역학 물질의 개발을 위해 BODIPY에서 유도된 일련의 나노 물질이 합성되었다. 크기가 작은 분자는 표적 영역에 대한 가용성의 이점을 가지고 있다. BODIPY인 AmH2, AmBr2 및 AmI2는 음전하를 띤 미토콘드리아에 편재화를 할 수 있는 양이온성 트라이메틸암모늄 기를 중간 위치에 가지고 있다. 이들 구조에 포함된 할로젠(브로민 및 아이오딘)의 중원자 효과는 향상된 시스템 간 교차(ISC)를 일으켜서 이들을 광역학적 물질로 적합하게 해준다. 그러나, 이들은 짧은 흡수 파장을 가지고 있어서 근적외선(NIR) 활성화를 방해한다. 근적외선은 조직 깊숙이 침투하여 자가형광을 극복할 수 있어서 바람직하다. PyBHI, PyBMI 및 PyBBrI는 흡수 스펙트럼을 NIR 영역으로 이동시키는 확장된 π-콘쥬게이션을 갖는 형광단과 친수성을 위한 PEG 코일을 가지고 있다. 브로민 원자는 염료의 형광 이미징 능력을 감소시키지 않으면서 감광 능력을 제공한다. 마지막으로, 염료의 효율적인 전달과 표적 외 효과를 줄이기 위하여 나노젤로 중합된 BN-H2 및 BN-Br2는 형광단/광역학제를 통합하여 가지고 있다. 나노젤은 열역학적 N-아이소프로필아마이드(N-isopropylacrylamide, NIPAM), 2-하이드록시에틸 메타크릴레이트(2-hydroxyethyl methacrylate, HEMA) 및 이중 색 형광 이미징 기능을 위한 두 개의 형광단인 나이트로벤조옥사다이아졸(nitrobenzoxadiazole, NBD)과 BODIPY로 구성되어 있다.

CHAPTER 1: Mitochondria-targeting BODIPY dyes

1. Cancer and Mitochondria

Cancer refers to a collection of diseases affecting any part of the body and accounts for one in six deaths worldwide in 2020.[1] The global cancer burden is expected to increase by 47% to 28.4 million cases by 2040, attributed to risk factors accompanying globalization and growing economy.[2] Hence, it is only appropriate that research for cancer treatments is actively pursued. Defining features generally present in the development and progress of cancer are: enabling growth signals, bypassing growth regulators, inhibiting apoptosis, immortalizing cancer cells, inciting the generation of new blood vessels, and invading and spreading to other sites. In addition, recent progress identified two enabling characteristics (genomic irregularity and inflammation) and added two more indicators (unrestricted energy generation, avoidance of immune recognition and eradication) to the list.[3] The deregulation of energy metabolism has been more studied in detail and has opened the door for targeted cancer therapy. Mitochondria, mostly known as the powerhouse of the cell, participate in a lot of essential cellular activities such as bioenergetic and biosynthetic pathways, antioxidant defense, redox status, apoptosis, and cell signaling. The relationship between mitochondrial dysfunction and cancer progression was first reported in the 1920s when Otto Warburg observed that cancer cells have elevated rates of glycolysis than their healthy counterparts. Mitochondria have so much important role to play in the progression of cancer. There are five proposed ways of how mitochondria participates in cancer development:1) mutations in mitochondrial DNA are found in a myriad of diseases; 2) mitochondria release reactive oxygen species (ROS) as by products which trigger cancer generation and progression; 3) mitochondria are major players in controlling cell death; 4) mutations in the genes encoding for the enzymes involved in

tricarboxylic acid cycle (TCA) promote malignant transformation; 5) sustained cell proliferation caused by multiple molecular changes.[4] Hence, mitochondria are the ideal place for detection of tumor growth since the environment of the mitochondria is sensitive to changes. It is important to develop therapeutics that are specific to mitochondria.

2. Photodynamic therapy for cancer treatment

The first observation of cytotoxic effect induced by the combination of light and dye was made by Oscar Raab in 1900 in Munich, Germany. In 1907, the phrase "photodynamic action" was conceived by von Tappeiner and Jodlbauer after they demonstrated that oxygen is necessary for the reaction to occur.[5] Currently, PDT is a minimally invasive treatment for tumor and non-tumor diseases with nonexistent recurrence. In addition, PDT exhibits the concept of dual selectivity wherein collateral damage to the normal tissues can be lessened by increasing the agglomeration of the PS in the tumor tissues.[6] In addition, the directionality of laser light and the short diffusion distance of ROS diminish toxicity to healthy tissues. PDT triggers antitumor responses which result to regression in distant neoplasms and produce immune memory that lasts a long time.[7] PDT has been successfully applied for treating various cancers.[8] The photodynamic effect works with the interaction of light of appropriate wavelength, oxygen, and photosensitizer. Light is delivered to the target site topically or using an optical fiber. Molecular oxygen is available inside the cells. Photosensitizers are substances capable of triggering photophysical processes after absorbing light.[9] Once the photosensitizer is inside the target site, light is absorbed to initiate the photophysical processes cascade. The absorption of light brings electrons of the PS from the ground state (S_0) to singlet excited states (S_n). The electrons then relax from the S_n to S_1. From the singlet excited state, the electrons undergo intersystem crossing (ISC) towards the triplet state (T_1). Then, the electrons can undergo two types of

photodynamic actions. The Type I mechanism of photodynamic action is electron transfer from the excited PS to a substrate resulting in the production of radicals and radical ion species. Meanwhile, Type II mechanism employs energy transfer reactions to produce the cytotoxic singlet oxygen ($^1O_2$).[10] PDT destroys cancer cells in three ways: 1) killing the tumor cell directly by necrosis; 2) ROS produces the damage by apoptotic pathway; and 3) photodynamic reaction-activated immunogenic cell death.[11]

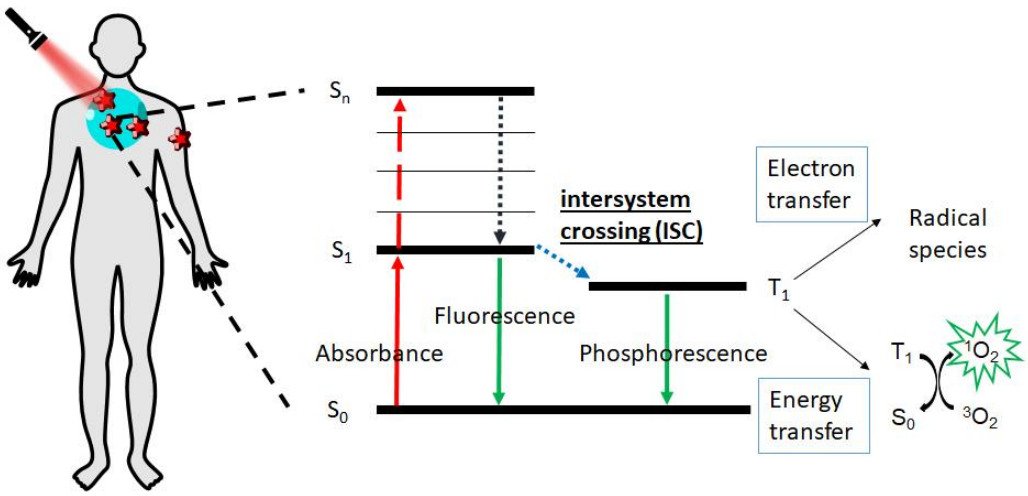

Figure 1. The photodynamic action inside the patient's body illustrated with a Jablonski diagram.

Crucial to the production of cytotoxic $^1O_2$ is an efficient ISC from the singlet to the triplet states. However, an electronic transfer from a singlet to a triplet excited state is a spin-forbidden process and does not occur for most compounds, especially for highly fluorescent dyes. To capacitate the transition of states with different spins, spin-orbit perturbation is necessary. Spin-orbit coupling (SOC) is a phenomenon that results to a quantum mechanical interaction between states with different spin multiplicities.[12,13] SOC between the singlet and triplet states of an atom or a molecule can be achieved by the heavy-atom effect (HAE). HAE has an important contribution in determining

many photophysical and photochemical processes, such as photocatalytic reactions, triplet-triplet annihilation, and photodynamic therapy.[13] HAE can be brought about by iodine, bromine, and ruthenium.[14]

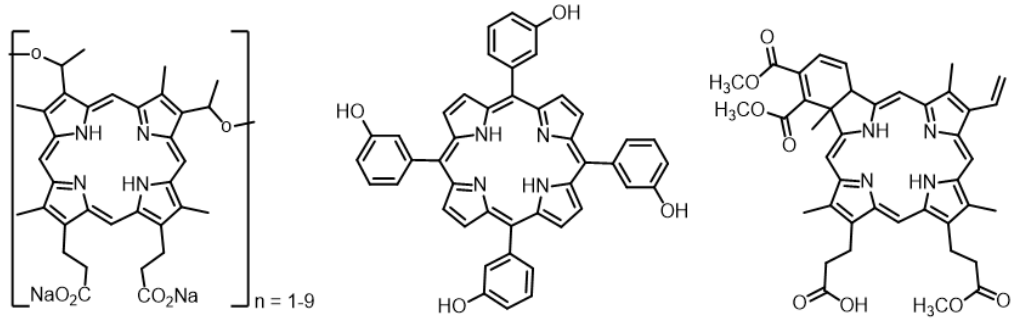

Figure 2. Some FDA-approved porphyrin-based photosensitizers.

FDA-approved photosensitizers include Photofrin, Foscan, Verteporfin, and Talaporfin sodium, among others.[5] Although Photofrin is the most widely used PDT agent for treating several kinds of cancer, the difficulty of isolating it from the mixture of oligomeric products greatly hampers its commercial availability.[12] In addition, synthesis and modification of the tetrapyrrole structure is difficult hence the interest in developing non-porphyrin dyes.[15]

3. Synthesis of BODIPY

BODIPY is the commercial name of 4,4-difluoro-4-bora-3a,4a-diaza-*s*-indacene with a structure composed of fused pyrrole rings. They were first synthesized and characterized in 1968 by Treibs and Kreutzer.[16] BODIPY dyes are one of the most common dye families because of their exceptional photophysical characteristics such as sharp absorption bands, narrow fluorescence spectrum and high fluorescence quantum yields.[17] Their outstanding spectral characteristics make them potential candidates for various applications such as sensors, light harvesters in artificial photosynthesis, optoelectronic devices, fluorescence cell imaging, and photodynamic therapy.[18-22] From an organic

synthesis point of view, the ease of synthesis and post-functionalization of BODIPY dyes are a few of its merits. Although the discovery of BODIPY is serendipitous, there are two distinctive routes to arrive at the dipyrrins followed by complexation using BF_3.[23] The first strategy is the condensation of 2-formylpyrrole with another pyrrole that is unsubstituted at the 2-position with the help of an acid catalyst. The second is the oxidation of dipyrromethene formed from the acid-catalyzed condensation of pyrrole with an aldehyde.

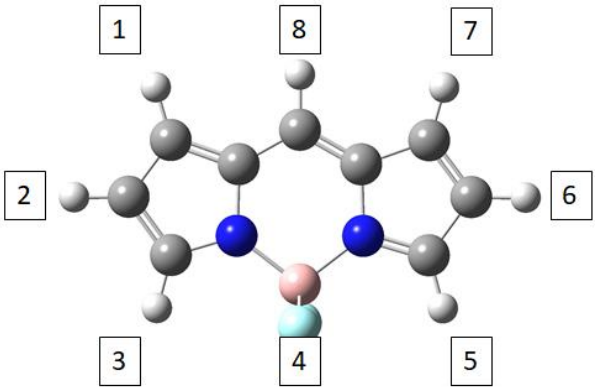

Figure 3. IUPAC numbering system on the BODIPY structure.

4. BODIPY-derived materials for synergistic cell imaging and photodynamic therapy applications

Despite the excellent optical properties displayed by BODIPY dyes, their potential towards biomedical applications is greatly hindered by their inherent hydrophobicity resulting from their conjugated ring structure.[24] Attaching hydrophilic groups to the BODIPY core greatly enhances its water solubility and its applicability to biological studies.[25] BODIPY with hydrophilic groups such as poly(ethylene) glycol (PEG), carboxylic acid, phosphonic acid, sulfonic acid, and ammonium groups have been reported.[26-28]

Another method is by incorporating BODIPYs into nanogels for optimized delivery. Nanogels are physically or covalently cross-linked three-dimensional polymer networks. The crosslinking strategy produces robust structures with porosity and mesh size dictated by the distance and distribution of bonds. The spaces between the chains are available for monomers or drugs to diffuse.[29] For example, a polypeptide nanogel with crosslinked BODIPY was employed for synergistic fluorescence cell imaging and photodynamic therapy and was also able to deliver doxorubicin.[30] On the other hand, nanogels held together by weaker hydrogen-bonding, van der Waals, electrostatic and hydrophobic interactions are prone to sol-gel transition caused by changes in the surroundings.[31] Additional advantages of nanogels include excellent capacity to encapsulate drugs or substrates, facile preparation, modifiability, and environment sensitivity.[32]

Background interferences in bioimaging due to autofluorescence of certain tissues under UV light and shallow tissue penetration of light prompted the preference for fluorophores that absorb in the longer wavelength as imaging agents.[33] The main BODIPY core typically absorbs in the yellow region of the visible spectrum, hence impractical for deeply penetrating *in vivo* studies. This drawback is solved by extending the π-conjugation of the BODIPY by *de novo* synthesis or by post-functionalization. Aza-boron-dipyrromethene (Aza-BODIPY) are BODIPY-derived dyes with a nitrogen atom replacing the carbon at the *meso* position. They are synthesized using γ-nitro-β -phenyl-butyrophenone instead of pyrrole and possess similar excellent photophysical properties as conventional BODIPY but with a more red-shifted absorption and emission maxima.[34] Virtually all positions of the BODIPY structure are available for post-functionalization and many derivatives have been reported which show red-shifted absorption and emission spectra.

Organelle-specific fluorescent imaging is becoming more in-demand for a more precise characterization of the cell to prevent off-target effects.[35] Mitochondria serves as an

excellent target because of its relationship to cancer. To specifically target mitochondria, the more commonly used method is to attach cationic groups to the labeling agent. Several BODIPY dyes with cationic groups are synthesized to selectively target the mitochondria. BODIPY nanoparticles with triphenylphosphonium groups localized within the mitochondria while also showing high photoconversion efficiency.[36] In addition, through the use of nanoparticles, BODIPY and targeting units need not be covalently bonded to produce the same mitochondria-targeted imaging and phototherapy.[37]

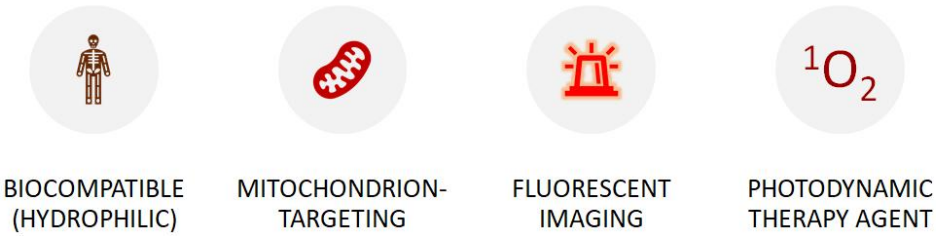

Figure 4. Main characteristics of ideal dual-functional cell imaging and PDT agents.

Ideal synthetic design is important to address the challenges needed to overcome and to realize the desired properties of BODIPY-based fluorophores and photodynamic agents. As discussed above, the principles that will be consistently shown in the next chapters are as follows: first, cationic groups contribute both hydrophilicity and mitochondria-targeting ability; second, extending the π-conjugation of the structure shifts the absorbance maximum wavelength but also affects the fluorescence and singlet oxygen quantum yield; lastly, using small molecules or incorporating dyes in nanogels both have advantages and disadvantages and should be considered.

CHAPTER 2: Cationic BODIPYs for mitochondria-targeted cell imaging and photodynamic therapy

1. Introduction

BODIPYs for photodynamic therapy typically employ heavy atoms and/or transition metals to induce intersystem crossing (ISC) from the singlet state to the triplet state. Aside from that, configuration and the presence of rotatable bonds can also induce phototoxic effect.[38] From the triplet state, the electrons collide with nearby molecular oxygen simultaneous with energy transfer which then elevate the molecular oxygen to its singlet state. This singlet oxygen is cytotoxic to cancer cells. Photodynamic therapy combined with diagnosis by fluorescence imaging is the future of advanced theragnostic applications.[39] Therefore, photosensitizers that generate $^1O_2$ while also able to function as fluorescent probes are highly sought after.

Mitochondria-targeting probes usually employ triphenylphosphine (TPP), dequalinium (DQA) and rhodamine.[40] Incorporating cations in the BODIPY dyes not only impart hydrophilicity to the dye but also organelle-targeting ability. TPP-functionalized BODIPY has been shown to localized in the mitochondria.[41,42] Herein, the cationic moiety is brought about by the quaternization of the dimethylamine group at the *meso* position. In addition, the substitution by either bromine or iodine at the C-2 and C-6 positions will impart a photodynamic ability to the dye. Although BODIPY dye H1 used here has been applied as optical pH-sensor before, this is the first report of the application of this BODIPY and its quaternized form in cell imaging and photodynamic therapy. The results described herein should fill the gap in the functionalities of this kind of BODIPY.[43,44]

2. Experimental Section

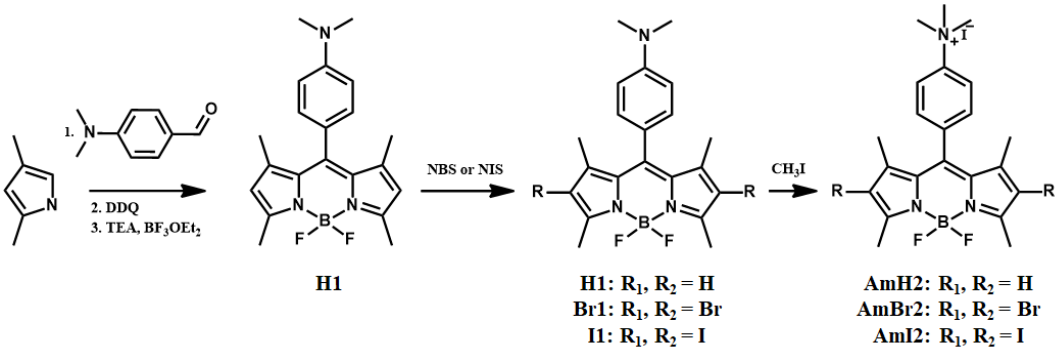

Figure 5. Synthetic scheme of cationic BODIPY dyes AmH2, AmBr2, and AmI2.

2.1. Materials

All chemicals were obtained commercially and used without additional purification unless mentioned. 2,4-Dimethylpyrrole, 4-(dimethylamine)benzaldehyde, trifluoroacetic acid (TFA) and boron trifluoride diethyl etherate ($BF_3 \cdot OEt_2$) were bought from Sigma Aldrich (USA). 2,3-Dichloro-5,6-dicyano-1,4-benzoquinone and *p*-Chloranil were purchased From Alfa Aesar (USA). *N*-Bromosuccinimide and *N*-Iodosuccinimide were sourced from TCI (Japan). Triethylamine (TEA), iodomethane, sodium hydrogen carbonate ($NaHCO_3$), and magnesium sulfate ($MgSO_4$) were obtained from Daejung Chemical (South Korea). Analytical grade solvents were distilled before use.

2.2. Synthesis of BODIPY H1

BODIPY H1 was synthesized as the same routine according to our previous publication.[45] In brief, 2,4-Dimethylpyrrole (0.9 g, 9.46 mmol), and 4-(Dimethylamine)benzaldehyde (0.58 g, 4.73 mmol) was dissolved in 120 mL of dry methylene chloride (MC) at room temperature under Argon gas in the presence of TFA. Next, DDQ (1.07 g, 4.73 mmol) dissolved in MC was added to the mixture, followed by TEA (4mL) and $BF_3.OEt_2$ (4.5 mL). The BODIPY H1 was afforded by column chromatography as a red-orange solid.

H1:(Yield: 260.1 mg, 18.2%) ^{1}H NMR (300 MHz, $CDCl_3$, 25°C, TMS): δ = 7.07 (d, 2H, J = 9 Hz, 2Ar-H), 6.79 (d, 2H, J = 9 Hz, 2 Ar-H), 5.97 (s, 2H, 2Ar-H), 3.02 (s, 6H, 2CH3), 2.55 (s, 6H, 2CH3),1.48 (s, 6H, 2CH3) ppm.

2.3. Halogenation reaction

Halogenation reaction of the C-2 and C-6 positions of the BODIPY dyes were carried out using either *N*-Bromosuccinimide or *N*-Iodosuccinimide. Briefly, H1 was dissolved in distilled methylene chloride at room temperature. Then 3.0 eq of either NBS or NIS were added to the reaction. After the reaction reached completion, the solvent was evaporated and the crude product was purified *via* silica gel column chromatography.

Br1: (Yield: 79.7 mg, 55.8%) ^{1}H NMR (300 MHz, $CDCl_3$, 25°C, TMS): δ = 7.04 (d, 2H, 2Ar-H), 6.80 (d, 2H, 2Ar-H), 3.04 (s, 6H, 2CH3), 2.60 (s, 6H, 2CH3), 1.49 (s, 6H, 2CH3) ppm.

I1: (Yield: 137.5 mg, 81.6%) ^{1}H NMR (300 MHz, $CDCl_3$, 25°C, TMS): δ = 7.03 (d, 2H, 2Ar-H), 6.80 (d, 2H, 2Ar-H), 3.04 (s, 6H, 2CH3), 2.64 (s, 6H, 2CH3), 1.50 (s, 6H, 2CH3) ppm.

2.4. Methylation reaction

Methylation reactions of the dimethylamine moiety at the *meso* position were carried out by dissolving BODIPY precursors (H1, Br1 and I1, respectively) with iodomethane in anhydrous acetonitrile. The reaction was allowed to stir at room temperature for two days and the final compounds were isolated by column chromatography using aluminium oxide.

AmH2: (Yield: 50.0 mg, 60.0 %) ^{1}H NMR (300 MHz, $CDCl_3$, 25°C, TMS): δ = 8.15 (d, 2H, 2Ar-H), 7.69 (d, 2H, 2Ar-H), 6.11 (s, 2H, 2Ar-H), 3.76 (s, 9H, 3CH3), 2.50 (s, 6H, 2CH3), 1.41 (s, 6H, 2CH3) ppm. ^{13}C NMR (300 MHz, $CDCl_3$, 25°C, TMS): δ

= 157.48, 149.39, 144.25, 140.43, 138.62, 131.82, 122.71, 122.51, 57.87, 14.86 ppm. HRMS (ESI) m/z calcd for $C_{22}H_{27}BF_2IN_3$+: 382.28; [M-I]+; found:382.2267.

AmBr2: (Yield: 80.0 mg, 79.0 %) ^{1}H NMR (300 MHz, $CDCl_3$, 25°C, TMS): δ = 8.30 (d, 2H, 2Ar-H), 7.60 (d,2H, 2Ar-H), 4.11 (s, 9H, 3CH3), 2.61 (s, 6H, 2CH3), 1.33 (s, 6H, 2CH3) ppm. ^{13}C NMR (300 MHz, $CDCl_3$, 25°C, TMS): δ = 154.92, 140.13, 132.80, 131.79, 121.93, 112.45, 57.98, 44.38, 27.33, 14.08 ppm. HRMS (ESI) m/z calcd for $C_{22}H_{25}BBr_2F_2IN_3$+: 540.07; [M-I]+; found:540.0468.

AmI2: (Yield: 120.0 mg, 71.0 %) ^{1}H NMR (300 MHz, $CDCl_3$, 25°C, TMS): δ = 8.22(d, 2H, 2Ar-H), 7.73(d, 2H, 2Ar-H), 3.80 (s, 9H, 3CH3), 2.61 (s, 6H, 2CH3), 1.44 (s, 6H, 2CH3) ppm. ^{13}C NMR (300 MHz, $CDCl_3$, 25°C, TMS): δ = 138.47, 131.88, 122.92, 113.71, 57.94, 40.48, 27.28, 17.71, 16.46, 16.28 ppm. HRMS (ESI) m/z calcd for $C_{22}H_{25}BF_2I_3N_3$+: 634.07; [M-I]+; found:634.0198.

2.5. Methods

Intermediate and final products AmX2 were analyzed by ^{1}H and ^{13}C NMR spectroscopy using a Bruker AM 250 spectrometer (USA). Furthermore, the molecular masses of the compounds were confirmed by high-resolution electrospray ionization mass spectrometry (HR-ESI-MS) using a SYNAPT G2-Si high-definition mass spectrometer (United Kingdom).

The absorption and emission spectra of AmX2 samples dissolved in different solvents were measured at 25 ℃ using a UH5300 UV/Vis spectrophotometer (Hitachi) and a F-7000 FL fluorometer (Hitachi), respectively.

2.6. Cells and cell culture

HeLa and MCF-7 cells were supplied by the Korean Cell Line Bank. They were maintained with 10% heat-inactivated fetal bovine serum (FBS) and antibiotics (100

U/mL penicillin and 100 mg/mL streptomycin) (Welgene Inc., South Korea) in RPMI 1640 medium (Gibco, Carlsbad, CA, USA) in a humidified 5% CO_2 incubator at 37ºC.

2.7. Cell proliferation assay

HeLa and MCF-7 cells (2×10^3 cells/well) were spread in 96-well plates and kept at 37°C in 5% CO_2 for one day. Then the cells were treated with the AmX2 dyes at different concentrations for another 24h. The cell proliferation was determined according to the prescribed procedure for CellTiter96® AQueousOne Solution Cell Proliferation Assay (Promega, Madison, WI, USA). Then the absorbance was measured at 490 nm using ELISA plate reader (ThermoFisher Scientific, Inc., Waltham, MA, USA).

2.8. Photodynamic activity

HeLa and MCF-7 cells (2×10^3 cells/well) were treated in the same way as above but with further incubation at 37°C in 5% CO_2 under dark conditions for 2h. Then, the media were replaced with phenol-red free RPMI 1640 followed by exposure to green light-emitting diode at 520 nm (100% power) for 10 min. The cells were incubated for additional 24h and the cell proliferation (% of the control) was measured using the same method described above.

2.9. Confocal laser scanning microscopy

HeLa and MCF-7 cells were incubated with the AmX2 dyes (1.6 μM) for 24h. Then, they were further stained with MitoTracker Red (Invitrogen) for 45 min. The cells were fixed with 4% paraformaldehyde for 10 min and permeabilized with 0.1% Triton X-100 for 10 min followed by counter staining with 4′ ,6-diamidino-2-phenylindole (DAPI) for 1h at room temperature. Finally, the treated cells were imaged using confocal microscopy (LSM-700, Carl Zeiss, Germany).

2.10. Statistical Analysis

Data are expressed as means ± standard deviations. Group means were considered significantly different at $p < 0.05$. GraphPad 6 Prism software (San Diego, CA, USA) was used for the one-way analysis of variance and Tukey's test of the data.

3. Results and Discussion

The synthesis of cationic BODIPYs is outlined in Figure 3. Initially, trifluoroacetic acid-catalyzed condensation reaction between 2,4-Dimethylpyrrole and 4-(Dimethylamine)benzaldehyde was carried out at room temperature while dissolved in distilled methylene chloride overnight. Next, DDQ was dissolved in MC and added dropwise into the reaction at 0℃ for 2 hours. Lastly, dropwise addition of TEA followed by BF_3OEt_2 completed the reaction. Halogenation reactions were carried out using either NBS or NIS in distilled MC room temperature. The three final compounds were obtained after methylation of the dimethylamino group. AmH2, AmBr2 and AmI2 were characterized by ^{1}H NMR,^{13}C NMR and mass spectroscopy.

3.1. Photophysical Properties

The final compounds were dissolved in different solvents and their photophysical properties were measured (Table 1). At a glance, the shape of the absorption and emission spectra are consistently mirror images of each other which is a typical characteristic of BODIPY.[46] AmH2 has a maximum absorbance wavelength of 500 nm, typical to those of similarly-constructed BODIPY. Evidently, with the presence of halogens, the absorbance wavelengths are red shifted, even more so with iodine, which is heavier than bromine. The *meso* phenyl group does not have a significant influence on the absorbance and fluorescence maximum wavelength before and after methylation, showing the effect of the overall nonplanar structure of BODIPY. The quaternization of the dimethyl group allowed the water solubility of the BODIPY dye as shown by the high fluorescence intensity of AmH2 in water. In contrast, AmI2 was not readily

soluble in water and needs to be sonicated. Furthermore, their fluorescence properties are greatly diminished, especially for AmI2. This points to aggregation due to presence of the hydrophobic halogens (Br and I). The fluorescence spectrum of AmI2 is almost non-existent despite having the most red-shifted absorption spectra. This further supports the existence of aggregation-induced quenching (ACQ) of the molecules. Based on the photophysical and solubility results, AmX2 dyes have the potential for fluorescence cell imaging.

	Solvent	**λ**	**λ**
AmH2	MC	506	515
	THF	502	515
	ACN	500	516
	EtOH	502	519
	H_2O	500	514
AmBr2	MC	530	554
	THF	526	548
	ACN	524	546
	EtOH	528	548
	H_2O	528	539
AmI2	MC	542	565
	THF	536	559
	ACN	534	556
	EtOH	538	549
	H_2O	538	549

Table 1. Absorbance and emission maximum wavelengths of AmX2 dyes in various solvents.

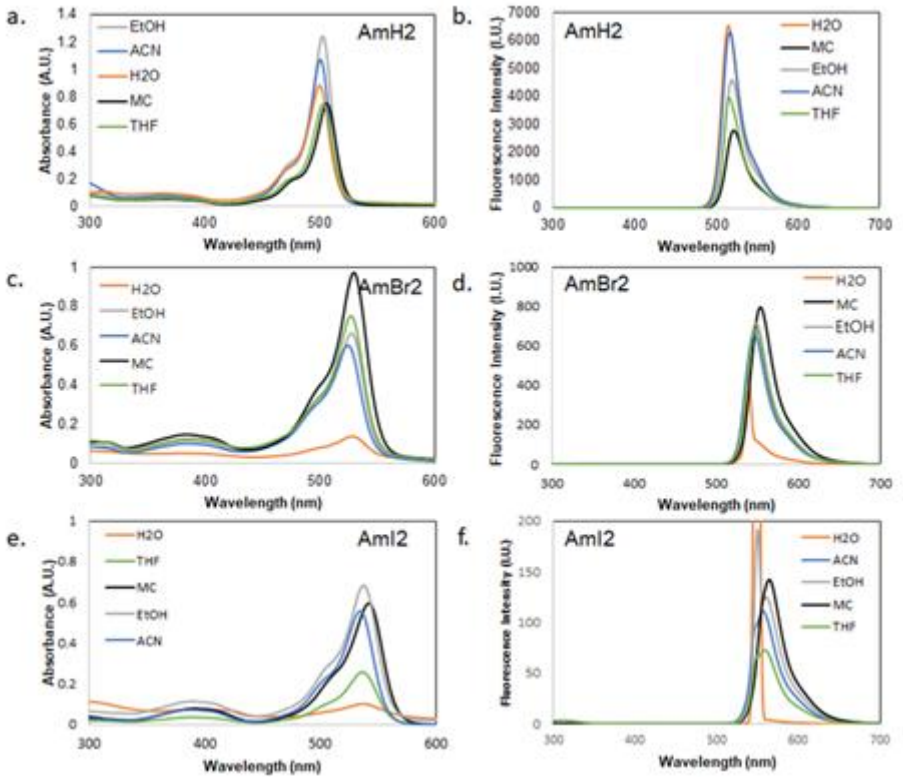

Figure 6. Absorption (a, c, e) and fluorescence intensity (b, d, f) spectra of AmH2, AmBr2, and AmI2 in different solvents.

3.2. Cell Proliferation

After examining the solubility and fluorescence emission, the dyes are subjected to biological experiments. The cell proliferation of the dyes was determined using MTS assay in increasing concentrations (0 to 1600 nM) conducted in two cell lines, namely HeLa and MCF-7. The cancer cells were incubated with the dyes under normal conditions first to evaluate their cytotoxicity and then were exposed to green LED light to measure the photoactivity of the dyes. Upon illumination, the halogenated AmBr2 and AmI2 will undergo photodynamic processes which end in the production of $^1O_2$

which is harmful to cells. Figure 7 depicts the observed results of the assay under dark (black bars) and light-activated (green bars) conditions. Under dark conditions, the dyes did not cause damage to the cells, as the cell proliferation remained consistently

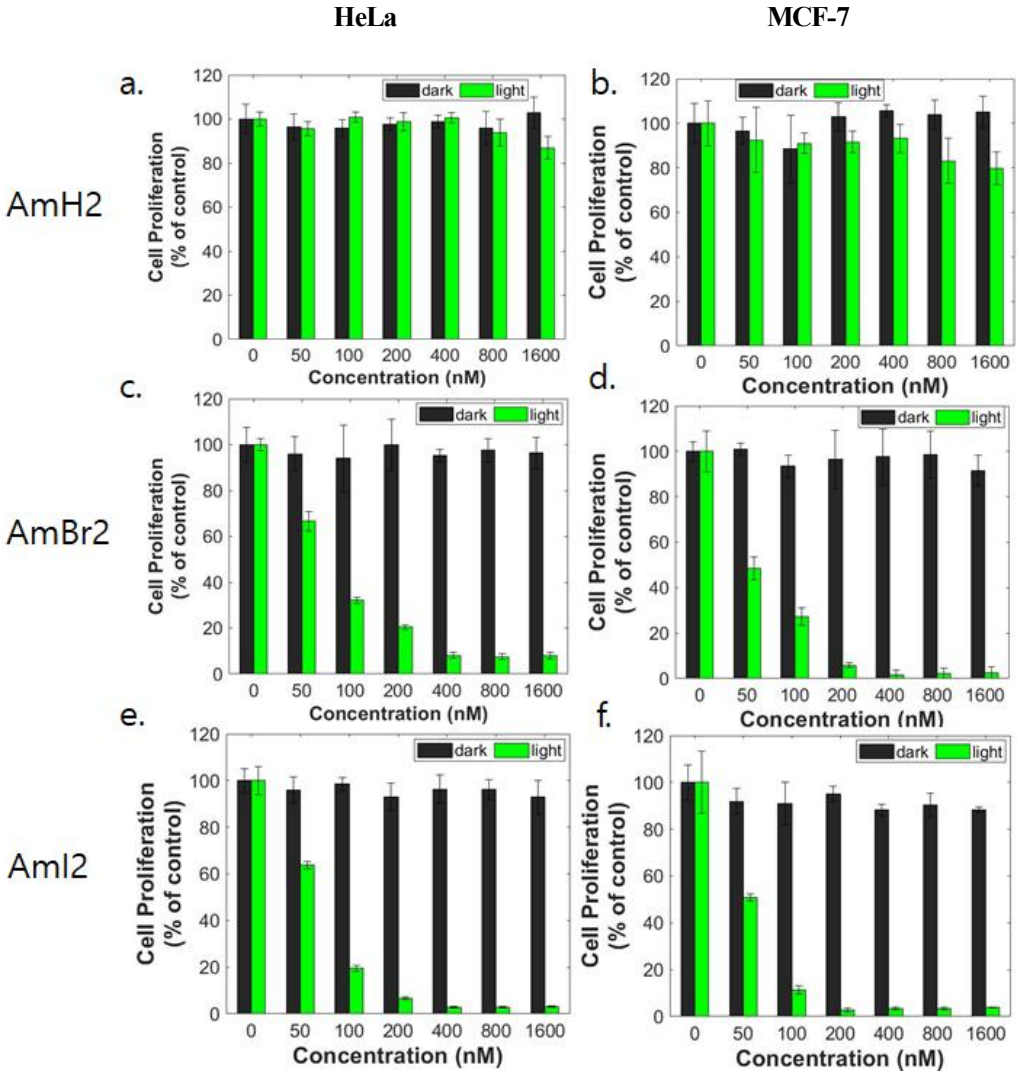

Figure 7. Cell proliferation (% of control) of HeLa (a,c,e) and MCF-7 (b,d,f) cancer cell lines after a 24-hour incubation with the dyes under dark and light conditions.

	HeLa	MCF-7
AmBr2	64.54 ± 3.00	48.57 ± 3.51
AmI2	59.27 ± 0.53	49.35 ± 0.52

Table 2. IC_{50} of AmBr2 and AmI2 dyes in HeLa and MCF-7cell lines in nM.

high (>90% of control) even with increasing concentration of the dyes in both cell lines. Therefore, the dyes are biocompatible and do not induce cell death under normal conditions. Even with light activation, AmH2 still did not cause death to the cell, further evidencing its nontoxicity. However, with light, the cell proliferation of the cancer cells incubated with AmBr2 and AmI2 drastically decreased, and the effect can be observed starting at 50 nM across all cell lines. This shows the efficacy of heavy-atom effect contributed by bromine and iodine. Calculating the IC_{50} reveals that the phototoxic effects of AmBr2 and AmI2 do not differ with each other.

3.3. Mitochondria-targeted cell imaging

Due to competing ISC and radiative relaxation processes, the singlet oxygen quantum yield and fluorescence quantum yield often show an inverse relationship. Thus, high emissive dyes do not possess photodynamic ability and effective PDT agents are typically non-emissive. However, as shown previously, when the dyes are in physiological environment, their photophysical behaviors can change. After proving the biocompatibility of the dyes, the fluorescent imaging of the cells is undertaken next. The confocal laser scanning microscopy images of HeLa and MCF-7 cell lines are collected in Figure 8 and 9. Clear images of the cells can be seen when dyed with BODIPY (green). This supports the successful permeation and accumulation of the dyes inside the cell without causing any toxic effect to the cell. Similarly, Mitotracker Red dye accumulated in the same manner as BODIPY dye. Both dyes showed a black area in the center, which is reserved for the nuclear dye DAPI (blue). Merged images showed that while the nuclear area is dyed blue, the peripheral area (cytoplasm) is stained with both BODIPY and Mitotracker Red. This shows the selectivity of BODIPY

dye, that is, it localized in the mitochondria more. The attachment of cation is effective in the selective accumulation of the dye around the nucleus. Further inspection of the fluorescence intensity profiles of the dyes relative to MitoTracker Red (Figure 10 and 11) showed the strong overlap of BODIPY dyes and MTR. This establishes the ability of the dyes to selectively localize into the mitochondria. Notably, all dyes were able to image the cells, particularly AmBr2 and AmI2 despite having low fluorescence quantum yield in water. This could be due to complex interactions of the dyes with the cellular environment.

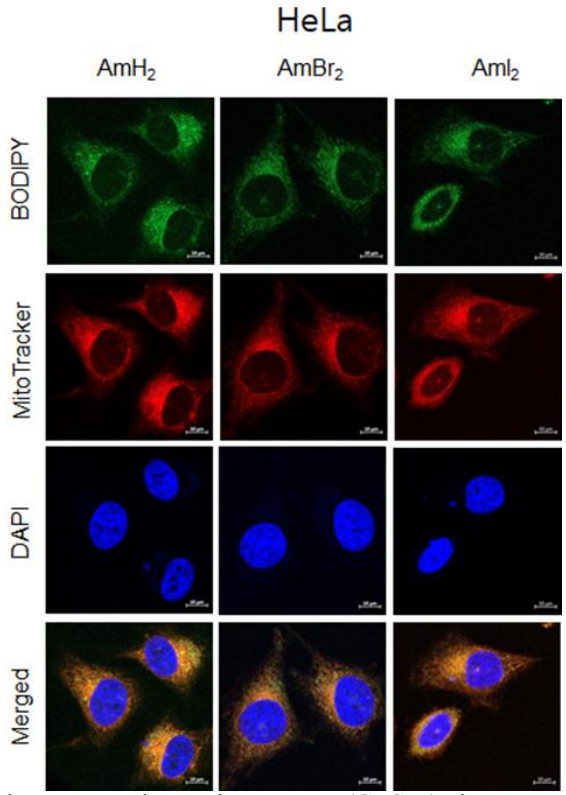

Figure 8. Confocal laser scanning microscopy (CLSM) images of HeLa cells treated with AmH2, AmBr2 and AmI2 (1.6 μM) with MitoTracker Red and DAPI as co-stains.

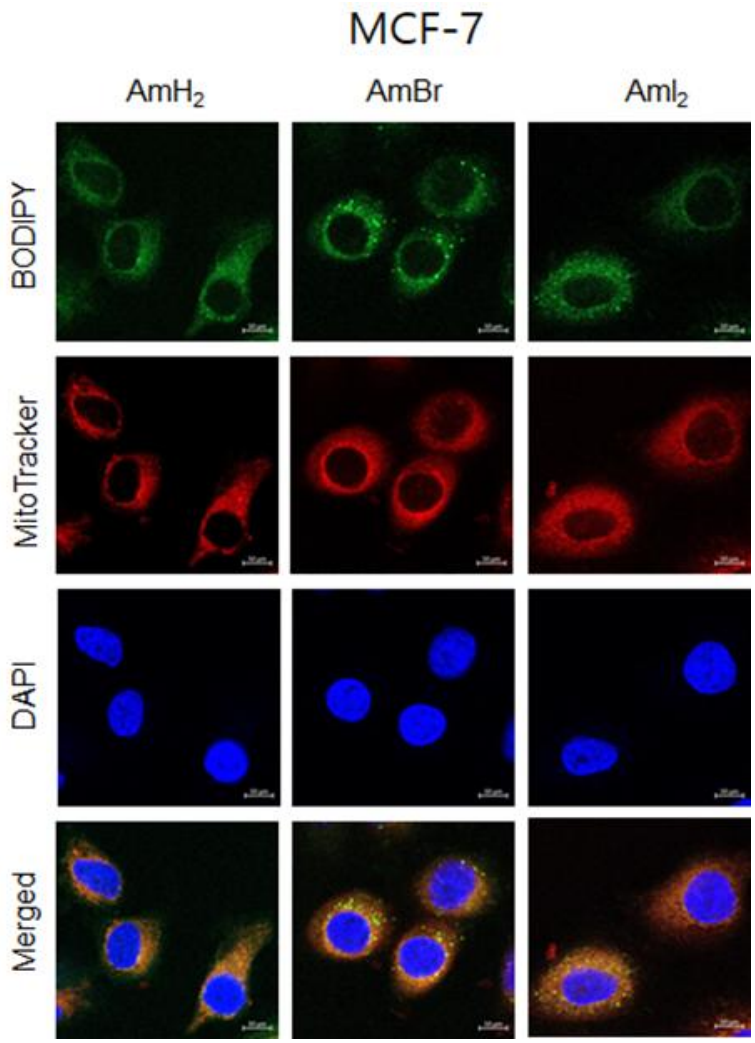

Figure 9. Confocal laser scanning microscopy (CLSM) images of MCF-7 cells treated with AmH2, AmBr2 and AmI2 (1.6μM) with MitoTracker Red and DAPI as co-stains.

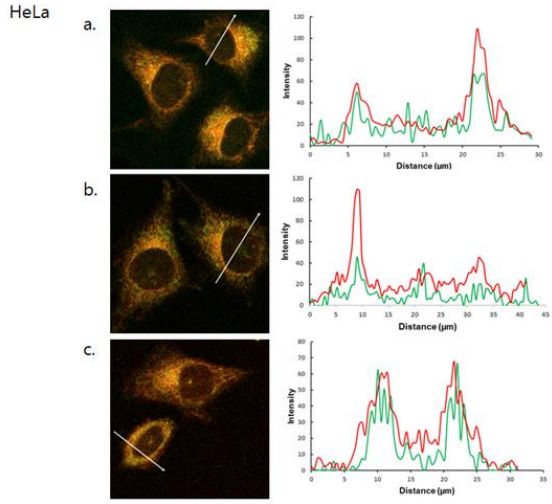

Figure 10. Fluorescence micrographs of HeLa cells co-stained with MitoTracker Red and AmX2 BODIPY dyes and fluorescence intensity profiles along the region of interest marked by a white arrow. The green topographic profile corresponds to each BODIPY dye while the red one is for MitoTracker Red.

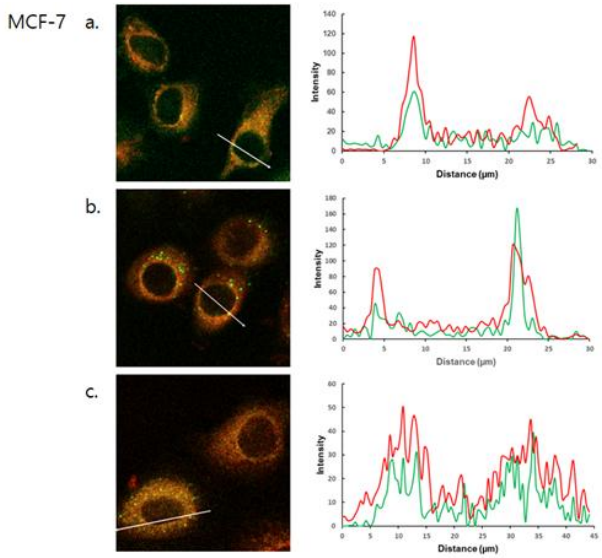

Figure 11. Fluorescence micrographs of MCF-7 cells co-stained with MitoTracker Red and AmX2 BODIPY dyes and fluorescence intensity profiles along the region of interest marked by a white arrow. The green topographic profile corresponds to each BODIPY dye while the red one is for MitoTracker Red.

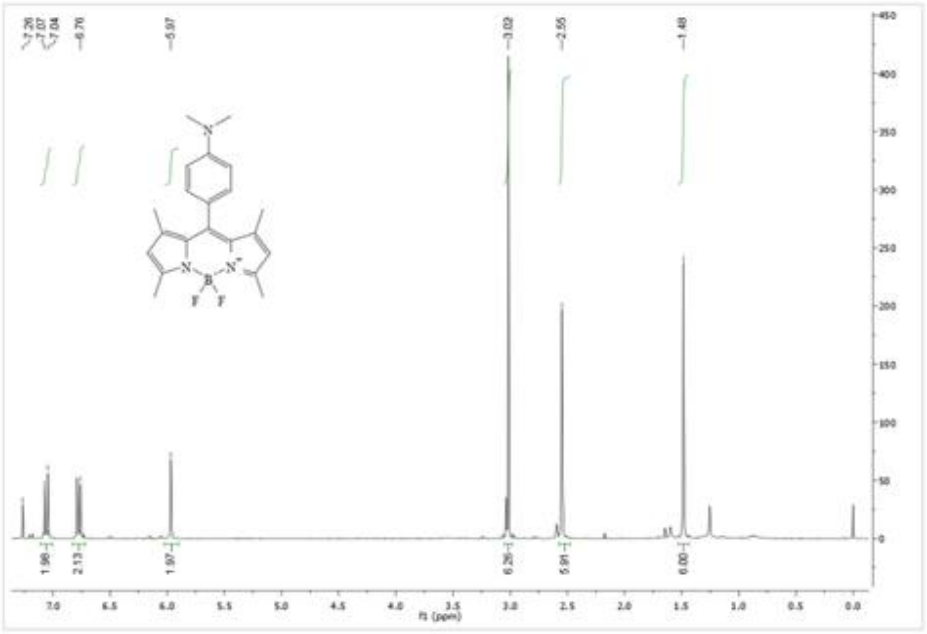

^{1}H NMR of H1

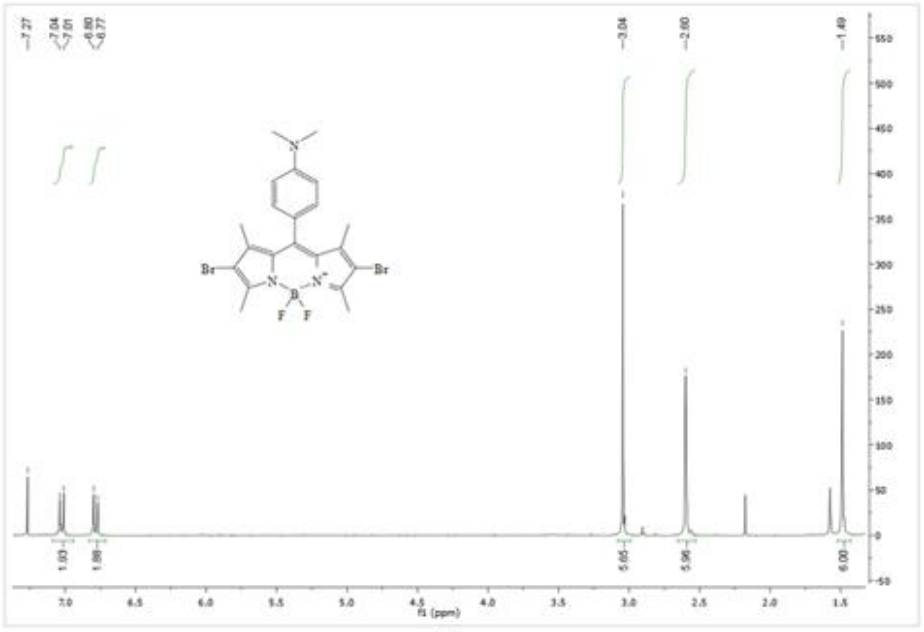

^{1}H NMR of Br1

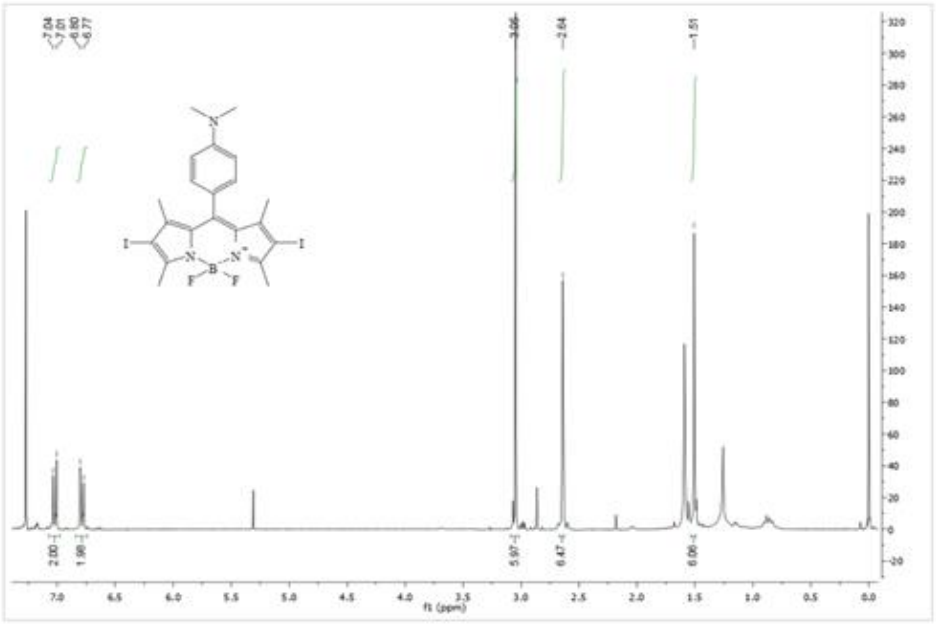

^{1}H NMR of I1

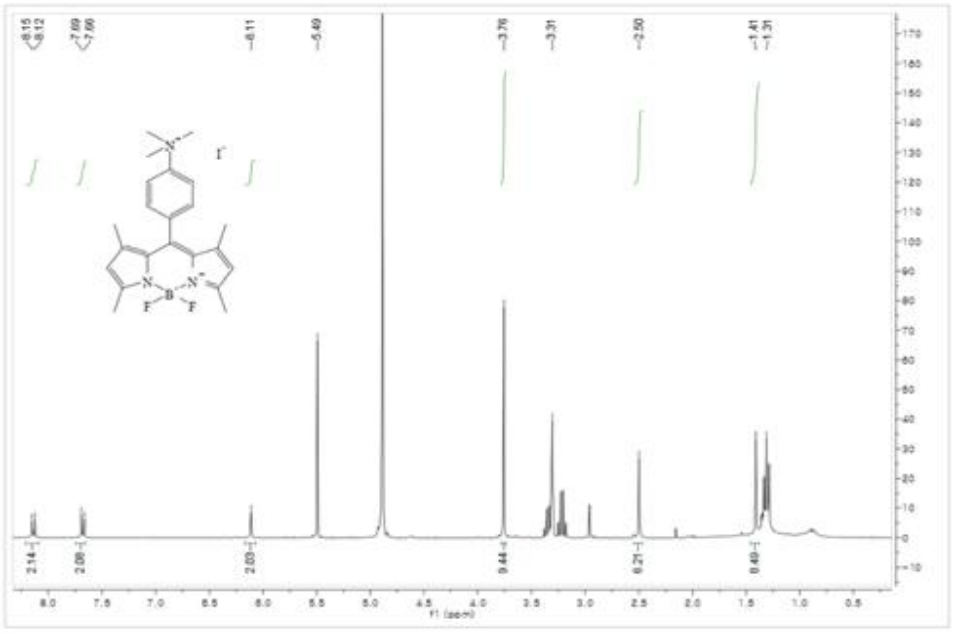

^{1}H NMR of AmH2

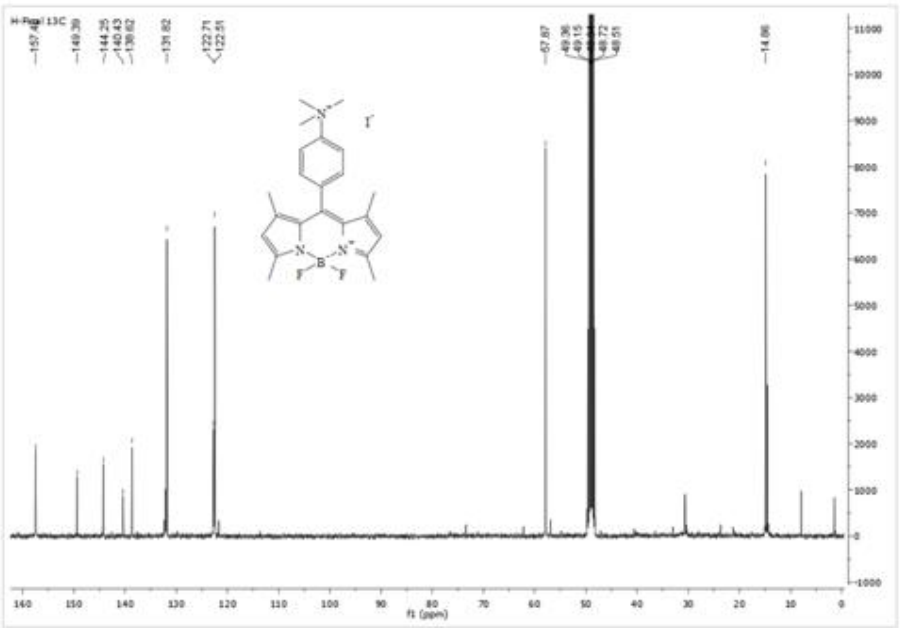

^{13}C NMR of AmH2

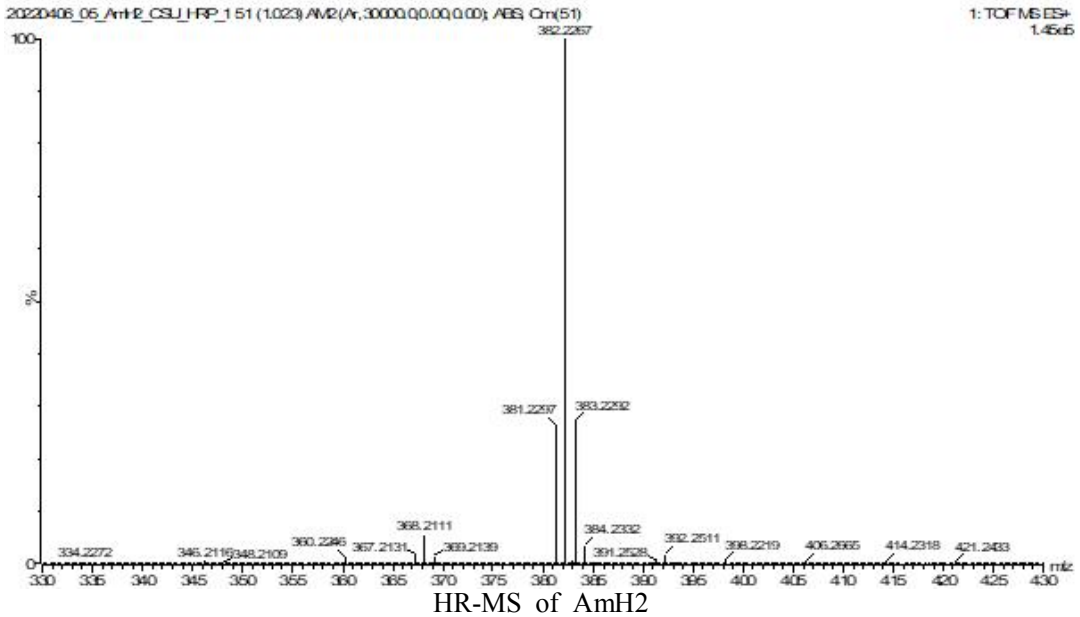

HR-MS of AmH2

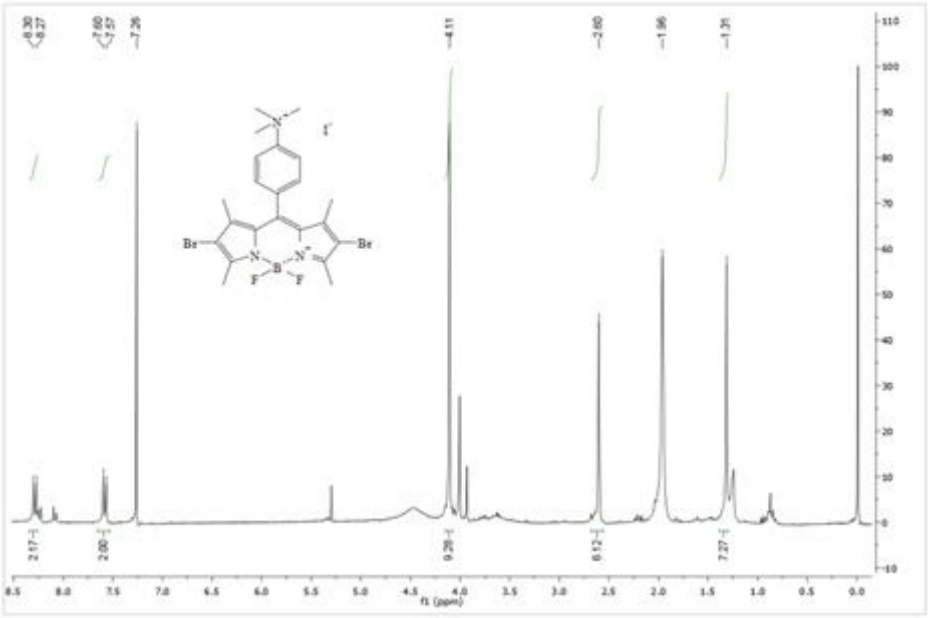

^{1}H NMR of AmBr2

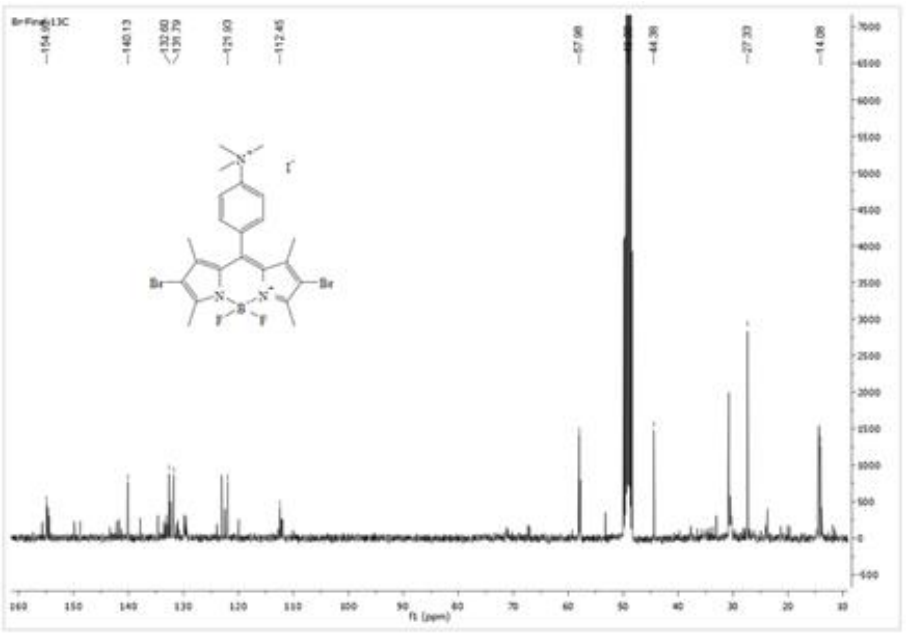

^{13}C NMR of AmBr2

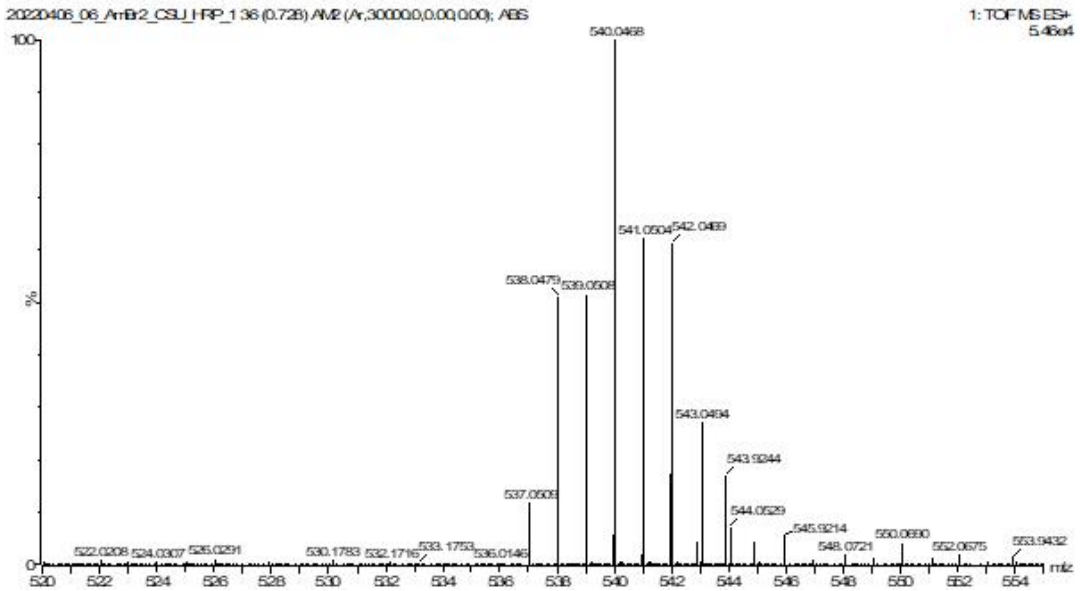

HR-MS of AmBr2

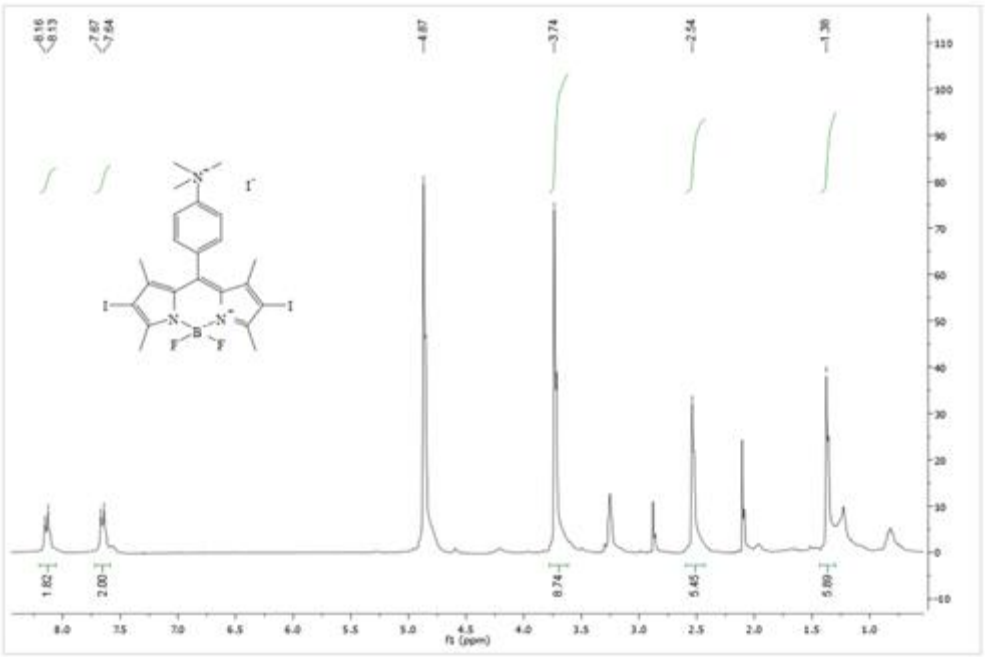

^{1}H NMR of AmI2

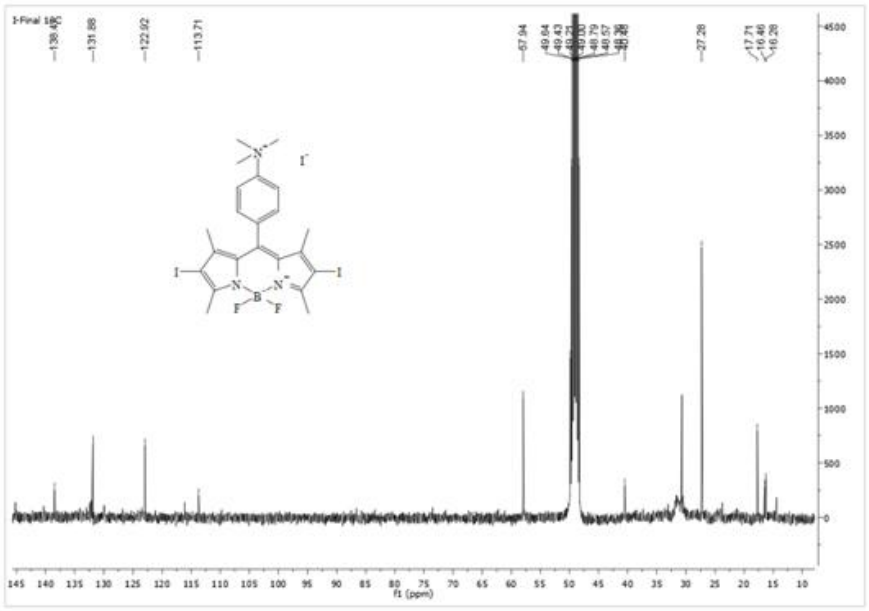

^{13}C NMR of AmI2

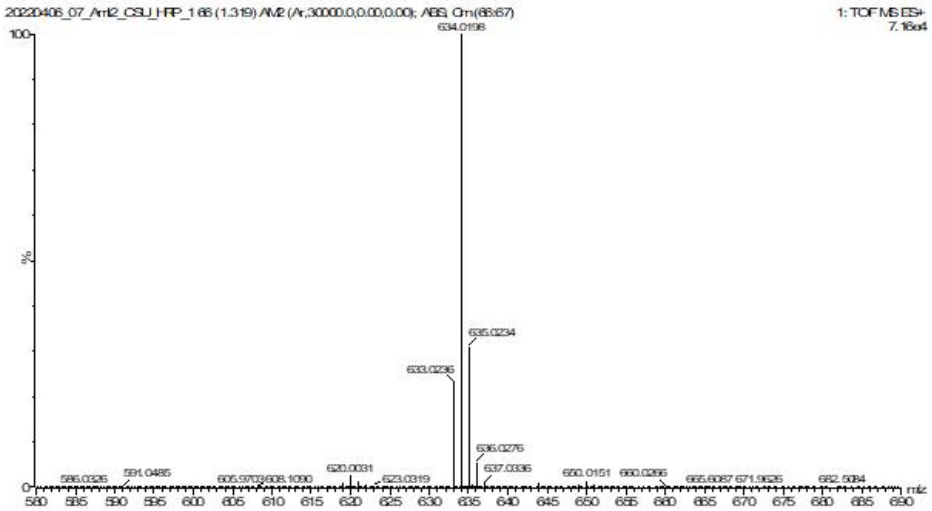

HR-MS of AmI2

CHAPTER 3: Near-Infrared BODIPY dye for synergistic mitochondria-targeted cell imaging and photodynamic therapy

1. Introduction

The near-infrared (NIR) is the shortest part of the infrared region of the electromagnetic spectrum ranging from 750 nm to 2500 nm. NIR absorption and emission is a desirable feature in PDT agents because of the deeper penetration of NIR light into tissues. However, the core BODIPY structure absorbs light in the UV region. This is circumvented by extending the delocalization pathway of the electrons by either substitution or aromatic fusion to the BODIPY backbone. Effective strategies reported in literature include: 1) extending the π-conjugation at the α-, β- and meso positions of the BODIPY (IUPAC system: C-1,-7,-3,-5 and 8-positions); 2) using substituted pyrroles as starting materials or fusing pyrrole with aromatic groups at the [a] bond, [b] bond and the "zig-zag" of the BODIPY; 3) synthesizing aza-BODIPYs.[47] Although most of these strategies are synthetically tedious, Knoevenagel condensation reaction at the α- and β-positions is rather easy to follow and allows for diverse synthetic addition to the BODIPY structure.

2. Experimental Section

2.1. Materials

All chemicals were obtained commercially and used without additional purification unless mentioned. 2,4-Dimethylpyrrole, 4-Pyridiniumcarboxaldehyde, trifluoroacetic acid, 3,4-Dihydroxybenzaldehyde and boron trifluoride diethyl etherate ($BF_3 \cdot OEt_2$) were bought from Sigma Aldrich (USA). 2,3-Dichloro-5,6-dicyano-1,4-benzoquinone and p-Chloranil were obtained from Alfa Aesar (USA). *N*-Bromosuccinimide was purchased from TCI

(Japan). Triethylamine (TEA), iodomethane, triethylene glycol monomethyl ether, sodium hydrogen carbonate ($NaHCO_3$), *p*-toluene sulfonyl chloride and magnesium sulfate ($MgSO_4$) were obtained from Daejung Chemical (South Korea). Analytical grade solvents were distilled before use.

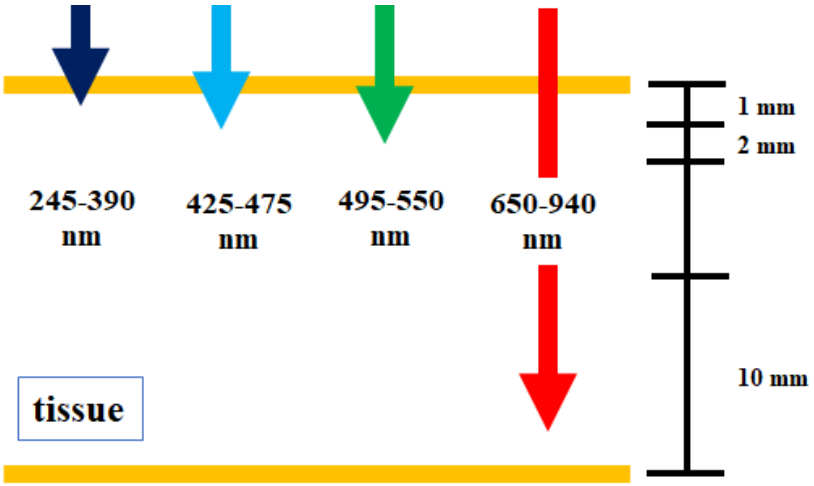

Figure 12. Depth of tissue penetration of different wavelengths of light.

2.2. Synthesis of BODIPY dye 1a

2,4-Dimethylpyrrole (1.0 g, 2.2 eq) and 4-Pyridiniumcarboxaldehyde (0.52 g, 1.0 eq) were mixed in dry MC under argon gas at 298 K.[84] Trifluoroacetic acid was added as catalyst and the mixture was left stirring overnight. p-Chloranil (0.90 g, 1.0 eq) was dissolved in dry MC and injected slowly to the mixture at 0°C and the reaction stirred for 2 hrs. Then, TEA (6.0 eq) was also added and stirred for 30 minutes, followed by the addition of BF_3OEt_2 (10.0 eq) in the same manner to the reaction. After stirring for 1.5 hrs, the reaction was washed with H_2O and extracted with MC, dried with magnesium sulfate, filtered, and the solvent was evaporated. Purification by column chromatography using MC/Hexane yielded the compound as orange crystals.

1a: (Yield: 440 mg, 25.7%) ^{1}H NMR (300 MHz, $CDCl_3$, 25°C, TMS): δ = 8.78 (d, 2H, J = 6Hz; 2Ar-H), 7.30 (d, 2H, J = 6Hz; 2Ar-H), 6.01 (s, 2H; 2Ar-H), 2.56 (d, 6H, 2CH3), 1.41 (s, 6H, 2CH3) ppm.

2.3. Mono- and dibromination of BODIPY 1a

The mono and dihalogenated BODIPY 1a was obtained after reaction with *N*-bromosuccinimide. 0.5 eq of NBS was used for monobromination and 3.0 eq was used for dibromination. Then, NBS and BODIPY 1 a were mixed in dry MC under inert atmosphere at 298 K. The reaction was stopped when the end of the reaction was reached as monitored by TLC. The solvent was removed and BODIPY 1a and b were afforded after purification by column chromatography using hexane/CH_2Cl_2 as eluents.

1b: 130 mg of 1a and 35.6 mg of NBS (Yield: 50.0 mg, 61.9 %) ^{1}H NMR (300 MHz, $CDCl_3$, 25°C, TMS): δ = 8.80 (d, 2H, J = 6 Hz; 2Ar-H), 7.29 (d, 2H, J = 6 Hz; 2Ar-H), 6.07 (d, 1H ;Ar-H), 2.58 (d, 6H, J = 6 Hz; 2CH3), 1.40 (d, 6H, J = 6Hz; 2CH3) ppm.

1c: 200 mg of 1a and 328.4 mg NBS (Yield: 250.0 mg, 84.2 %) ^{1}H NMR (300 MHz, $CDCl_3$, 25°C, TMS): δ = 8.83 (d, 2H, J = 6 Hz; 2Ar-H), 7.32 (d, 2H, J = 6 Hz; 2Ar-H), 2.62 (s, 6H, 2CH3), 1.40 (s, 6H, 2CH3) ppm.

2.4. Synthesis of triethylene glycol tosylate

Triethylene glycol was tosylated based on the procedure from reported literature.[45] *p*-toluene sulfonyl chloride (6.97 g, 1.2 eq) dissolved in anhydrous methylene chloride was added dropwise to triethylene glycol monomethyl ether (5.0 g, 1.0 eq) dissolved in 5 mL pyridine. The reaction was left stirring for 2 days or until reaction is complete. The tosylated intermediate compound was obtained after extraction with methylene chloride, washing with 6 M HCl (25 mL) and drying with magnesium sulfate. (Yield: 8.6 g, 88.7 %) ^{1}H NMR (300 MHz, $CDCl_3$, 25°C, TMS): δ = 7.78 (d, 2H, *J* = 9 Hz;

2Ar-H), 7.34 (d, 2H, *J* = 9 Hz; 2Ar-H), 4.14-4.17 (m, 2H; CH_2), 3.66-3.70 (m, 2H; CH_2), 3.59-3.63 (m, 6H; $3CH_3$), 3.51-3.55 (m, 2H; CH_2), 3.37 (s, 3H; CH_3), 2.45 (s, 3H; Ar-CH_3) ppm.

2.5. Synthesis of diPEGylated benzaldehyde (PEG-CHO)

Triethylene glycol tosylate (8.6 g, 2.5 eq) from the previous reaction was directly used and dissolved in 40 mL DMF together with 3,4-dihydroxybenzaldehyde (1.5, 1.0 eq) and anhydrous potassium carbonate (6.6, 4.4 eq).[45] The reaction was refluxed at 80°C for 12 hours under inert atmosphere. After cooling to room temperature, the reaction mixture was poured into ice-cold water. This was followed by extracting with MC three times, washing with water and brine, and drying with magnesium sulfate. The solvent was removed under reduced pressure and the desired compound was isolated after purification using column chromatography with ethyl acetate/MeOH (9:1). (Yield: 1.3 g, 28.4 %) ^{1}H NMR (300 MHz, $CDCl_3$, 25°C, TMS): δ = 9.84 (s,1H;Ar-H), 7.45 (s, 2H; 2Ar-H), 7.04 (s, 1H; Ar-H), 4.24 (m, 4H; $2CH_2$), 3.92 (m, 4H; $2CH_2$), 3.77 (m, 4H; $2CH_2$), 3.37 (s, 6H; $2CH_3$), 3.67 (m, 8H; $4CH_2$), 3.56 (m, 4H; $2CH_2$) ppm.

2.6. Knoevenagel Condensation Reaction

The Knoevenagel condensation reaction was carried out the same way as reported literature.[49] In around-bottomed flask, the BODIPY dyes and the diPEGylated benzaldehyde derivative (3.0 eq) were dissolved in 15 mL of DMF, then a drop of piperidine and of acetic acid were added to the reaction. The reaction was refluxed at until the reaction is complete, as indicated by the appearance of bluish-green color. DMF was evaporated under reduced pressure. The compounds 2a-c were separated from the mixture using column chromatography with ethyl acetate/MeOH (90/10) as eluents.

2a: 110 mg of **1a** and 436.9 of PEG-CHO (Yield: 65.0 mg, 16.7 %) ^{1}H NMR (300 MHz, $CDCl_3$, 25°C, TMS): δ=8.79 (d, 2H, J = 9 Hz), 7.53 (d, 2H, J = 9 Hz), 7.36 (d, 2H, J = 6 Hz), 7.29 (s, 1H), 7.23 (s, 1H), 7.17 (s, 1H), 7.13 (s, 1H), 6.93 (d, 2H,

J = 9 Hz), 6.64 (s, 2H), 4.21-4.27 (m, 8H), 3.89-3.92 (m, 8H), 3.75-3.80 (m, 8H), 3.64-3.70 (m, 16H), 3.52-3.58 (m, 8H), 3.36-3.39 (d, 12H, J = 9 Hz), 1.47 (s, 6H) ppm. ^{13}C NMR: 150.77, 150.52, 149.07, 137.05, 130.34, 124.15, 121.78, 118.40, 117.49, 114.58, 72.03, 72.02, 70.96, 70.79, 70.66, 70.63, 69.88, 69.74, 69.29, 68.78, 59.15, 59.11, 53.53, 14.92 ppm.

2b: 50.0 mg of **1b** and 159.8 mg of PEG-CHO (Yield: 33.1 mg, 21.8 %) ^{1}H NMR (300 MHz, $CDCl_3$, 25°C, TMS): δ = 8.81 (d, 2H, J=6Hz), 7.96 (d, 1H, J = 15 Hz), 7.53 (d, 2H, J = 15 Hz), 7.35 (d, 2H, J = 6 Hz), 7.30 (m, 3H), 7.13 (dd, 2H, J = 9 Hz), 6.94 (dd, 2H, J = 12 Hz), 6.70 (s, 1H), 4.21-4.27 (m, 8H), 3.89-3.92 (m, 8H), 3.76-3.78 (m, 8H), 3.63-3.70 (m, 16H), 3.52-3.58 (m, 8H), 3.36 (d, 12H, J = 9 Hz),1.45 (d, 6H, J = 9 Hz) ppm. ^{13}C NMR: 150.87, 150.69, 150.21, 148.91, 130.76, 130.35, 129.68, 122.01, 114.71, 114.47, 114.34, 71.85, 71.82, 70.78, 70.60, 70.48, 70.45, 69.68, 69.58, 69.52, 69.14, 69.04, 68.65, 68.57, 58.96, 58.91, 14.94, 13.56.

2c: 250 mg of **1c** and 668.5 mg PEG-CHO (Yield: 36.4 mg, 5.4 %) ^{1}H NMR (300 MHz, $CDCl_3$, 25°C, TMS): δ = 8.85-8.83 (d, 2H), 8.10-8.05 (d, 2H), 7.59-7.54 (d, 2H), 7.35-7.34 (m, 4H), 7.15 (s, 2H), 6.98-6.95 (d, 2H), 4.26-4.22 (m, 8H), 3.92-3.88 (m, 8H), 3.78-3.75 (m, 8H), 3.70-3.68 (m, 17H), 3.57-3.51 (m, 8H), 3.38 (s, 6H), 3.36 (s, 6H), 1.45 (s, 6H) ppm. ^{13}C NMR: 151.02, 150.84, 149.08, 139.96, 130.56, 124.03, 121.82, 114.64, 114.30, 72.03, 70.96, 70.95, 70.77, 70.65, 70.61, 69.84, 69.72, 69.18, 68.78, 59.13, 59.08, 53.53, 37.16, 34.72, 32.80, 31.99, 31.64, 30.09, 29.76, 29.72, 29.43, 27.14, 22.74, 22.70, 19.76, 14.22, 14.16, 14.06, 11.44 ppm.

2.7. Methylation of BODIPY compounds

BODIPY compounds **2a-c** and 2.0 mL of methyl iodide were mixed and stirred in 5 mL anhydrous MeCN for 2 days at room temperature according to literature.[45] The reaction was monitored to completion using TLC.

PyBHI: (Yield: 66.0 mg, 90.4 %) ^{1}H NMR (300 MHz, $CDCl_3$, 25°C, TMS): δ =9.69 (d, 2H, J = 9 Hz), 8.07 (d, 2H, J = 6 Hz), 7.47 (d, 2H, J = 18 Hz), 7.18-7.28 (m, 4H), 7.07 (s, 2H), 6.91 (d, 2H, J = 9Hz), 6.62 (s, 2H), 4.86 (s, 3H), 4.16-4.23 (m, 8H), 3.89-3.92 (m, 4H), 3.83-3.86 (m, 4H), 3.74-3.79 (m, 8H), 3.62-3.71 (m, 16H), 3.51-3.56 (m, 8H), 3.35-3.37 (d, 12H, J = 6 Hz), 1.43 ppm (s, 6H). ^{13}C NMR: 152.79, 150.91, 148.82, 130.43, 72.03, 71.99, 70.91, 70.77, 70.71, 70.61, 69.86, 59.13, 59.10, 15.11 ppm. HRMS (ESI) m/z calcd for $C_{61}H_{85}BF_2N_3O_{16}$+: 1165.1454 [M-I]+; found: 1164.6036.

PyBMI: (Yield: 33.0 mg, 89.3 %) ^{1}H NMR (300 MHz, $CDCl_3$, 25°C, TMS): δ = 9.80 (d, 2H, J = 6Hz), 8.10 (d, 2H, J = 6Hz), 7.97 (d, 1H, J = 15Hz), 7.46 (dd, 2H, J = 15Hz), 7.33 (m, 2H), 7.09 (s, 1H), 7.02 (s, 1H), 6.94 (t, 2H, J = 9Hz), 6.65 (s, 1H), 4.88 (s, 3H), 4.09-4.22 (m,8H), 3.90-3.93 (m,4H), 3.77-3.85 (m,8H), 3.71-3.76 (m,8H), 3.61-6.69 (m,12H), 3.50-3.57 (m,8H), 3.35-3.37 (m, 12H) 1.38 (s, 6H) ppm. ^{13}C NMR: 149.51, 149.36, 149.12, 147.95, 147.84, 147.44, 129.80, 117.01, 115.28, 114.93, 114.69, 72.64, 71.53, 71.37, 71.25, 70.47, 69.73, 59.81, 59.67, 50.05, 30.53, 17.04, 16.93, 15.53, 15.44 ppm. HRMS (ESI) m/z calcd for $C_{61}H_{84}BBrF_2N_3O_{16}$+: 1244.0414 [M-I]+; found: 1244.5093

PyBBrI: (Yield: 40.0 mg, 99.0 %) ^{1}H NMR (300 MHz, $CDCl_3$, 25°C, TMS): δ =9.83 (d, 2H, J = 6 Hz), 8.13 (d, 3H, J = 9 Hz), 8.07 (s, 1H), 7.48 (d, 2H, J = 15 Hz), 7.32 (d, 2H, J = 6 Hz), 7.09 (s, 2H), 6.96 (d, 2H, J = 9 Hz), 4.89 (s, 3H), 4.21-4.24 (m, 4H), 4.14-4.18 (m, 4H), 3.9-3.93 (m, 4H), 3.81-3.84 (m, 4H), 3.60-3.78 (m, 24H), 3.49-3.57 (m, 8H), 3.34-3.36 (d, 12H, J = 6 Hz), 1.34 ppm (s, 6H). ^{13}C NMR: 150.60, 148.89, 130.19, 72.02, 72.00, 70.92, 70.77, 70.73, 70.62, 69.83, 69.19, 68.83, 59.14, 59.10, 16.09 ppm. HRMS (ESI) m/z calcd for $C_{61}H_{83}BBr_2F2N_3O_{16}$+: 1322.9375 [M-I]+; found:1322.4263.

2.8. Methods

Intermediate and final products PyBXI were analyzed by ^{1}H and ^{13}C NMR spectroscopy using a Bruker AM 250 spectrometer (USA). Furthermore, the molecular masses of the compounds were confirmed by high-resolution electrospray ionization mass spectrometry (HR-ESI-MS) using a SYNAPT G2-Si high-definition mass spectrometer (United Kingdom).

The steady-state absorption and emission spectra of PyBXI dyes dissolved in methanol were measured using a LAMBDA 25 spectrophotometer (PerkinElmer) and a LS-55 fluorometer (PerkinElmer) at 298 K, respectively. The fluorescence quantum yields (ϕ_F) of the dyes were measured relative to that of Rhodamine 6G (ϕ_F = 0.95 in ethanol) and calculated according to the equation given:

$$\phi_F^S = \phi_F^R \left(\frac{A_R}{A_S}\right)\left(\frac{E_S}{E_R}\right)\left(\frac{n_S}{n_R}\right)$$

where S and R stand for sample and reference, respectively. A refers to the absorbance of the solution; E represents the integrated fluorescence intensity, and n indicates the refractive index of the solvent, respectively.

2.9. Singlet oxygen quantum yield measurements

For the singlet oxygen quantum yield (ϕ_Δ) measurements, 1,3-diphenylisobenzofuran (DPBF) bleaching experiment was conducted where DPBF is used to trap $^{1}O_2$ and methylene blue (MB) is used as the reference standard (ϕ_Δ = 0.50 in methanol). DPBF solutions containing each of the BODIPY dyes were carefully irradiated by an LED light at 660 nm at an illumination intensity of 8 mW/ cm^2. Then the loss of the absorption peak at 410 nm corresponding to DPBF was monitored every five minutes. Finally, the singlet oxygen quantum yield was calculated by the equation below:

$$\phi_\Delta^S = \phi_\Delta^R \left(\frac{m_S}{m_R}\right)\left(\frac{F_R}{F_S}\right)$$

where m refers to the slope of the photobleaching curve and F is the correction factor

accounting for the gap in the absorption of the sample and of the reference ($F=1-10^{-A}$).

2.10. Quantum chemical calculations

The structures and electronic states of PyBXI dyes were optimized according to density functional theory (DFT) and time-dependent DFT (TD-DFT) at B3LYP-6-31G(d) level, respectively. Water is designated as solvent for these calculations. The TD-DFT calculation of the spin-orbit coupling was done in ORCA 5.0.1 at the B3LYP/ZORA-def2-TZVP level[46], where ZORA indicates zero-order relativistic approximation and takes relativistic effects into account. Unless mentioned otherwise, the triethylene glycol chains of the BODIPY dyes were replaced by hydrogen atoms in all calculations to save computation costs.

2.11. Cells and cell culture

HeLa and MCF-7 cells were supplied by the Korean Cell Line Bank. They were maintained with 10% heat-inactivated fetal bovine serum (FBS) and antibiotics (100 U/mL penicillin and 100 mg/mL streptomycin) (Welgene Inc., South Korea) in RPMI 1640 medium (Gibco, Carlsbad, CA, USA) in a humidified 5% CO_2 incubator at 37 ºC.

2.12. Cell proliferation assay

HeLa and MCF-7 cells (2×10^3 cells/well) were spread in 96-well plates and kept at 37°C in 5% CO_2 for one day. Then the cells were treated with the PyBXI dyes at different concentrations for another 24 h. The cell proliferation was determined according to the prescribed procedure for CellTiter96® AQueousOne Solution Cell Proliferation Assay (Promega, Madison, WI, USA). Then the absorbance was measured at 490 nm using ELISA plate reader (ThermoFisher Scientific, Inc., Waltham, MA, USA).

2.13. Photodynamic activity

HeLa and MCF-7 cells (2×10^3 cells/well) were treated in the same way as above but with further incubation at 37°C in 5% CO_2 under dark conditions for 2h. Then, the media were replaced with phenol-red free RPMI 1640 followed by exposure to red light-emitting diode at 680 nm (70% power) for 30 min. The cells were incubated for additional 24 h and the cell proliferation (% of the control) was measured.

2.14. Confocal laser scanning microscopy

HeLa and MCF-7 cells were treated with the PyBXI dyes (16 μM) for 24 h. Then, they were further treated with MitoTracker Red (Invitrogen) for 45 min. The cells were fixed with 4% paraformaldehyde for 10 min and permeabilized with 0.1% Triton X-100 for 10 min followed by counter staining with 4′,6-diamidino-2-phenylindole (DAPI) for 1 h at room temperature. Finally, the treated cells were imaged using confocal microscopy (LSM-700, Carl Zeiss, Germany).

2.15. Statistical Analysis

Data are expressed as means ± standard deviations. Group means were considered significantly different at $p < 0.05$. GraphPad 6 Prism software (San Diego, CA, USA) was used for the one-way analysis of variance and Tukey's test of the data.

3. Results and Discussion

Pyridinium-conjugated BODIPY dyes with mitochondria-targeting ability was accessed following the route outlined in Figure 13. BODIPY 1 was synthesized *via* acid-catalyzed condensation reaction of 2,4-Dimethylpyrrole and 4-Pyridiniumcarboxaldehyde, followed by *p*-chloranil, and dropwise additions of TEA and BF_3OEt_2. Controlled substitutions of bromine atoms produced monobrominated and dibrominated BODIPYs. Two equivalents of tosylated triethylene glycol was conjugated to 3,4-Hydroxybenzaldehyde to yield diPEGylated benzaldehyde. Then, Knoevenagel

condensation reaction between the precursor BODIPY 1a-c and benzaldehyde derivative produced intermediate compound 2a and halogenated analogues 2b-c. Finally, quantitative methylation of the pyridinium group yielded final compounds PyBHI, PyBMI and PyBBrI. The current synthetic design attempts to circumvent the limitations of parent BODIPY by making full use of available sites for modifications. All structures of the compounds were confirmed by ^{1}H NMR and ^{13}C NMR and further characterized by mass spectrometry.

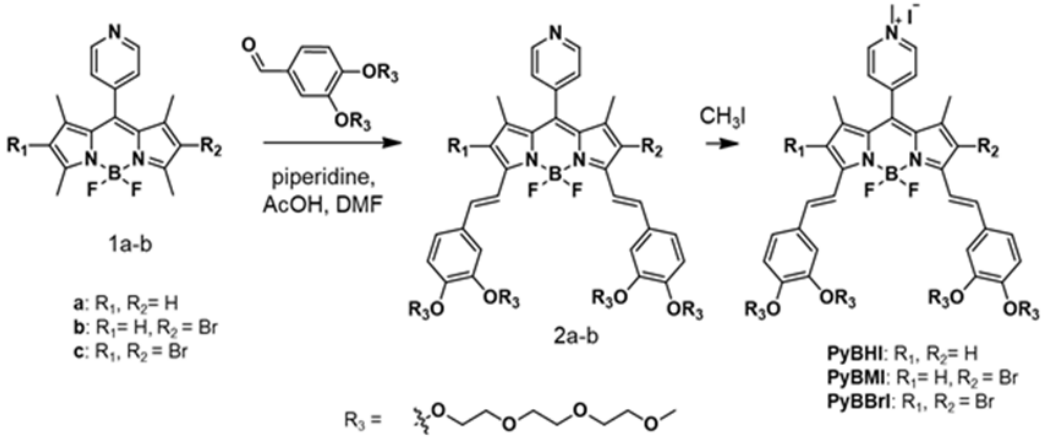

Figure 13. Pyridinium-based BODIPY photosensitizers with different substitutions at the C-2 and C-6 positions.

3.1. Photophysical Properties

The steady-state absorption and emission spectra of PyBXI dyes are presented in Figure 14a and b. PyBXI features a pronounced red shift of up to ca. 180-200 nm relative to intermediate BODIPY compounds 1a-c. Because of the methyl groups found at the C-1 and C-7 positions of parent BODIPY, substituents at the C-8 position are oriented orthogonally to BODIPY and exert negligible influence on the absorption and emission bands.[51] Thus, the observed bathochromic shift can only be attributed to the extension of the π-π conjugation of the BODIPY core *via* Knoevenagel condensation reaction. In

addition, bromination at the C-2 and C-6 positions also contributed to the red shift of the absorption and emission spectra.[52] The observed values are also in agreement with that of similar BODIPY compounds in literature.[45]

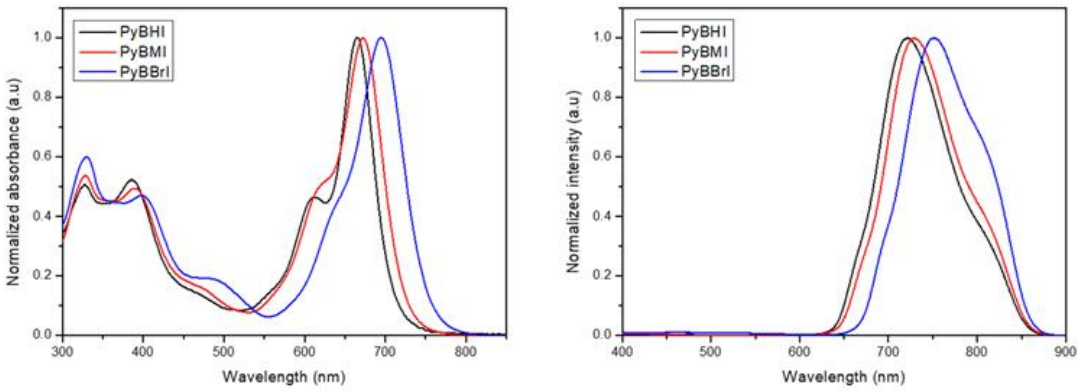

Figure 14. Normalized absorbance and fluorescence intensity spectra of PyBHI, PyBMI and PyBBrI in methanol.

	λ_{abs}(nm)	λ_{em}(nm)	Φ_F	Φ_Δ
PyBHI	666	721	0.0014	0.0008
PyBMI	672	729	0.0013	0.0034
PyBBrI	696	751	0.0010	0.0075

Table 3. Photophysical properties of PyBXI dyes in methanol.

However, the fluorescence quantum yields of the PyBXI dyes are unexpectedly poor even for the halogen-free PyBHI, as shown in Table 3. This could be due to multiple compounding factors. First, the free rotation of the PEG chains and vinyl bonds lead to nonradiative pathways resulting to the fluorescence quenching. Second, the presence of electronegative nitrogen atoms on the pyridine ring strongly attracts electrons from the main BODIPY, contributing to the reduction of fluorescence quantum yield. Finally, upon the methylation of the sp^2-hybridized nitrogen atom in the pyridine, migration of

electrons — be it *via* photoinduced electron transfer (PET) or charge transfer (CT) – contributes to fluorescence quenching.[48,53] In fact, there are only small variations in the fluorescence quantum yields among the PyBXI dyes.

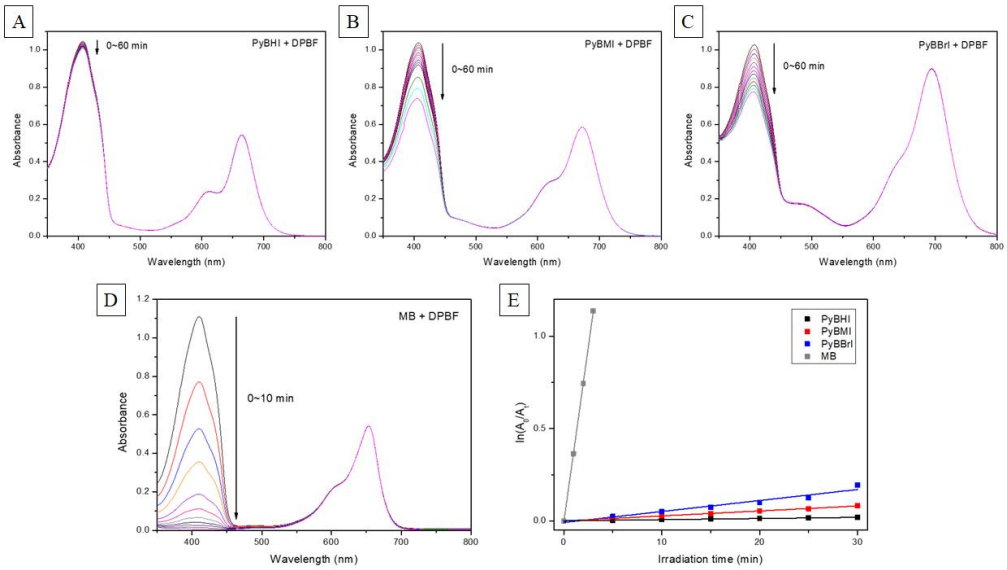

Figure 15. The changes in the absorption spectra of DPBF solutions added with PyBHI (A), PyBMI (B), PyBBrI (C) and MB (D) under the illumination of 660 nm light tracked with time. E) Linear fitting of the photodegradation of DPBF with PyBXI and MB in methanol.

To measure the $^1O_2$-generation efficiency of the PyBXI dyes, 1,3-Diphenylisobenzofuran (DPBF) bleaching experiment is performed on the dyes. DPBF, a fluorophore that absorbs at 410 nm and emit light at ~455 nm, reacts with $^1O_2$ to produce 1,2-dibenzoylbenzene (DBB) *via* a cycloaddition reaction. The loss of absorbance of DPBF at 410 nm has been utilized for the precise measurement of $^1O_2$ for many years.[55] Similarly, methanolic solutions of PyBXI were mixed with DPBF to trap the

generated $^1O_2$ after LED irradiation. Figure15a-c shows the absorption spectra of the methanolic solution containing DPBF and PyBXI dyes, respectively. Figure 15d shows the absorption spectra of the solution containing DPBF and MB, a reference PS. Figure 15e shows the linearly fitted comparison of the individual results of the photobleaching experiment. As summarized in Table 3, the singlet oxygen quantum yields of PyBXI dyes increased from the nonhalogenated PyBHI (0.0008) to PyBMI (0.0034) and to PyBBrI (0.0075), respectively. Expectedly, the ϕ_Δ increased in accordance to the degree of bromination. In order produce a PDT effect, an efficient intersystem crossing should be met. Historically, nonhalogenated BODIPY dyes have been shown to have low intersystem crossing. To circumvent this problem, installing a heavy atom (bromine) facilitates ISC process through vibronic spin-orbit coupling.[54] However, as will be shown later, even with the low ϕ_F and lowϕ_Δ, PyBXI dyes can still induce light-triggered damage to cancer cells while also allowing for mitochondria visualization.

Computational study using time-dependent density functional theory at B3LYP/6-31G(d) level were conducted to see the correlation of the spectral data of PyBXI with their electronic structures (Figures 16-18). PEG chains are precluded from the calculation to lessen computation costs and as they do not have any electronic contribution to the electronic structures because of their saturated nature. Based on the optimized geometries of PyBXI, the BODIPY core and the distyryl moieties are coplanar with each other leading to the delocalization of the HOMOs and LUMOs among the styryl compounds. In addition, the electron density also spreads to the bromine atoms resulting to the narrowing of HOMO-LUMO energy gap (HLG) causing the bathochromic shift of the absorption and emission spectra.[56]

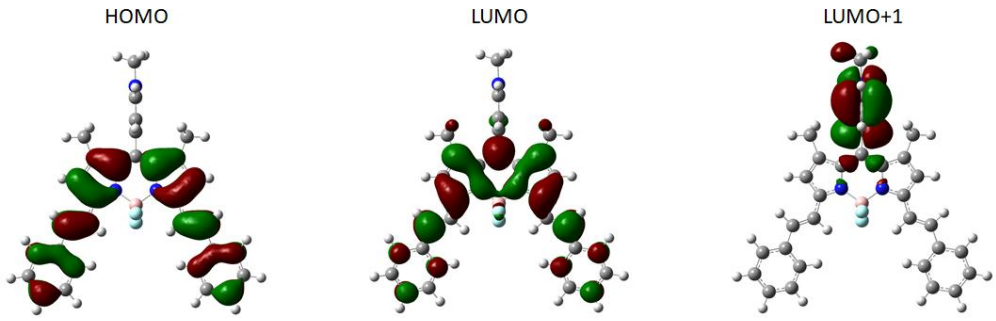

HOMO is 135

No.	Energy (cm-1)	Wavelength (nm)	Osc. Strength	Symmetry	Major contribs	Minor contribs
1	15528.69968	643.968922451	0.0	Singlet-A	HOMO->L+1 (99%)	
2	16560.28992	603.854162476	1.0685	Singlet-A	HOMO->LUMO (101%)	
3	23253.93136	430.034811972	0.0414	Singlet-A	H-1->LUMO (45%), HOMO->L+2 (50%)	HOMO->L+3 (4%)

CT state = 1.93 eV / S_1 state = 2.05 eV

Figure 16. Energy levels of the HOMO and LUMO of PyBHI calculated using the B3LYP/6-31G(d) level (solvent:water).

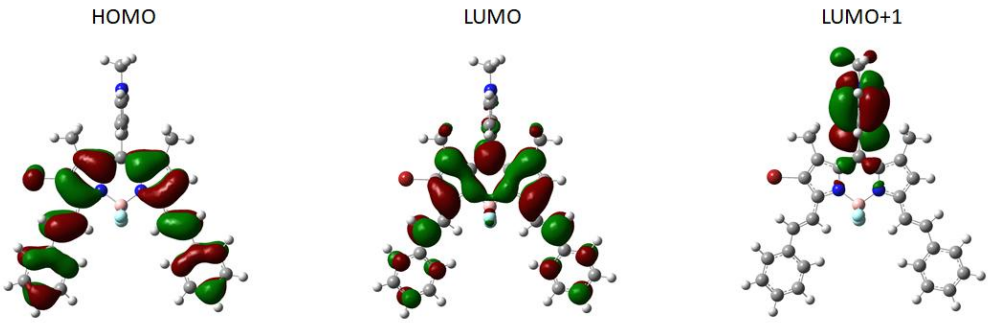

HOMO is 152

No.	Energy (cm-1)	Wavelength (nm)	Osc. Strength	Symmetry	Major contribs	Minor contribs
1	16039.25216	623.470464847	0.2526	Singlet-A	HOMO->LUMO (31%), HOMO->L+1 (68%)	
2	16398.97792	609.794101119	0.7485	Singlet-A	HOMO->LUMO (70%), HOMO->L+1 (31%)	
3	23034.54704	434.130525017	0.2379	Singlet-A	H-1->LUMO (80%), HOMO->L+2 (12%)	HOMO->L+3 (7%)

CT state = 1.99 eV / S_1 state = 2.03 eV

Figure 17. Energy levels of the HOMO and LUMO of PyBMI dye calculated using the B3LYP/6-31G(d) level (solvent:water).

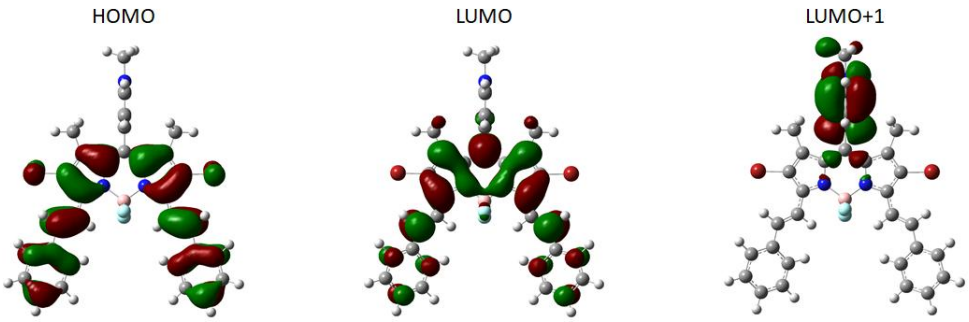

HOMO is 169

No.	Energy (cm-1)	Wavelength (nm)	Osc. Strength	Symmetry	Major contribs	Minor contribs
1	15980.37328	625.767610355	0.951	Singlet-A	HOMO->LUMO (101%)	
2	16640.94592	600.927378051	0.0001	Singlet-A	HOMO->L+1 (99%)	
3	22526.41424	443.923293493	0.331	Singlet-A	H-1->LUMO (89%)	HOMO->L+2 (4%), HOMO->L+3 (6%)

CT state = 2.06 eV / S_1 state = 1.98 eV

Figure 18. Energy levels of the HOMO and LUMO of PyBBrI dye calculated using the B3LYP/6-31G(d) level (solvent:water).

Another interesting result obtained from the TD-DFT study reveals that charge transfer states are formed in PyBXI dyes. Charge transfer states are states that correspond to full or partial transfer of electrons from a donor to an acceptor.[57] In this case, the BODIPY core acts as the electron donor while the pyridinium moiety acts as the acceptor. The charge transfer phenomenon appears to be the primary reason of the low fluorescence quantum yields and singlet oxygen quantum yields of PyBXI dyes.[58]

3.2. Cell proliferation and phototoxicity

To evaluate the light-controlled cytotoxicity of the dyes, HeLa and MCF-7 cells were treated with different concentration of the dyes for 24 hrs. As shown by the black bars in Figure 19, the three dyes did not elicit cytotoxic effects to both cell lines up to 640 nM. However, with irradiation for 30 mins, a significant portion of the cells died. The phototoxic effect is more pronounced with PyBBrI-treated cell lines at high concentrations (> 80 nM). For cells treated with singly brominated PyBMI, a significant

phototoxic effect can only be observed at 640 nM. In contrast, the cells treated with nonhalogenated PyBHI did not show any reduced cell viability. PyBBrI has an IC_{50} of 219 and 96 nM for HeLa and MCF-7 cells, respectively. PyBMI has a higher IC_{50} of 329 and 326 nM for the same cell lines. Expectedly, the results point to the presence of bromine atoms as the contributing factor to the phototoxicity of the cells.

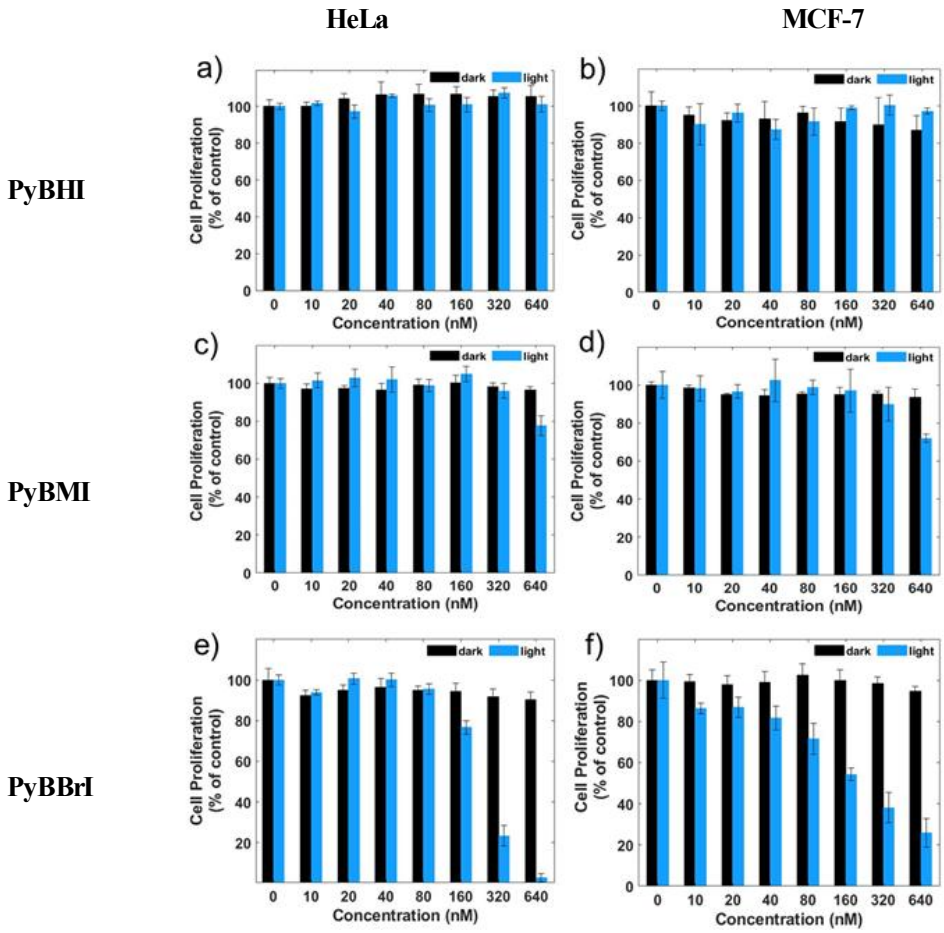

Figure 19. Dose-dependent cell proliferation assay of PyBHI, PyBMI and PyBBrI using HeLa and MCF-7 cells under dark and irradiated conditions at 680 nm for 30 min (70%, 40 mW).

	HeLa	MCF-7
PyBMI	329	326
PyBBrI	219	96

Table 4. IC_{50} of PyBMI and PyBBrI dyes in HeLa and MCF-7 cell lines in nM.

3.2. Mitochondria-targeted cell imaging

After establishing the biocompatibility of the dyes, the same cancer cell lines were imaged using confocal laser scanning microscopy (CLSM). Figure 20 and 21 show the cell imaging results of MCF-7 and HeLa cells, respectively. In Figure 20a and 21a, the BODIPY dyes can be distinctly observed in the red areas surrounding the nucleus (dark area). MitoTracker Green can also be observed in this same area around the nucleus (Fig. 20b and 21b). Furthermore, DAPI staining confirms the position of the nucleus (Fig. 20c and 21c). Additional analysis of the co-stained cells of the BODIPY dyes and MitoTracker Green show the agreement of their fluorescence intensities (Figure 22 and 23). This evidences the strong preference of the BODIPY dyes to the mitochondria.

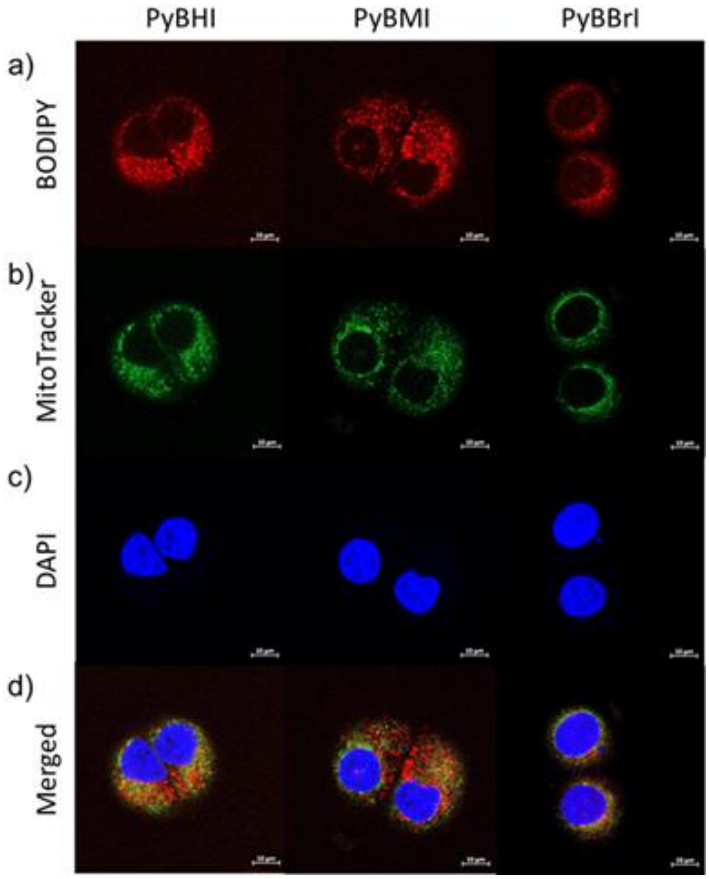

Figure 20. CLSM images of MCF-7 cells co-stained with 16 μM each of PyBHI, PyBMI, PyBBrI (a), MitoTracker Green (b), DAPI (c), and merged images (d).

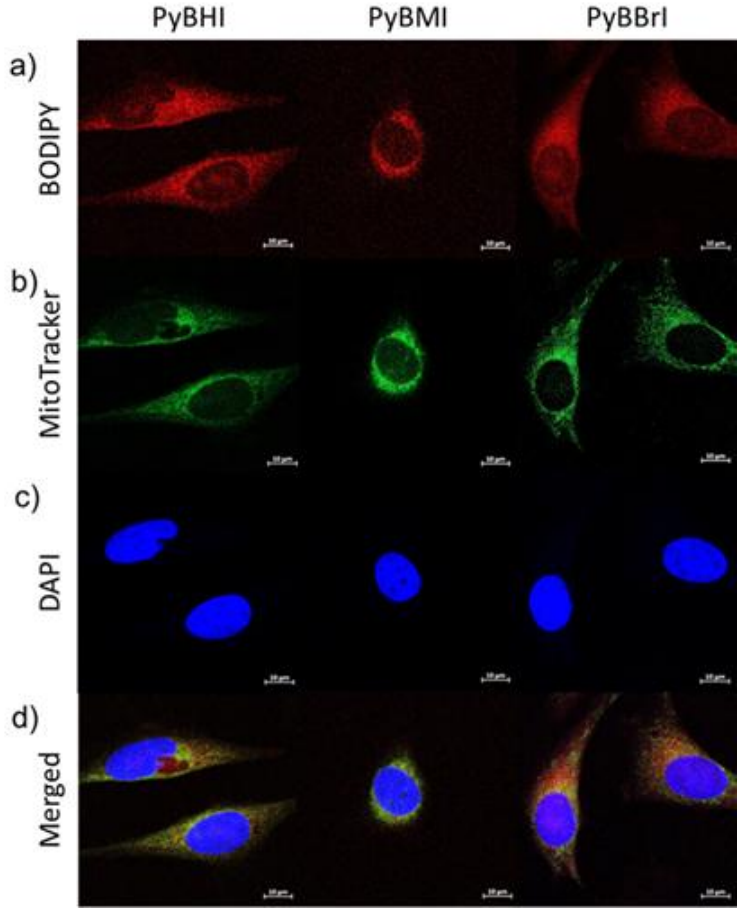

Figure 21. CLSM images of HeLa cells co-stained with 16 μM each of PyBHI, PyBMI, PyBBrI (a), MitoTracker Green (b), DAPI (c), and merged images (d).

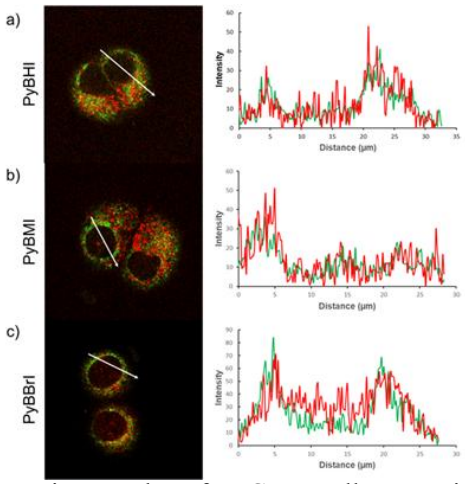

Figure 22. Fluorescence micrographs of MCF-7 cells co-stained with MitoTracker Green and PyBXI BODIPY dyes and fluorescence intensity profiles along the region of interest marked by a white arrow.

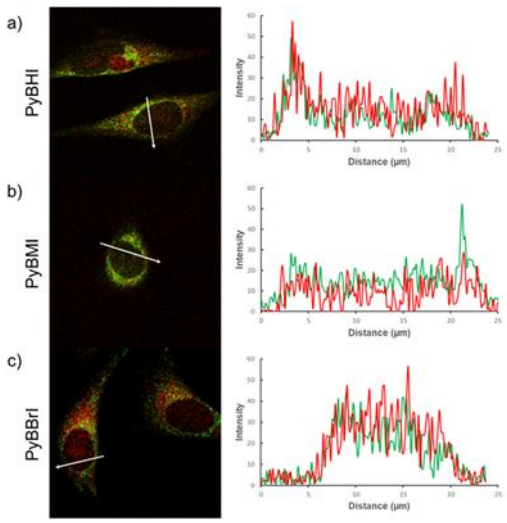

Figure 23. Fluorescence micrographs of HeLa cells co-stained with MitoTracker Green and PyBXI BODIPY dyes and fluorescence intensity profiles along the region of interest marked by a white arrow.

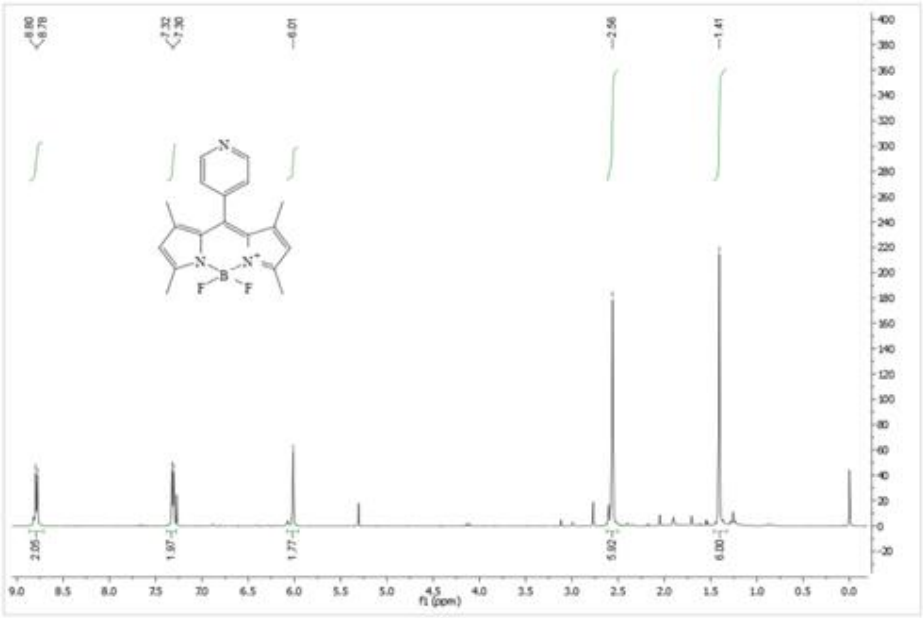

^{1}H NMR of 1a

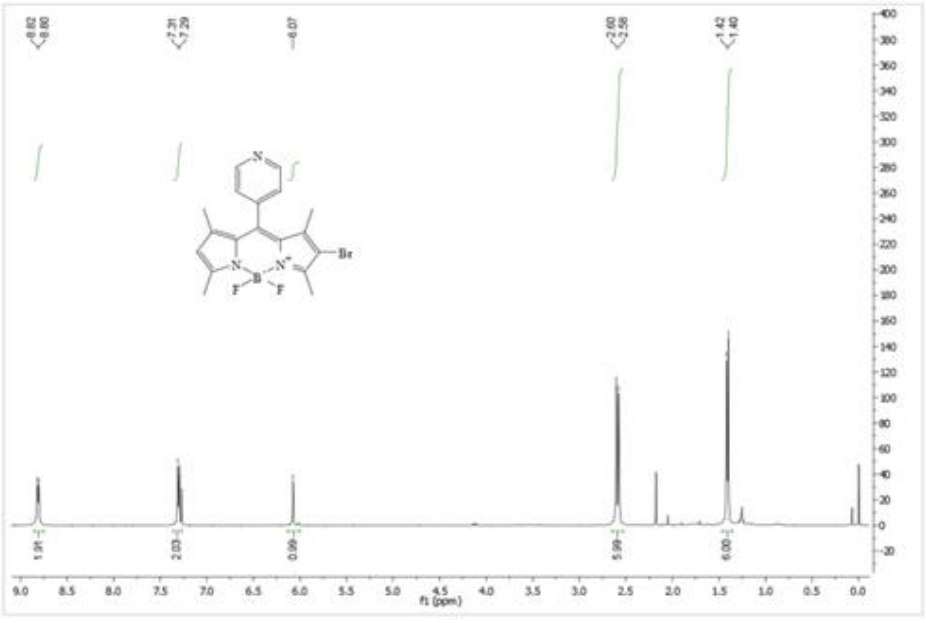

1H NMR of 1b

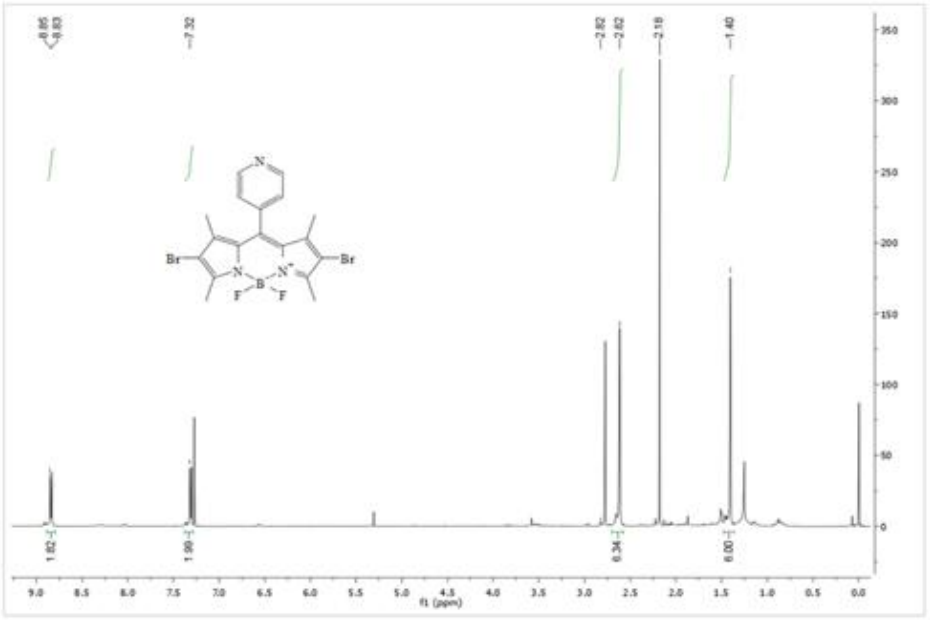

^{1}H NMR of 1c

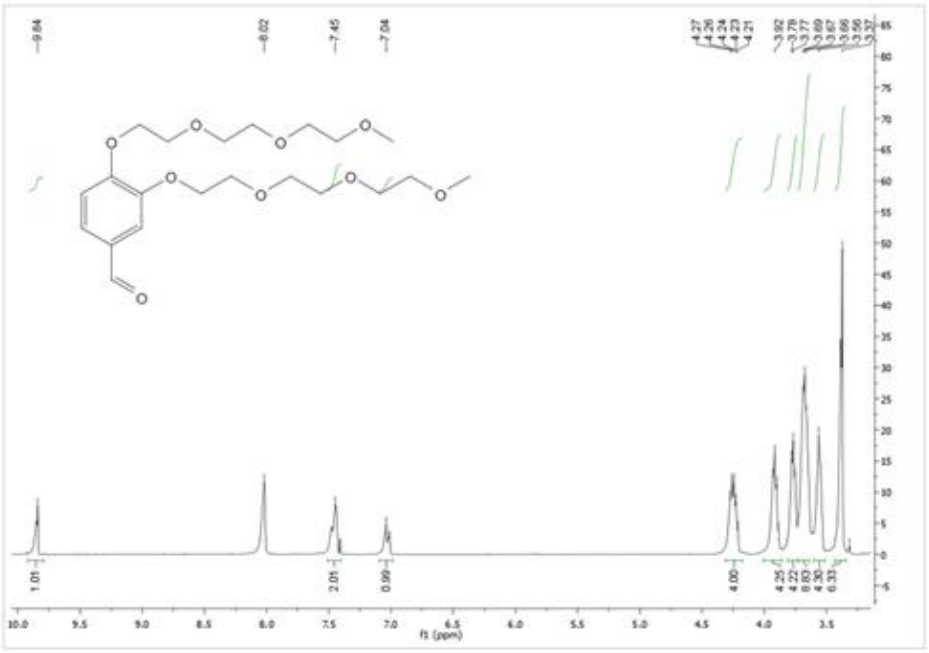

^{1}H NMR of diPEGylated benzaldehyde

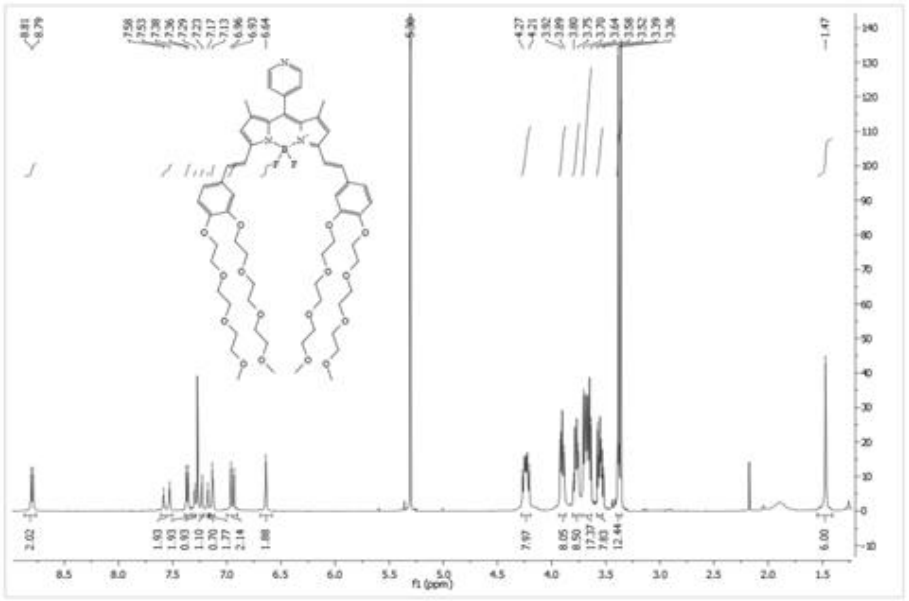

^{1}H NMR of 2a

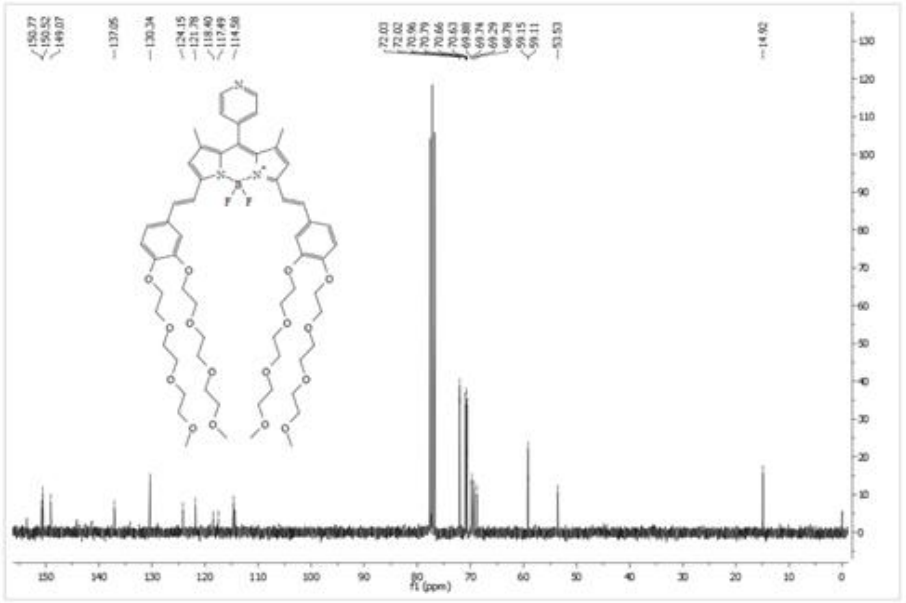

^{13}C NMR of 2a

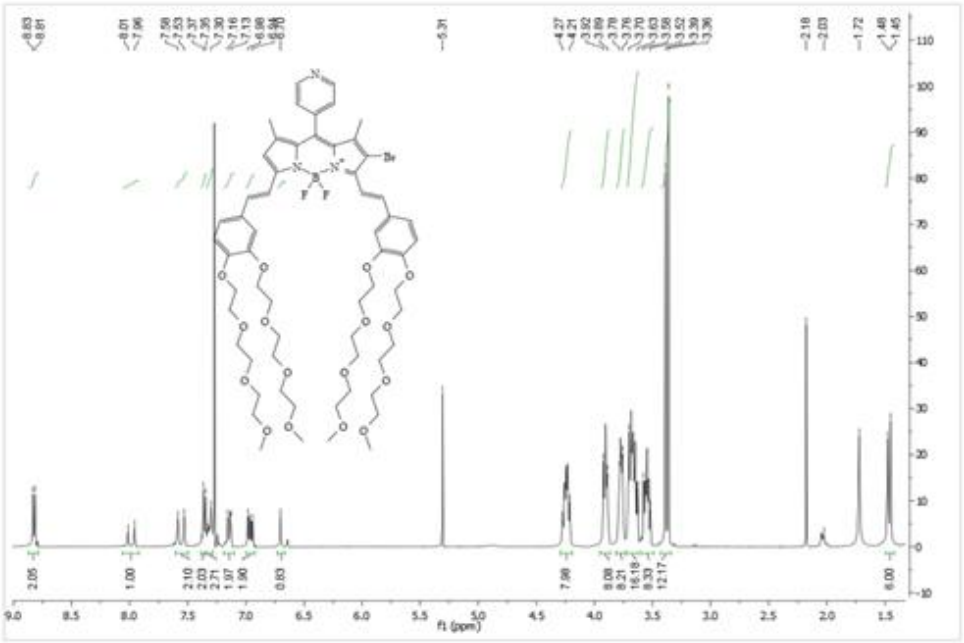

^{1}H NMR of 2b

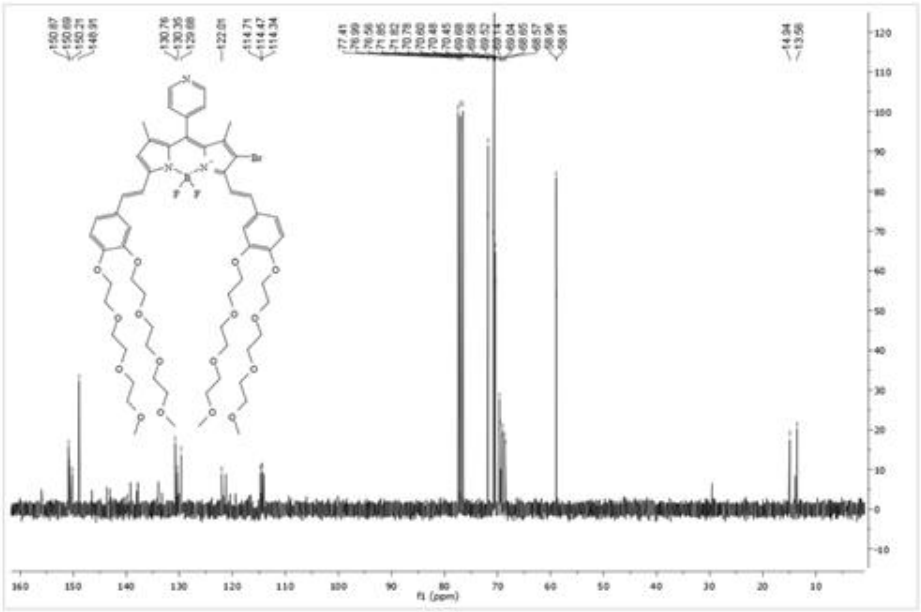

^{13}C NMR of 2b

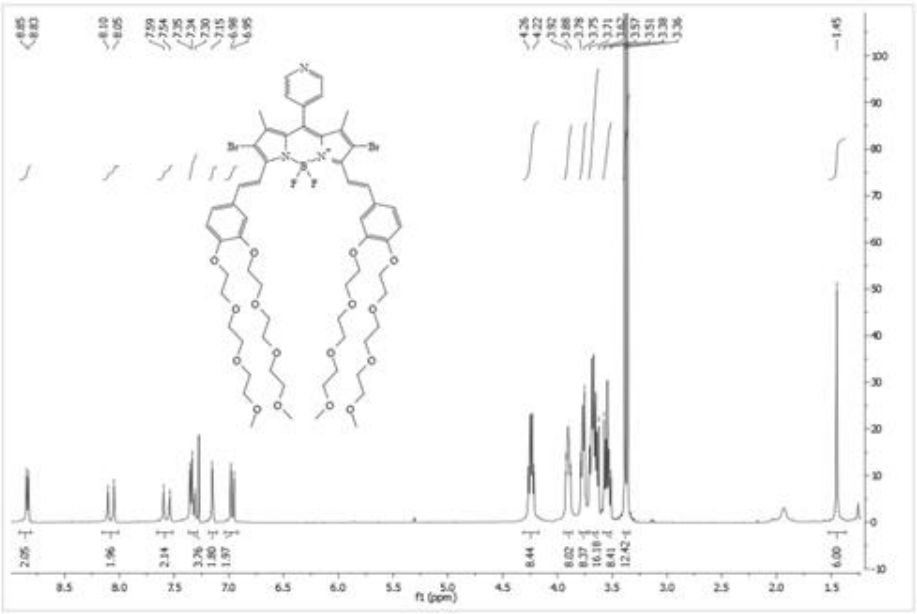

^{1}H NMR of 2c

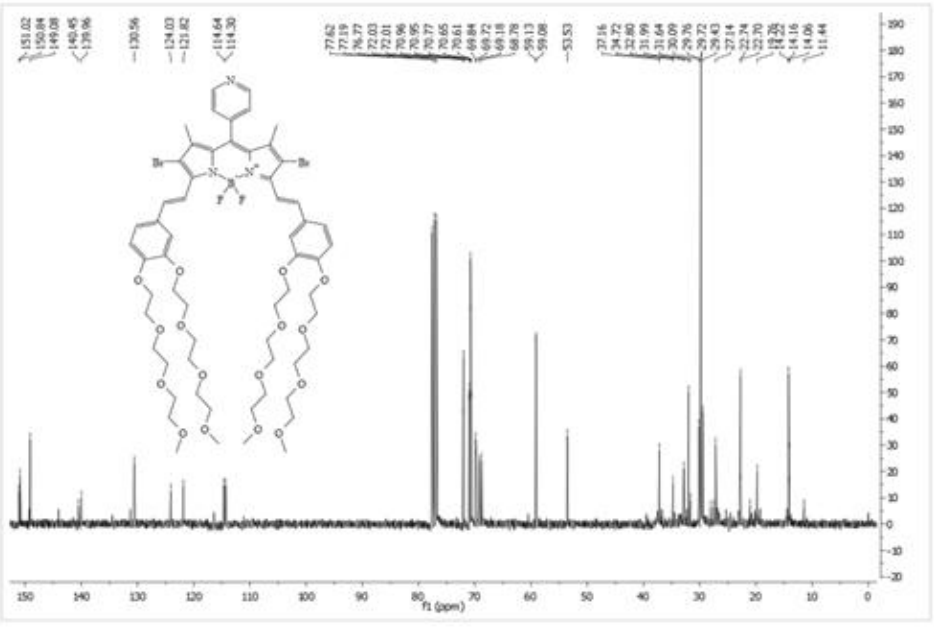

^{13}C NMR of 2c

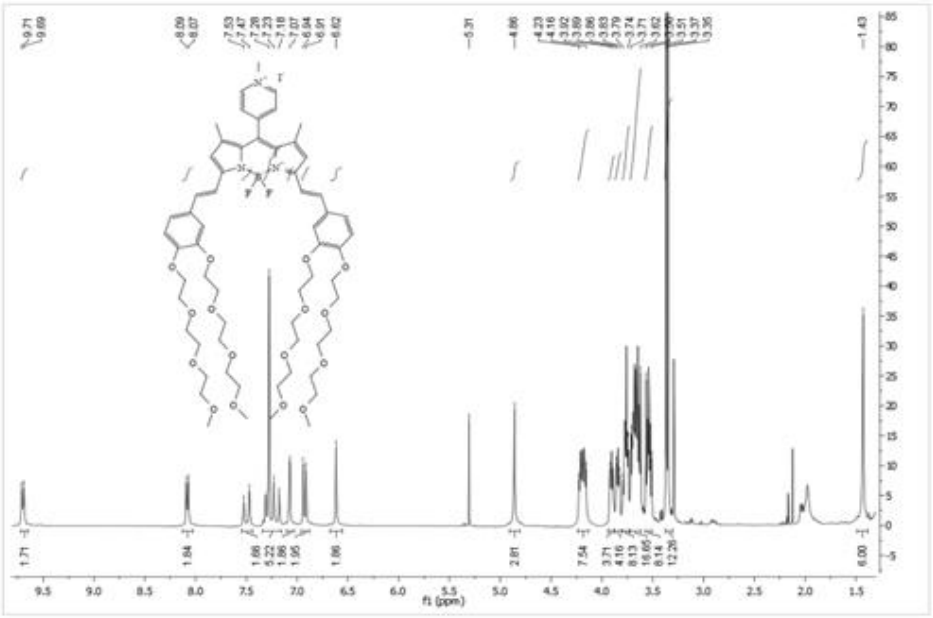

^{1}H NMR of PyBHI

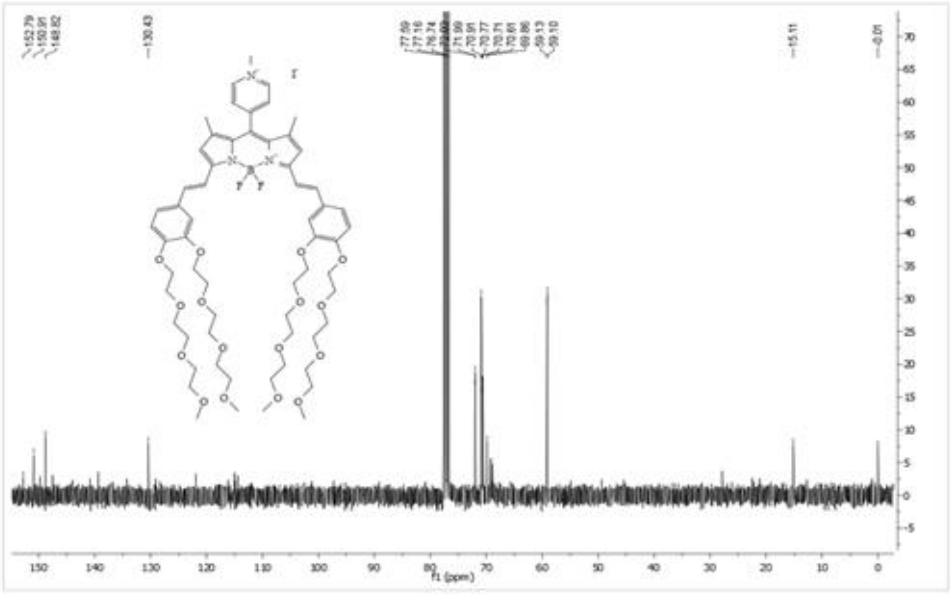

^{13}C NMR of PyBHI

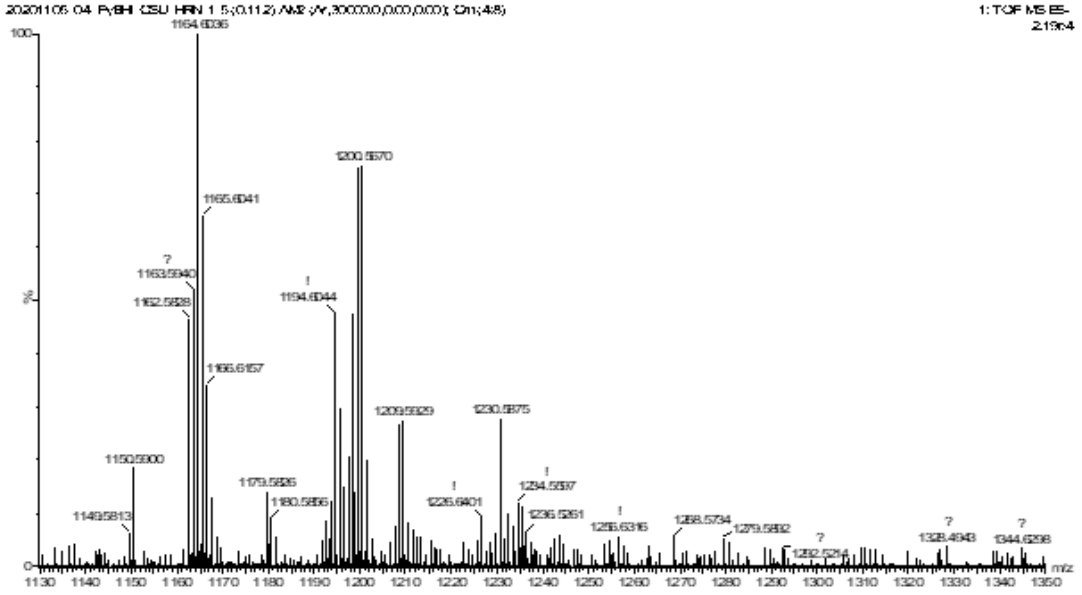

HR-MS of PyBHI

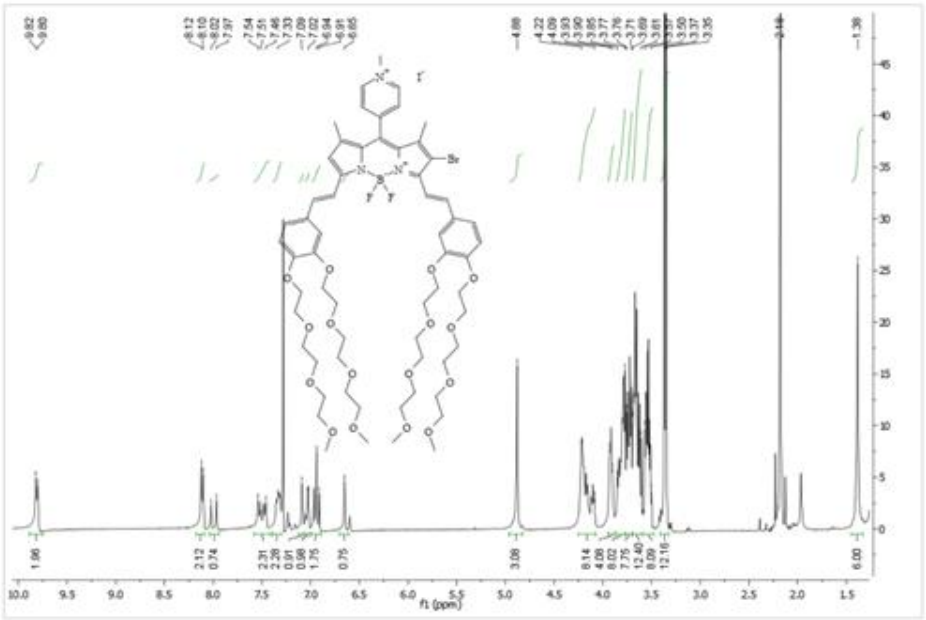

^{1}H NMR of PyBMI

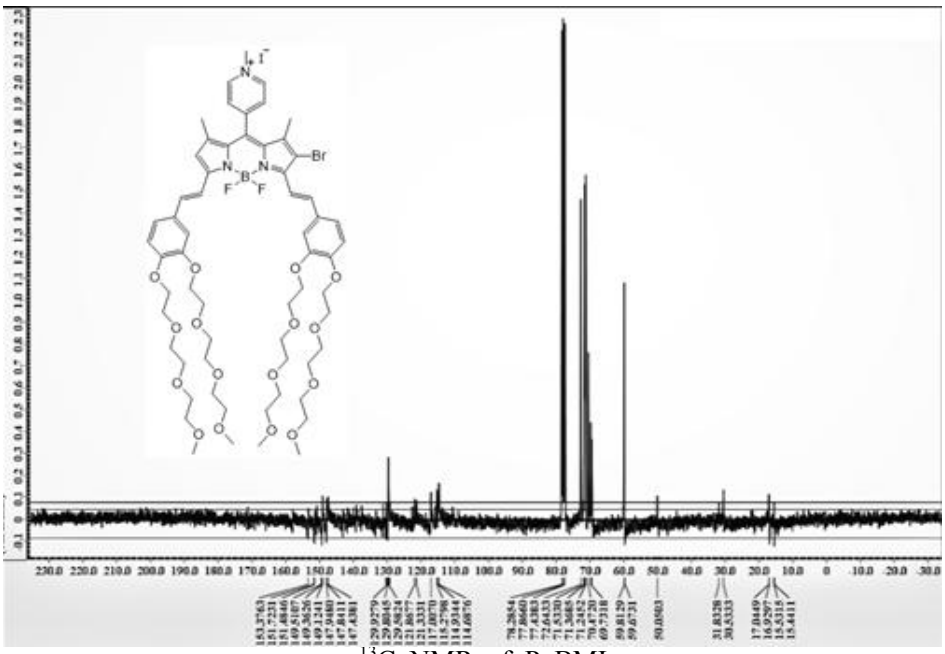

^{13}C NMR of PyBMI

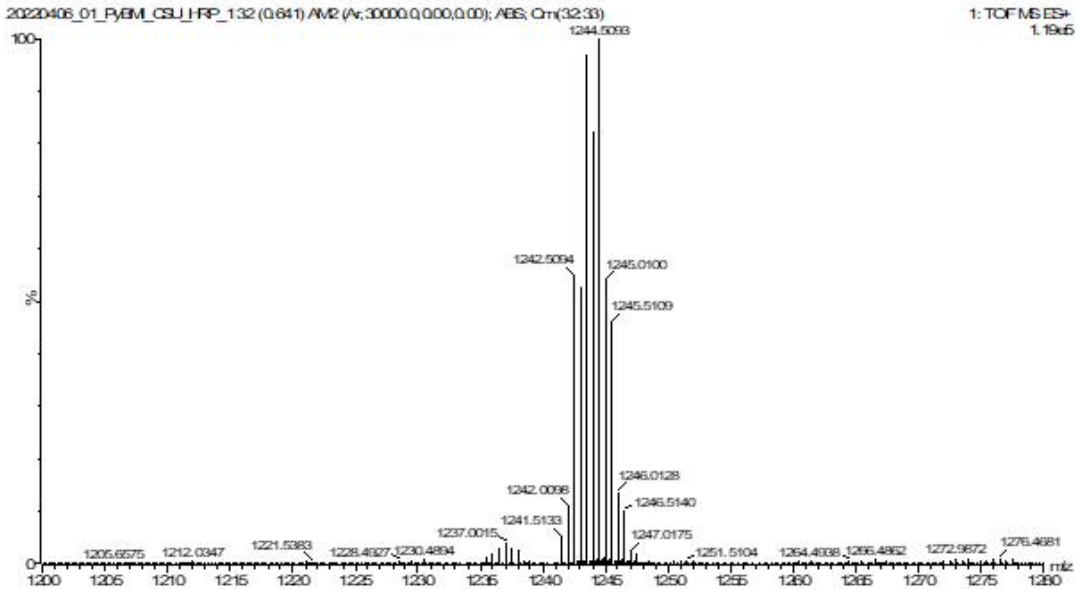

HR-MS of PyBMI

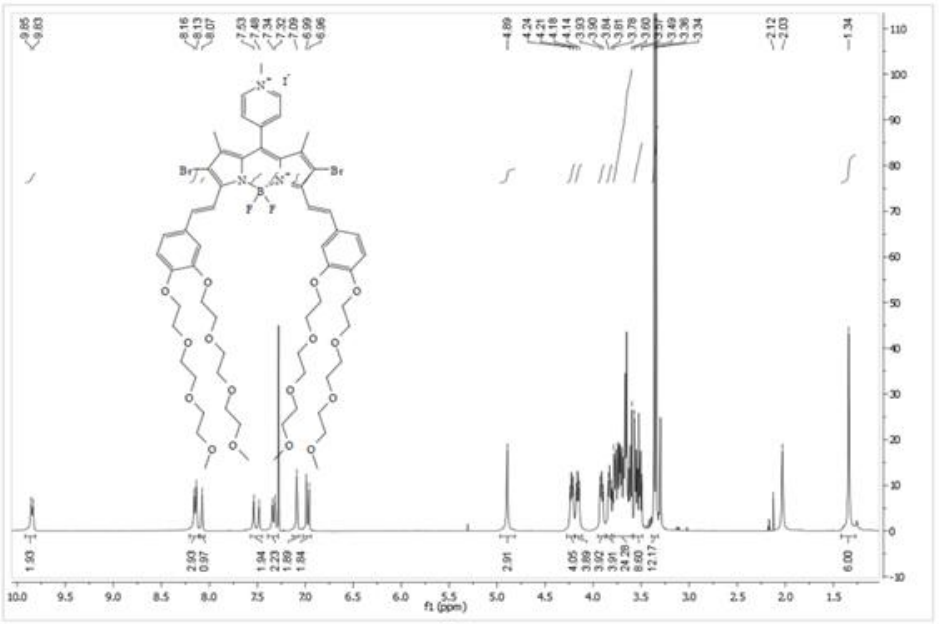

^{1}H NMR of PyBBrI

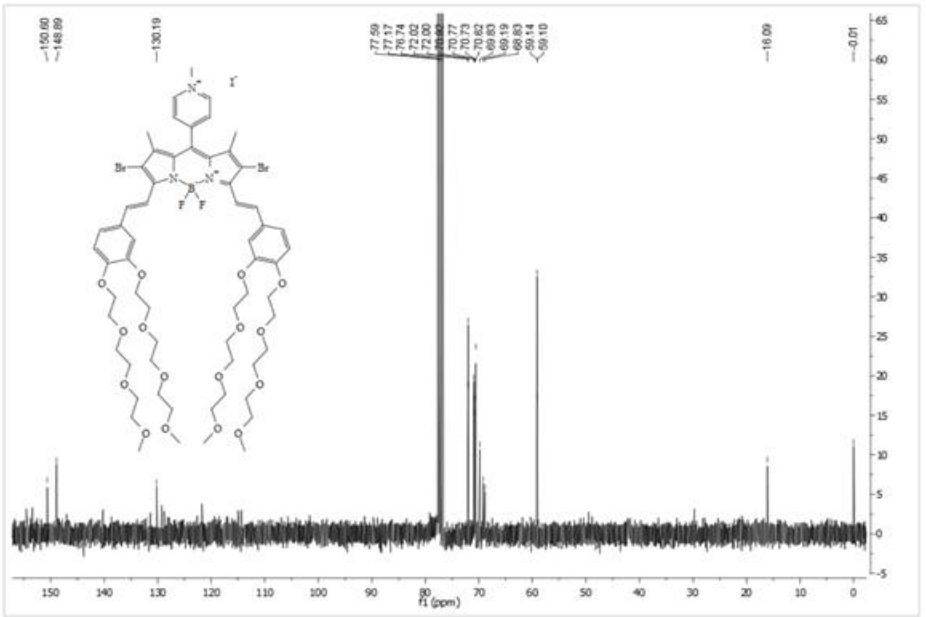

^{13}C NMR of PyBBrI

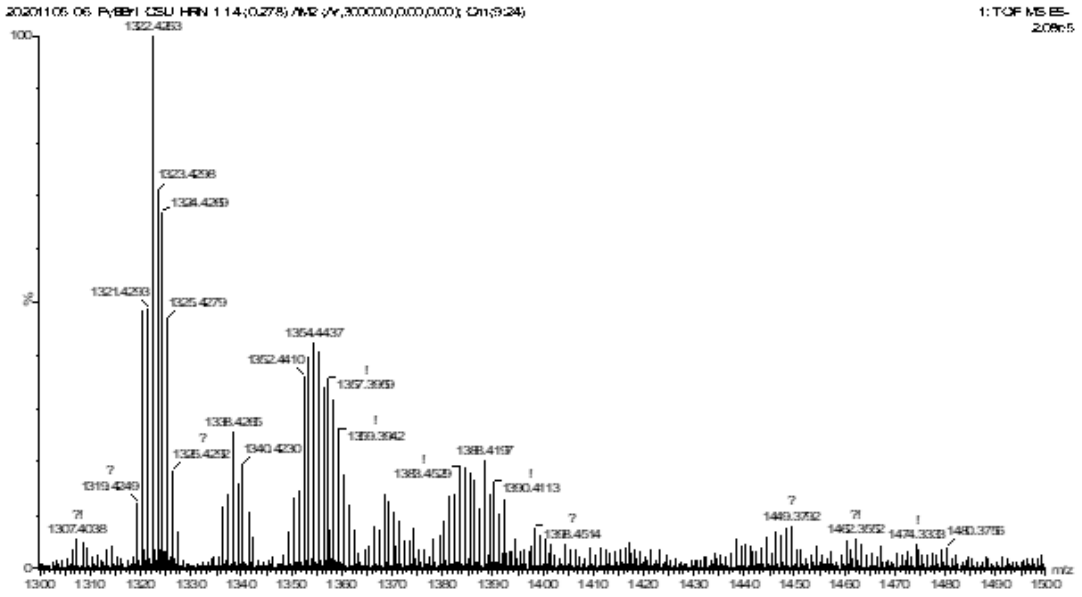

HR-MS of PyBBrI

CHAPTER 4: BODIPY functionalized NIPAM nanogels for dual-chromatic cell imaging and photodynamic therapy

1. Introduction

Nanogels are useful platforms in which several functionalities can be combined to form superstructures with innovative properties for disease diagnosis and therapies.[59-61] They are stimuli-responsive, crystallize at high volume fractions like colloids, and adsorb to interfaces like surfactants. The permeable network-like architecture, swelling behavior and deformability make them ideal for various applications such as in nanoreactors, actuators, catalysis, drug delivery systems and detection systems.[62] In contrast to free molecules, the components of a nanogel are contained within crosslinked polymer matrix which prevents direct contact with biological milieu. Furthermore, the surface of the nanogel is available for surface functionalization of targeting ligands.[63] Crosslinked poly(*N*-isopropylacrylamide) (pNIPAM) is the most relevant class of nanogel due to its temperature-dependent swelling, with a volume phase transition temperature (VPTT) of ~32°C. pNIPAM nanogel loses most of its water content and shrinks in size at this temperature.[64]

Herein, mitochondria-targeting nanogels for two-color fluorescence imaging and photodynamic activity are fabricated. Firstly, the nanogels composed of NBD and BODIPY fluorescent dyes covalently crosslinked with NIPAM and HEMA are accessed via free radical emulsion copolymerization technique. Next, the photophysical properties of the dyes were investigated to determine the effect of having two fluorophores within the crosslinked structure. Thirdly, the hydrodynamic and dehydrated size were measured. Finally, the ability of the nanogels to produce two color fluorescence micrographs of cancer cells were determined.

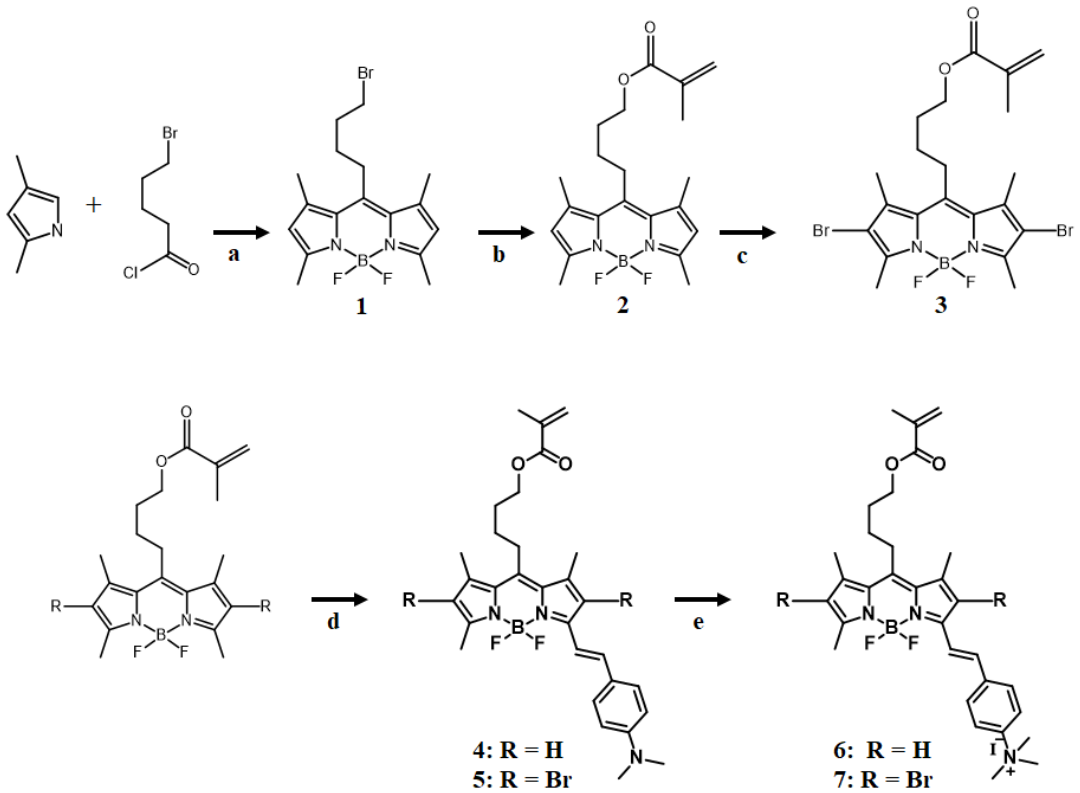

Figure 24. The synthetic route to obtain the methacrylated monostyryl BODIPY. a) TEA, BF_3OEt_2. b) sodium methacrylate, tetrabutylammonium bromide, DMF. c) *N*-Bromosuccinimide, dry MC. d) 4-(dimethylamine)benzaldehyde, piperidine, acetic acid. e) iodomethane, acetonitrile.

2. Experimental Section

2.1. Materials

All chemicals were obtained commercially and used without additional purification unless specified. 2,4-Dimethylpyrrole, tetrabutylammonium bromide, piperidine, 2-aminoethyl methacrylate HCl, ammonium persulfate and boron trifluoride diethyl etherate ($BF_3{\cdot}OEt_2$) were purchased from Sigma Aldrich (USA).

2,3-Dichloro-5,6-dicyano-1,4-benzoquinone, 4-chloro-7-nitrobenzofurazan and methacrylic acid were obtained from AlfaAesar (USA). *N*-Bromosuccinimide and 5-bromovaleryl chloride were obtained from TCI (Japan). Triethylamine (TEA), iodomethane, sodium hydroxide, sodium hydrogen carbonate ($NaHCO_3$), and magnesium sulfate ($MgSO_4$) were bought from Daejung Chemical (South Korea). *N*,*N*-diisopropylethylamine was obtained from Acros. Analytical grade solvents were distilled before use.

2.2. **Synthesis of Bromobutyl-BODIPY 1**

The synthesis of bromobutyl-BODIPY was carried using reported literature.[65] Briefly, 874.0 mg of 5-Bromovaleryl chloride and 1.0 g of 2,4-Dimethylpyrrole were refluxed in distilled methylene chloride overnight. After the reaction was cooled to room temperature, the solvent was evaporated. The reaction was dissolved in toluene:MC (1:10) solvent system. Then, TEA was added dropwise to the solution. After 30 minutes, BF_3OEt_2 was added dropwise to the reaction as well. The reaction was refluxed again overnight at 80°C. After quenching, the reaction was extracted with MC, washed with water, and dried with $MgSO_4$. Then the solution was concentrated and purified *via* silica gel column chromatography to obtain the product in green crystals.

1: (Yield: 694 mg, 41.3%) ^{1}H NMR (300 MHz, $CDCl_3$, 25°C, TMS): δ = 6.07 (s, 2H), 3.46 (t, 2H), 2.99 (t, 2H), 2.52 (s, 6H), 2.43 (s, 6H), 2.06 (m, 2H), 1.83 (m, 2H) ppm.

2.3. **Methacrylation of Bromobutyl-BODIPY 1**

The methacrylation of BODIPY was done by dissolving 694.0 mg of Bromobutyl-BODIPY 1 and sodium methacrylate in DMF with a catalytic amount of tetrabutylammonium bromide.[65] The reaction was refluxed for 2 days at 40°C. After that, extraction removed excess sodium methacrylate followed by washing with water,

and drying with $MgSO_4$. The reaction was concentrated and purified *via* silica gel column chromatography to obtain an orange solid.

2: (Yield: 600 mg, 85.5%) ^{1}H NMR(300 MHz, $CDCl_3$, 25°C, TMS): δ = 6.09 (s, 1H), 6.06 (s, 2H), 5.57 (s, 1H), 4.21 (t, 2H), 2.98 (t, 2H), 2.52 (s, 6H), 2.41 (s, 6H), 1.94 (s, 3H), 1.89 (m, 2H), 1.78 (m, 2H) ppm.

2.4. **Dibromination reaction of BODIPY 2**

Bromination reactions at the 2,6-positions of the BODIPY were carried out by dissolving 292.0 mg of methacrylated BODIPY together with *N*-Bromosuccinimide in distilled MC at room temperature. The reaction was monitored by TLC. The solvent was removed, and the crude product purified by silica gel chromatography to obtain red solid as product.

3: (Yield: 396 mg, 96.5%)

2.5. **Knoevenagel condensation reaction (Monostyryl) of BODIPY 3**

A single Knoevenagel reaction to produce monostyryl product were carried out by dissolving 1.0 eq of non-halogenated and halogenated BODIPYs (160.0 mg of **2** or 241.0 mg of **3**, respectively) in DMF with 4-(Dimethylamino)benzaldehyde with piperidine and acetic acid as catalysts.[45] The reaction was refluxed at 100°C overnight. After completion of the reaction, DMF was removed, and the reaction was directly purified by column chromatography to give the products.

4: (Yield: 60.0 mg, 28.0%) ^{1}H NMR (300 MHz, $CDCl_3$, 25°C, TMS): δ = 7.51 (d, 2H, J = 9 Hz), 7.42 (s, 1H), 7.23 (d, 1H, J = 18 Hz), 6.69 (m, 3H), 6.09 (s, 1H), 6.05 (s, 1H), 5.57 (s, 1H), 4.22 (t, 2H, J = 6 Hz), 3.02 (s, 8H), 2.55 (s, 3H), 2.46 (s, 3H), 2.41 (s, 3H), 1.94 (s, 3H), 1.89 (m, 2H), 1.78 (m, 2H) ppm.

5: (Yield: 80.0 mg, 26.8%) ^{1}H NMR (300 MHz, CDCl3, 25°C, TMS): δ = 7.51 (d, 2H, J = 9 Hz), 7.42 (s, 1H), 7.23 (d, 1H, J = 18 Hz), 6.69 (m, 3H), 6.09 (s, 1H), 6.05 (s, 1H), 5.57 (s, 1H), 4.22 (t, 2H, J = 6 Hz), 3.02 (s, 8H), 2.55 (s, 3H), 2.46 (s, 3H), 2.41 (s, 3H), 1.94 (s, 3H), 1.89 (m, 2H), 1.78 (m, 2H) ppm.

2.6. **Methylation reactions of 4 and 5**

The monotyryl BODIPY compounds (60.0 mg of **4** or 80.0 mg of **5**, respectively) were dissolved in 5.0 mL acetonitrile with 2.0 mL iodomethane.[45] The reaction was stirred for 2 days at room temperature. This was followed by purification using aluminum oxide.

6: (Yield: 51.0 mg, 66.8%) ^{1}H NMR (300 MHz, CDCl3, 25°C, TMS): δ = 7.86 (d, 2H, J = 9 Hz), 7.75 (d, 2H, J = 9 Hz), 7.70 (d, 1H, J = 18 Hz), 7.17 (d, 1H, J = 15 Hz), 6.73 (s, 1H), 6.16 (s, 1H), 6.09 (s, 1H), 5.58 (s, 1H), 4.23 (t, 2H, J = 6 Hz), 4.02 (s, 9H), 3.05 (m, 2H), 2.57 (s, 3H), 2.49 (s, 3H), 2.45 (s, 3H), 1.95 (s, 3H), 1.92 (m, 2H), 1.77 (m, 2H) ppm.

7: (Yield: 70.0 mg, 72.3%) ^{1}H NMR (300 MHz, CDCl3, 25°C, TMS): δ = 7.51 (d, 2H, J = 9 Hz), 7.42 (s, 1H), 7.23 (d, 1H, J = 18 Hz), 6.69 (m, 3H), 6.09 (s, 1H), 6.05 (s, 1H), 5.57 (s, 1H), 4.22 (t, 2H, J = 6 Hz), 3.02 (s, 8H), 2.55 (s, 3H), 2.46 (s, 3H), 2.41 (s, 3H), 1.94 (s, 3H), 1.89 (m, 2H), 1.78 (m, 2H) ppm.

2.7. **Synthesis of Nitrobenzoxadiazole-methacrylate (NBD-MA)**

2-aminoethyl methacrylate HCl and *N*,*N*-diisopropylethylamine were dissolved in distilled MC. 4-chloro-7-nitrobenzofurazan was added and the reaction was stirred for three hours. The reaction mixture was poured into a separatory funnel and washed with HCl and 5% $NaHCO_3$.

NBD-MA: (Yield: mg, %) ^{1}H NMR (300 MHz, $CDCl_3$, 25°C, TMS): δ = 8.53 (d, 1H), 6.29 (d, 1H), 6.17 (s, 1H), 5.67 (s, 1H), 4.55 (t, 2H), 3.85 (t, 2H), 1.94 (s, 3H) ppm.

2.8. **Synthesis of BN-H2 and BN-Br2 nanogels**

	NIPAM	NBD	HEMA	BODIPY
BN-H2	71%	4%	8%	17%
BN-Br2	69%	4%	8%	19%

Table 5. Composition of the BN-H2 and BN-Br2 nanogels

SDS (7.2 eq.), HEMA (10 eq.), NIPAm (100 eq.) and BIS (3 eq.) were dissolved in distilled water. The reaction was allowed to reach 70℃ under inert conditions. After 30 min, the BODIPY (4 eq) and NBD-MA (2 eq) dyes were dissolved in ethanol and added dropwise to the reaction while maintaining the 70℃ temperature. Then, ammonium persulfate dissolved in distilled water was added at once to the reaction to initiate the polymerization. After 4 hours, the reaction was stopped and cooled down to room temperature. The reaction mixture was transferred to cellulose tubes and dialyzed for several days, changing the dialysate thrice a day and changing the dialysate from ethyl acetate to water. After three days, the solution is freeze-dried to obtain the polymerized nanogel. BN-H2 (Yield: 54 mg) BN-Br2 (Yield: 144 mg).

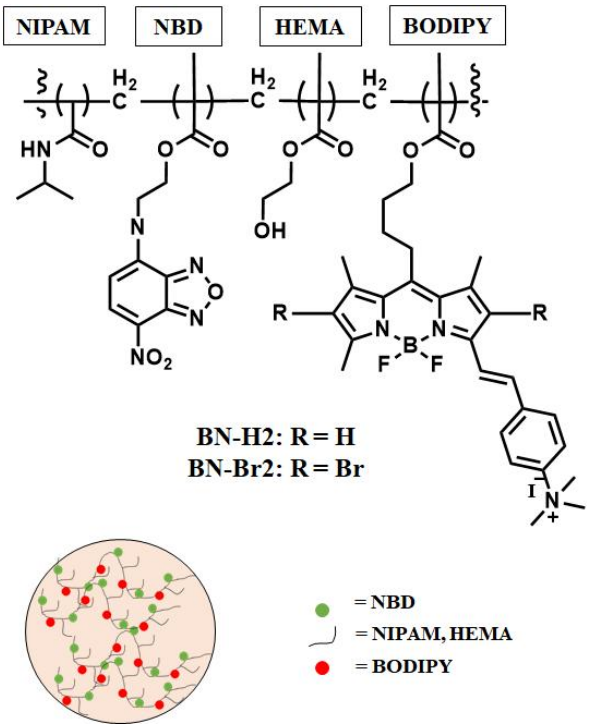

Figure 25. The components of BN-H2 and BN-Br2 nanogels.

2.9. **Methods**

All compounds were characterized by ^{1}H and ^{13}C NMR spectroscopy on a Bruker AM250 spectrometer (USA) and high-resolution electrospray ionization mass spectrometry (HR-ESI-MS) on a SYNAPTG2-Si high-definition mass spectrometer (United Kingdom).

Steady-state absorption and emission spectra of BODIPY nanogel samples dissolved ethanol were measured at room temperature using a UH5300 UV/Vis spectrophotometer (Hitachi) and a F-7000 FL fluorometer (Hitachi), respectively.

The hydrodynamic diameter of BODIPY nanogels were determined using dynamic light scattering (DLS) on Malvern Zetasizer Nano ZS90 and TEM images of the nanogels were observed using transmission electron microscopy (TEM) on JEOL- JEM 2100F at an accelerating voltage of 200 kV.

3.3. Cells and cell culture

HeLa and MCF-7 cells were supplied by the Korean Cell Line Bank. They were maintained with 10% heat-inactivated fetal bovine serum (FBS) and antibiotics (100 U/mL penicillin and 100 mg/mL streptomycin) (Welgene Inc., South Korea) in RPMI 1640 medium (Gibco, Carlsbad, CA, USA) in a humidified 5% CO_2 incubator at 37 ºC.

3.4. Cell proliferation assay

HeLa and MCF-7 cells (2×10^3 cells/well) were spread in 96-well plates and kept at 37°C in 5% CO_2 for one day. Then the cells were treated with BN-H2 and BN-Br2 nanogels at different concentrations for another 24h. The cell proliferation was determined according to the prescribed procedure for CellTiter96® AQueousOne Solution Cell Proliferation Assay (Promega, Madison, WI, USA). Then the absorbance was measured at 490 nm using ELISA plate reader (ThermoFisher Scientific, Inc., Waltham, MA, USA).

3.5. Photodynamic activity

HeLa and MCF-7 cells (2×10^3 cells/well) were treated in the same way as above but with further incubation at 37°C in 5% CO_2 under dark conditions for 2 h. Then, the media were replaced with phenol-red free RPMI 1640 followed by exposure to red light-emitting diode at 680 nm (100% power) for 15 min. The cells were incubated for additional 24h and the cell proliferation (% of the control) was measured.

3.6. Confocal laser scanning microscopy

HeLa and MCF-7 cells were treated with BN-H2 and BNBr2 nanogels (26.5 μg/mL) for 24 h. Then, they were further treated with MitoTracker Red (Invitrogen) for 45 min. The cells were fixed with 4% paraformaldehyde for 10 min and permeabilized with 0.1% Triton X-100 for 10 min followed by counter staining with 4′ ,6-diamidino-2-phenylindole (DAPI) for 1 h at room temperature. Finally, the treated cells were imaged using confocal microscopy (LSM-700, Carl Zeiss, Germany).

2.14. Annexin V/PI assay

Total apoptotic cells were determined using an Annexin V/PI assay kit (BD Biosciences, San Diego, CA, USA) following the prescribed protocol. Triplicate samples of HeLa and MCF-7 cells (2×10^5) were seeded in 6-well plates and incubated overnight to allow cell attachment. The cells were treated with either DMSO (control) or BN-H2 and BN-Br2 nanogels for 4 h and then exposed to red light-emitting diode at 680 nm (3 mW) for 30 min. Afterwards, the adherent cells were harvested by trypsinization and then resuspended in Annexin V/PI solution. This is followed by incubation of the cells for 15 min at room temperature in the dark with light agitation. The apoptotic cells were analyzed using a FC500 flow cytometer (Beckman coulter, CA, USA).

2.15. Statistical Analysis

Data are expressed as means ± standard deviations. Group means were considered significantly different at $p < 0.05$. GraphPad 6 Prism software (San Diego, CA, USA) was used for the one-way analysis of variance and Tukey's test of the data.

3. Results and Discussion

The synthetic scheme was shown in Figure 24. Briefly, BODIPY starting materials were synthesized by the condensation reaction between 4-bromovaleryl chloride and

2,4-Dimethylpyrrole in distilled MC. This was followed by complexation with BF_3OEt_2 in the presence of triethylamine. The bromide functional group was replaced by methacrylate after esterification reaction with sodium methacrylate. Next, bromination in the C-2 and C-6 positions of the core BODIPY was conducted using *N*-bromosuccinimide in distilled MC. Then, a controlled Knoevenagel reaction was conducted to obtain monostyryl BODIPY derivatives. Finally, methylation of the dimethylamino group produced the desired BODIPY monomers. For the synthesis of nanogel, a free radical polymerization reaction was conducted with HEMA, NIPAM and SDS in distilled water. The reaction was subjected to inert conditions while gradually raising the temperature to 70°C. After 30 mins, the dyes NBD and BODIPY were dissolved in ethanol and added dropwise to the reaction while keeping the temperature constant. Lastly, the initiator ammonium persulfate was dissolved in water and added to the reaction in one step. The reaction was refluxed for 4 hours, after which they were cooled down to room temperature and transferred to cellulose dialysis tubes and purified for several days. The components of the nanogels are elucidated in Figure 25.

3.1. Photophysical Properties

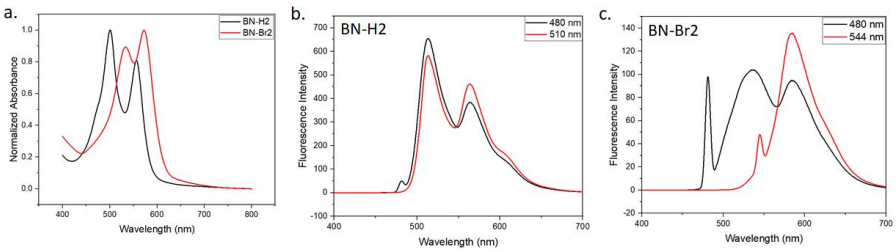

Figure 26. The absorbance (a) and emission spectra (b and c) of BN-H2 and BN-Br2 in ethanol.

	λ_{abs}	λ_{em}
BN-H2	500/556	513/563
BN-Br2	534/572	545/584

Table 6. The absorption and emission spectra maximum wavelengths of BN-H2 and BN-Br2 measured in ethanol.

Figure 26a shows the absorbance spectra of the nanogels in ethanol and features two maxima, wherein the first peak is ascribed to NBD and the second peak belongs to BODIPY. BN-H2 has absorbance peaks at 500 and 556 nm, respectively. Free NBD has an absorption maximum at 470 nm so this ~30 nm shift is rather interesting. On the other hand, for BN-Br2, the first peak appears at 536 nm while the second is found at 578 nm. The shift of the BODIPY peak can be attributed to the red shift brought about by the addition of two bromine atoms. In addition, the first peak (NBD peak) is also red-shifted to ~30 nm relative to the first peak in BN-H2. The difference in the absorbance peaks between NBD and BODIPY is closer in BN-Br2 (38 nm) than in BN-H2 (56 nm). Hence, a brief discussion on the implication of this behavior follows, mainly on the possibility of FRET processes.

Figure 26b and 26c show the fluorescence intensity spectra measured for the ethanolic solutions of BN-H2 and BN-Br2 nanogels in two excitation wavelengths. For BN-H2, the fluorescence emission peaks appear at 513 and 563 nm when excited at 480 nm, which is attributed to the fluorescence emission of NBD and BODIPY, respectively. When excited at 510 nm, the same fluorescence emission peaks can be observed, albeit a negligible change in the fluorescence intensity. This signifies that no fluorescence resonance energy transfer (FRET) interaction can be observed in BN-H2, expectedly because of the nonoverlap of their absorption spectra. For BN-Br2, two peaks can also be observed similarly when excited at 480 nm. Surprisingly, when the nanogel is excited at 544 nm, the first peak disappears while the peak at 584 nm increases in intensity. Assuming a similar proximity among nanogel components, the efficient FRET process could be due to the overlap of the fluorescence emission of NBD and the absorption of BODIPY. Although further experiments are needed to fully characterize the FRET behavior of the BN-Br2 nanogel with regards to the effect of different temperature, pH and medium, the results observed will suffice for the dual color imaging and PDT experiments desired.

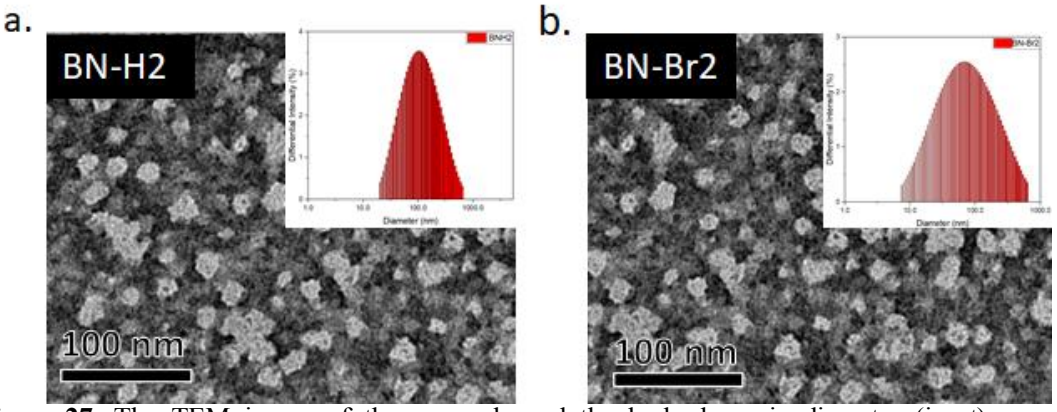

Figure 27. The TEM image of the nanogels and the hydrodynamic diameter (inset) analyzed using DLS. The nanogels are 143.5 nm (BN-H2) and 112.6 nm (BN-Br2) in hydrated state and 17-25 nm in the dehydrated state.

Cell uptake of nanoparticles usually depend on surface characteristics to preclude the reticuloendothelial system. Hydrophobic nanoparticles have tendencies to be absorbed by the liver, spleen, and lungs.[66] Whereas hydrophilic nanoparticles with 100 nm diameter or less can avoid clearance by macrophages, hence, they have longer blood circulation times, efficient uptake and reach target sites.[67] As shown by the TEM result in Figure 27, the dehydrated state of BN-H2 and BN-Br2 nanogels have diameters of 17-25 nm. They can swell up to ~150 nm when hydrated, which is 6x more than that of dried state. This shows the beneficial effect of incorporating the hydrophilic HEMA in the structure. Nanogels with hydrophilic coatings or prepared from block copolymers with both hydrophobic and hydrophilic domains usually form a cloud of chains that hinder interactions with plasma proteins.[68]

3.2. Flow Cytometry

Although the DLS hydrodynamic diameter shows a broad topographic profile, the cell uptake of the nanogels can be further evidenced by flow cytometry. Flow cytometry is a powerful tool for the classification and isolation of sample cells and particles.

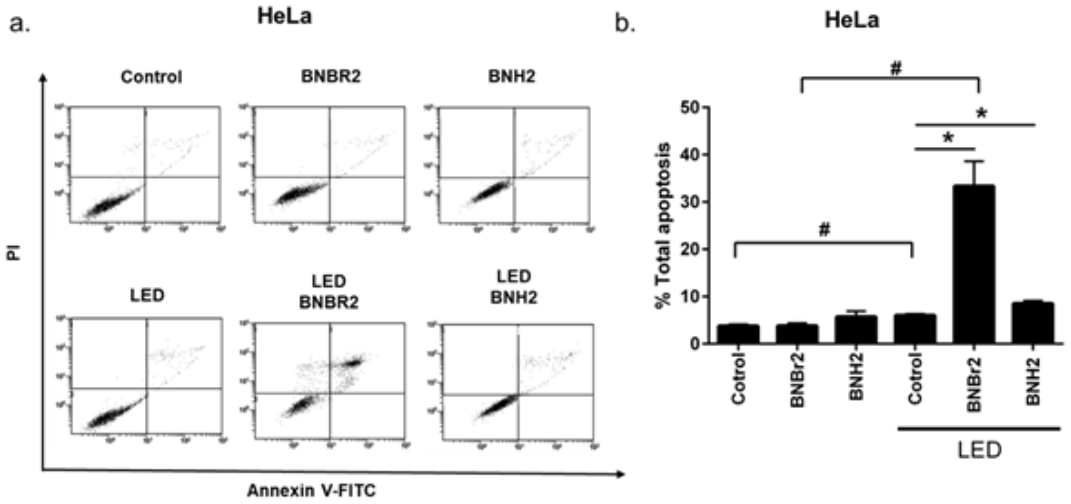

Figure 28. Apoptotic effects of BODIPY dyes on cancer cells. (a) The apoptotic cells were classified after annexin V-FITC/PI assay using flow cytometry after BODIPY dyes or LED treatment. (b) Quantification of the total apoptotic cell population (early + late) is shown.

Annexin V, a phospholipid binding protein, reacts to phosphatidylserine once translocated outside the cellular membrane during apoptosis. To confirm that the binding process occurs outside the cellular membrane, propidium iodide dye (or any viability exclusion dye) should be used.[69] Apoptosis is a programmed cellular death initiated by the cell without release of contents to the external environment whereas necrosis is an uncontrolled death process characterized by the rupture of the cell structure.[70] To interpret Figure 28a, each quartile represents the status of the cell population. In Q1, where PI = + and Annexin V = -, the cells are in necrotic stage. In Q2, where PI = + and Annexin V = +, the cells are in late apoptotic stage. In Q3, where PI = - and Annexin V = -, the cells are healthy and viable. In Q4, where PI = - and Annexin = +, the cells are in early apoptotic stage. Before LED excitation (upper three graphs), cells incubated with control, BN-Br2 and BN-H2 can be observed in Q3, signifying the internal accumulation and non-cytotoxicity of the nanogels (relative to the control

sample). After LED excitation (lower three graphs), the control cells did not exhibit any obvious change as before excitation. Similarly, cells incubated with BN-H2 remained in Q3, signifying the non-phototoxicity of BN-H2. Lastly, a significant portion of the cells incubated with BN-Br2 can be found in Q2, showing the photodynamic ability of BN-Br2. Further quantification (Figure 28b) shows that statistically significant difference in apoptosis was observed in BN-Br2 relative to the control reaching up to 35% total (early+late) apoptosis.

3.7. Cell Proliferation

The biocompatibility of BN-H2 and BN-Br2 nanogels were assayed using HeLa and MCF-7 cancer cell lines and the results are shown in Figure 29. Both nanogels did not induce damage to the cells even at the highest concentration used (25.6 μg/mL) in dark conditions. Even after irradiation with light, the cell proliferation of the cells incubated with BN-H2 were still consistently high. In contrast, the cells incubated with BN-Br2 were killed after being irradiated with LED light. This points to the phototoxicity of the nanogel brought about by the heavy atom effect of bromine atoms.[45] The results of the MTS cell proliferation assay described here show that the prepared nanogels are non-cytotoxic and BN-Br2 only induced cytotoxic effect under irradiation with light. Finally, the IC_{50} of BN-Br2 was calculated to be 6.14 μg/mL and 11.44 μg/mL, in HeLa and MCF-7 cell lines, respectively (Table7)

3.8. Dual-color fluorescence cell imaging

Two dyes were employed to enable dual-color imaging of cancer cells. As shown in Figure 30, both BN-H2 and BN-Br2 can be used to image the green and red channels. Obviously, BN-H2 contains both NBD (green) and BODIPY (red) dyes. Surprisingly, BN-Br2 still show two colors: green from NBD and red from BODIPY even when the BODIPY has bromine atoms. It has been shown in previous studies that halogenated

BODIPY that has low fluorescence quantum yield still show fluorescent imaging inside the cell, due to non-specific interactions with the biological environment.

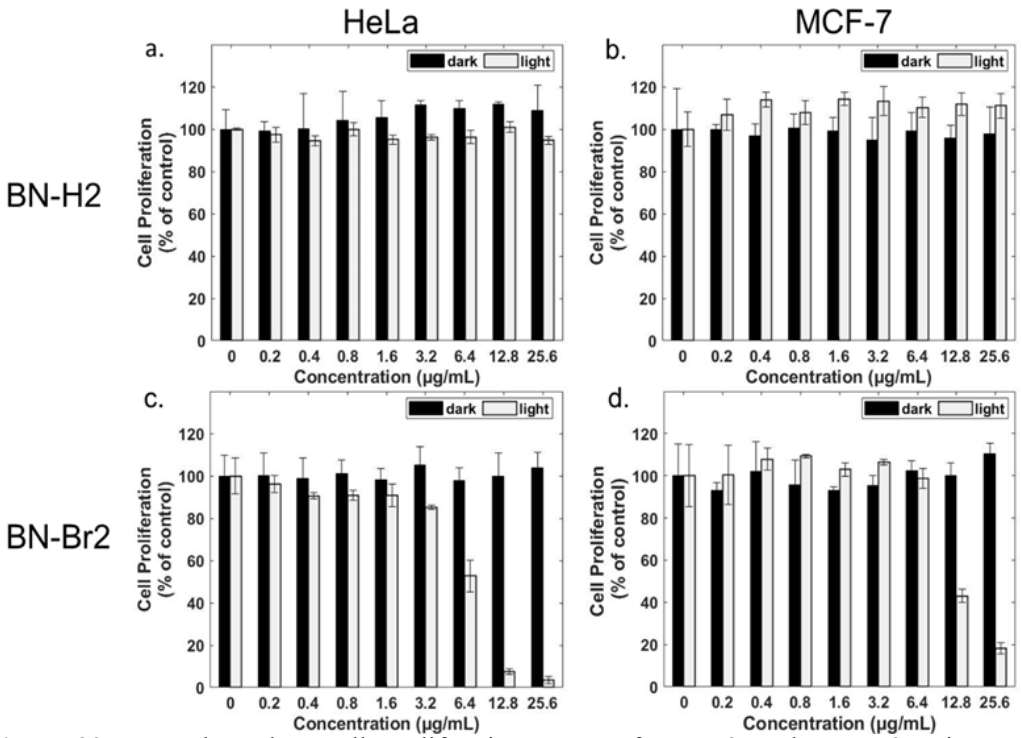

Figure 29. Dose-dependent cell proliferation assay of BN-H2 and BN-Br2 using HeLa and MCF-7 cells under dark and irradiated conditions at 680 nm for 15 min (100%, 40 mW).

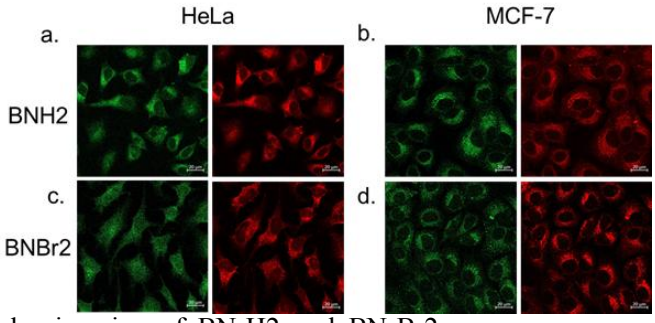

Figure 30. Dual-color imaging of BN-H2 and BN-Br2.

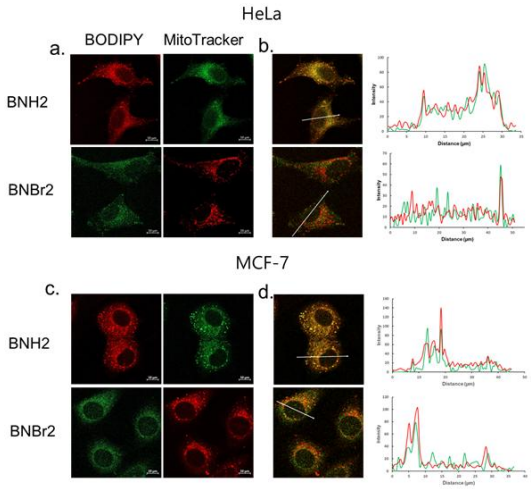

Figure 31. Dual color fluorescence micrographs of HeLa (a) and MCF-7 (c) cells stained with BODIPY nanogels and MitoTrackers Green and Red. b) Overlap of the fluorescence intensity profiles of the nanogels and MitoTrackers along the white line.

3.9. Mitochondria-targeted cell imaging

To evaluate the intracellular localization of the nanogels, the mitochondria-specific dye MitoTracker Green/Red are used together with them. As indicated in the overlapping fluorescence intensity profiles of the dyes in Figure 31b, the nanogels are localized in the mitochondria together with MitoTracker commercial dyes. This also shows that the mitochondria-targeting cationic group was not shielded despite being encapsulated by the nanogel.

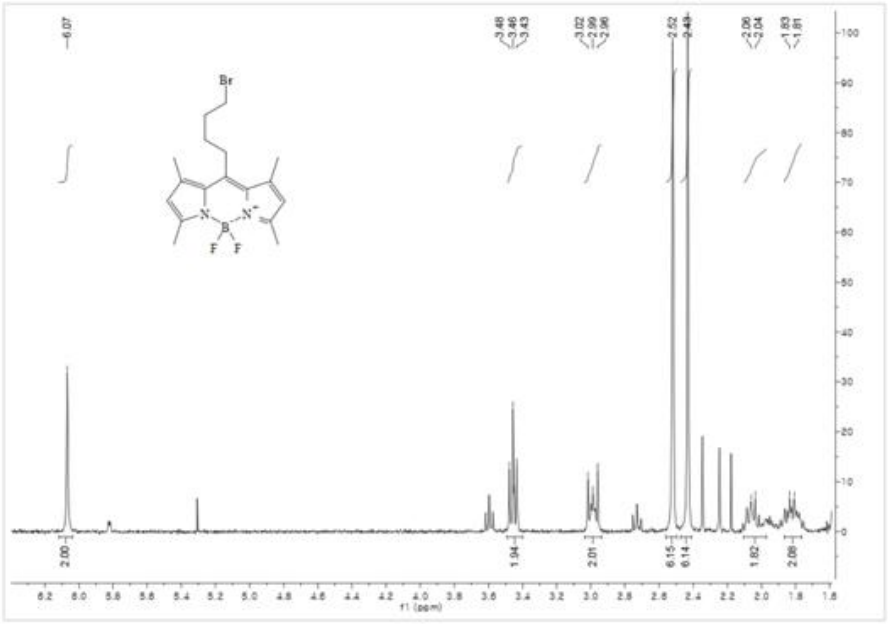

^{1}H NMR of Bromobutyl BODIPY 1

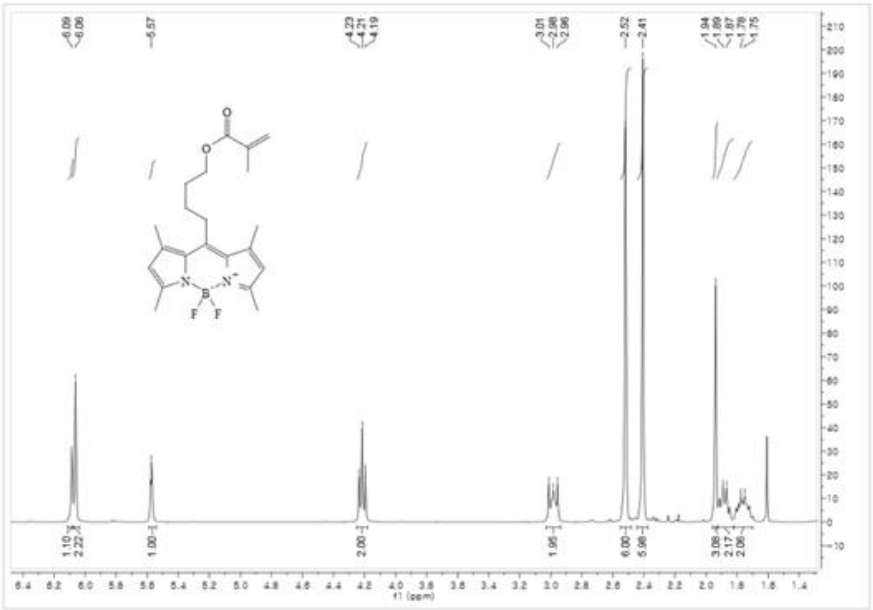

^{1}H NMR of methacrylated BODIPY 2

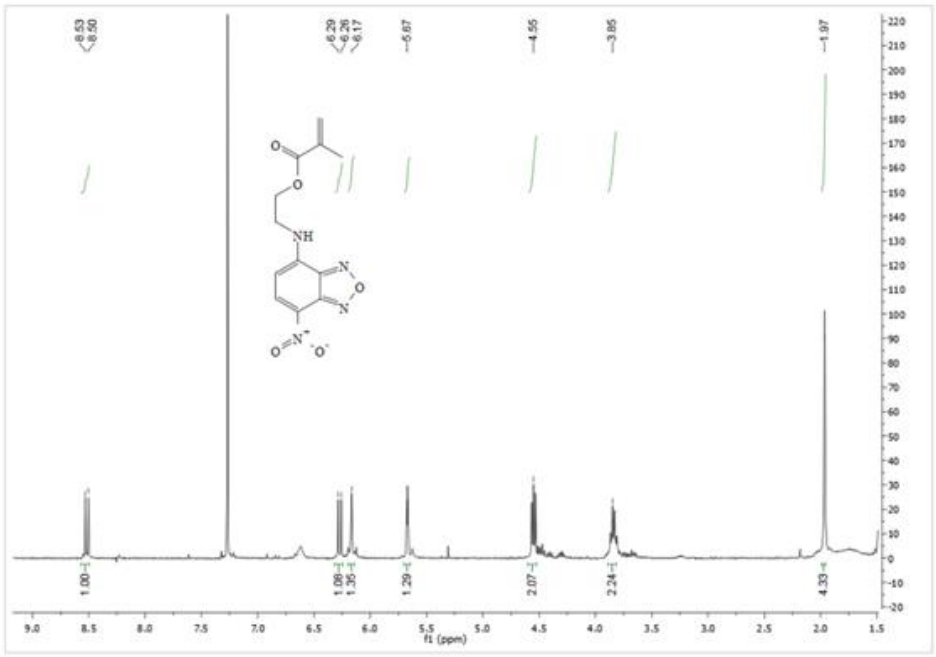

^{1}H NMR of methacrylated NBD-MA

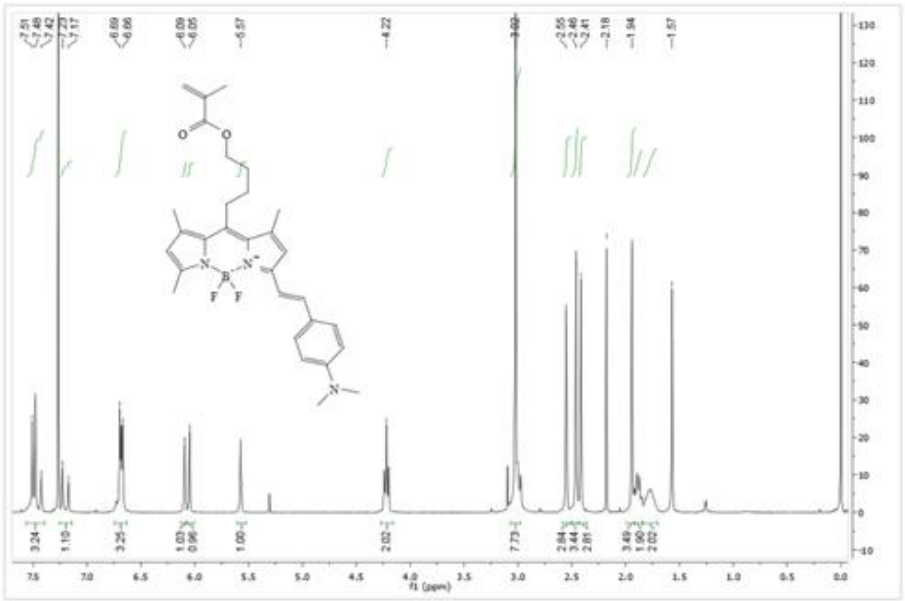

^{1}H NMR of monostyryl BODIPY 4

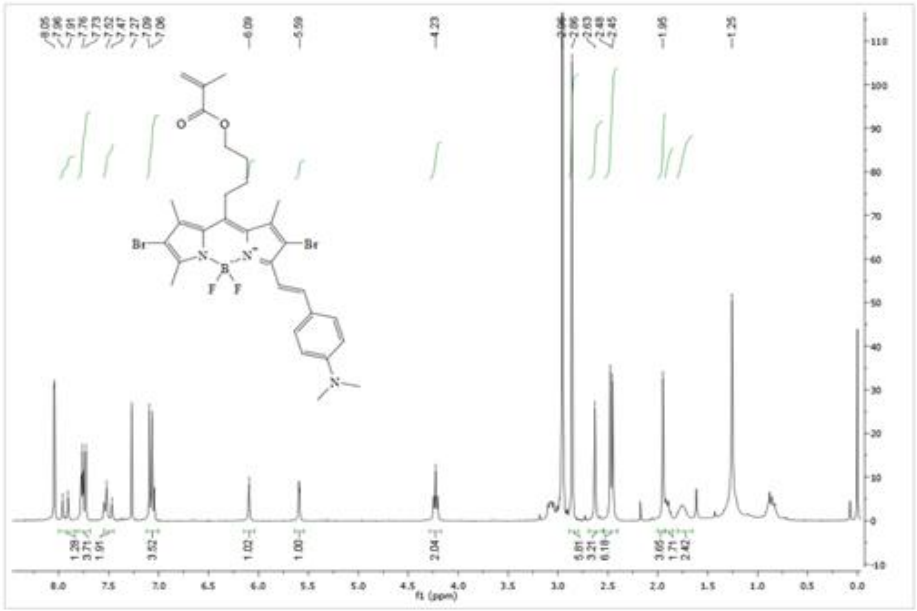

^{1}H NMR of monostyryl BODIPY 5

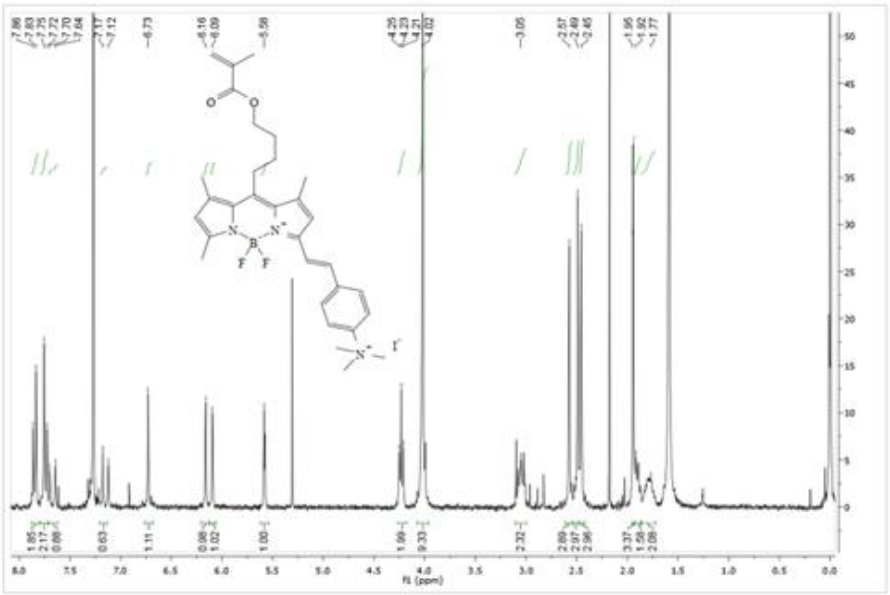

^{1}H NMR of BN-H2 monomer 6

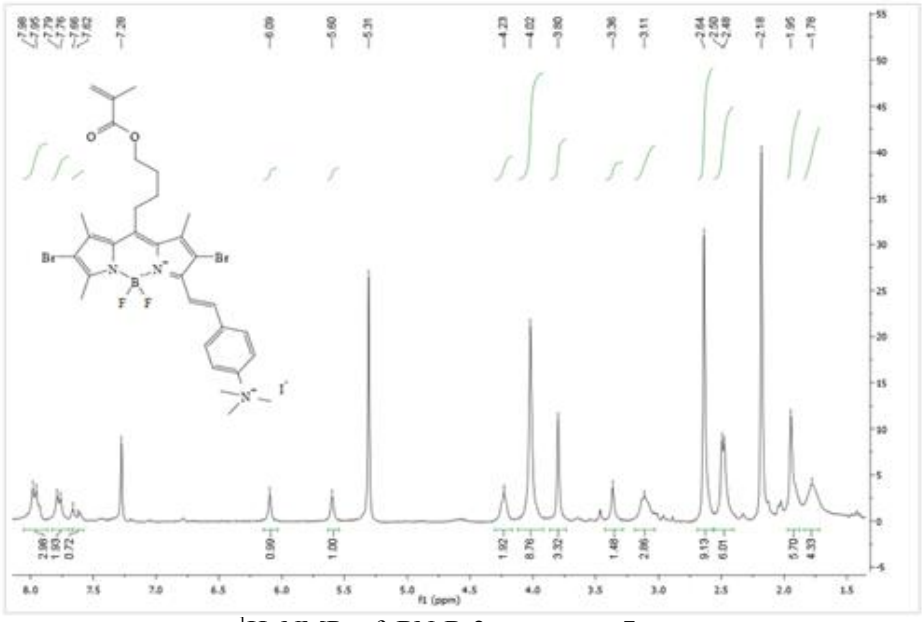

^{1}H NMR of BN-Br2 monomer 7

Conclusions

Efficient synthesis of different kinds of BODIPY-derived dyes for fluorescence cell imaging and photodynamic therapy was reported and their properties evaluated. Based on the empirical data presented here, the use quaternary ammonium and pyridinium groups is effective as mitochondria-targeting moiety. Hence, these nitrogen-based compounds may serve as alternatives to the bulky triphenylphosphonium group. Heavy-atom effect can be brought about even with only one bromine atom if the structural configuration is right (C-2 and C-6 positions). In the case of AmX2 dyes, the cationic moiety also conferred hydrophilicity to the dye, thereby making the dyes biocompatible. For PyBXI dyes, the Knoevenagel condensation reactions at the C-3 and C-5 positions resulted to red-shifted absorption and emission maxima. NIR-absorbance and emission have been achieved in PyBXI but with a reduced fluorescence and singlet oxygen quantum yield. Hence, the observed photodynamic activities for PyBMI and PyBBrI were modest relative to that of AmBr2 and AmI2 dyes. This shows that electronic properties should also be considered in choosing functional groups. Finally, the fabrication of nanogels with two different fluorophores resulted to a dual-color fluorescence imaging with photodynamic therapy.

References

[1] World Health Organization. (2022, February 3). *Cancer*. https://www.who.int/news-room/fact-sheets/detail/cancer

[2] Sung, H., Ferlay, J., Siegel, R. L., Laversanne, M., Soerjomataram, I., Jemal, A., & Bray, F. (2021). *CA: a cancer journal for clinicians*, 71(3), 209-249.

[3] Hanahan, D., & Weinberg, R. A. (2011). *Cell*, 144(5), 646-674.

[4] Grasso, D., Zampieri, L. X., Capelôa, T., Van de Velde, J. A., & Sonveaux, P. (2020). *Cell stress*, 4(6), 114.

[5] Hamblin, M. R. / *Photochemistry and photobiology* 96 (2020), 506-516.

[6] Castano AP, Demidova TN, Hamblin MR / *Photodiagnosis and photodynamic therapy* 1 (2004) 279-93.

[7] Arnaut, L. G., Pereira, M. M., Dąbrowski, J. M., Silva, E. F., Schaberle, F. A., Abreu, A. R., ... & Brett, C. M. (2014). *Chemistry–A European Journal*, 20(18), 5346-5357.

[8] Algorri, J. F., Ochoa, M., Roldán-Varona, P., Rodríguez-Cobo, L., & López-Higuera, J. M. (2021). *Cancers*, *13*(17), 4447.

[9] Agostinis, P., Berg, K., Cengel, K. A., Foster, T. H., Girotti, A. W., Gollnick, S. O., ... & Golab, J. (2011). *CA: a cancer journal for clinicians*, *61*(4), 250-281.

[10] Ding H, Yu H, Dong Y, Tian R, Huang G, Boothman DA, Sumer BD, Gao J. *Journal of controlled release*. 2011 Dec 20;156(3):276-80.

[11] Hou YJ, Yang XX, Liu RQ, Zhao D, Guo CX, Zhu AC, Wen MN, Liu Z, Qu GF, Meng HX. *International Journal of Nanomedicine*. 2020;15:6827.

[12] Gorman, A., Killoran, J., O'Shea, C., Kenna, T., Gallagher, W. M., & O'Shea, D. F. (2004). *Journal of the American Chemical Society*, 126(34), 10619-10631.

[13] De Simone, B. C., Mazzone, G., Russo, N., Sicilia, E., & Toscano, M. (2017). Molecules, 22(7), 1093.

[14] Bell, J. D., & Murphy, J. A. (2021). Chemical Society Reviews.

[15] Kamkaew, A., Lim, S. H., Lee, H. B., Kiew, L. V., Chung, L. Y., & Burgess, K. (2013). *Chemical Society Reviews*, *42*(1), 77-88.

[16] Treibs, A., & Kreuzer, F. H. (1968). *Justus Liebigs Annalen der Chemie*, 718(1), 208-223.

[17] Ziessel, R., Ulrich, G., & Harriman, A. (2007). *New Journal of Chemistry*, 31(4), 496-501.

[18] Niu, L. Y., Guan, Y. S., Chen, Y. Z., Wu, L. Z., Tung, C. H., & Yang, Q. Z. (2012). *Journal of the American Chemical Society*, *134*(46), 18928-18931.

[19] El-Khouly, M. E., Fukuzumi, S., & D'Souza, F. (2014). *ChemPhysChem*, *15*(1), 30-47.

[20] Debnath, S., Singh, S., Bedi, A., Krishnamoorthy, K., & Zade, S. S. (2015). *The Journal of Physical Chemistry C*, *119*(28), 15859-15867.

[21] Gai, L., Mack, J., Liu, H., Xu, Z., Lu, H., & Li, Z. (2013). *Sensors and actuators B: chemical*, *182*, 1-6.

[22] Padrutt, R., Babu, V., Klingler, S., Kalt, M., Schumer, F., Anania, M. I., ... & Spingler, B. (2021). *ChemMedChem*, *16*(4), 694-701.

[23] Wood, T.E. and Thompson, A., 2007. *Chemical reviews*, 107(5), pp.1831-1861.

[24] Kowada, T., Maeda, H., & Kikuchi, K. (2015). *Chemical Society Reviews*, *44*(14), 4953-4972.

[25] Fan, G., Yang, L., & Chen, Z. (2014). *Frontiers of Chemical Science and Engineering*, *8*(4), 405-417.

[26] Badon, I. W., Lee, J., Vales, T. P., Cho, B. K., & Kim, H. J. (2019). *Journal of Photochemistry and Photobiology A: Chemistry*, *377*, 214-219.

[27] Romieu, A., Massif, C., Rihn, S., Ulrich, G., Ziessel, R., & Renard, P. Y. (2013). *New Journal of Chemistry*, *37*(4), 1016-1027.

[28] Bura, T., & Ziessel, R. (2011). *Organic Letters*, *13*(12), 3072-3075.

[29] Amamoto, Y.; Kikuchi, M.; Masunaga, H.; Ogawa, H.; Sasaki, S.; Otsuka, H.; Takahara, A. *Polym. Chem*. 2011, 2, 957−962.

[30] Liu, L., Li, T., Ruan, Z., Yuan, P., & Yan, L. (2018). *Materials Science and Engineering: C*, 92, 745-756.

[31] Lalitha, K., Prasad, Y. S., Maheswari, C. U., Sridharan, V., John, G., & Nagarajan, S. (2015). *Journal of Materials Chemistry B*, 3(27), 5560-5568.

[32] Neamtu, I., Rusu, A. G., Diaconu, A., Nita, L. E., & Chiriac, A. P. (2017). *Drug Delivery*, 24(1), 539-557.

[33] Bittel, A. M., Davis, A. M., Wang, L., Nederlof, M. A., Escobedo, J. O., Strongin, R. M., & Gibbs, S. L. (2018). *Scientific reports*, *8*(1), 1-12.

[34] Shi, Z., Han, X., Hu, W., Bai, H., Peng, B., Ji, L., & Huang, W. (2020). *Chemical Society Reviews*, 49(21), 7533-7567.

[35] Kand, D., Pizarro, L., Angel, I., Avni, A., Friedmann-Morvinski, D., & Weinstain, R. (2019). *Angewandte Chemie International Edition*, *58*(14), 4659-4663.

[36] Wang, J. L., Zhang, L., Zhao, M. J., Zhang, T., Liu, Y., & Jiang, F. L. (2021). *ACS Applied Bio Materials*, 4(2), 1760-1770.

[37] Chen, D., Zhang, J., Tang, Y., Huang, X., Shao, J., Si, W., ... & Dong, X. (2018). *Journal of Materials Chemistry B*, 6(27), 4522-4530.

[38] Zou, J., Yin, Z., Ding, K., Tang, Q., Li, J., Si, W., ... & Dong, X. (2017). *ACS applied materials & interfaces*, *9*(38), 32475-32481.

[39] R. Prieto-Montero, A. Prieto-Castañeda, R. Sola-Llano, A. R. Agarrabeitia, D.García-Fresnadillo, I. López-Arbeloa, A. Villanueva, M. Ortiz, S. de la Moya, V. Martínez-Martínez / *Photochemistry and Photobiology* 96 (2020) 458-477.

[40] Ma, C., Xia, F., & Kelley, S. O. (2020). *Bioconjugate Chemistry*, 31(12), 2650-2667.

[41] Vales, T. P., Cho, S., Lee, J., Bui, H. T., Mai, D. K., Badon, I. W., ... & Kim, H. J. (2021). *Journal of Molecular Structure*, 1246, 131284.

[42] Gao, T., He, H., Huang, R., Zheng, M., Wang, F. F., Hu, Y. J., ... & Liu, Y. (2017). *Dyes and Pigments*, 141, 530-535.

[43] Werner, T., Huber, C., Heinl, S., Kollmannsberger, M., Daub, J., & Wolfbeis, OS (1997). *Fresenius' journal of analytical chemistry*, 359 (2), 150-154.

[44] Kollmannsberger, M., Gareis, T., Heinl, S., Daub, J., & Breu, J. (1997). *Angewandte Chemie International Edition in English*, 36 (12), 1333-1335.

[45] Badon, I. W., Kim, C., Lim, J. M., Duy, M. K., Vales, T. P., Kang, D., Cho, S., Lee, J., Kim, H.J., & Yang, J. (2022). *Journal of Materials Chemistry B*, 10(8), 1196-1209.

[46] Zlatić, K., El Ayouchia, H. B., Anane, H., Mihaljević, B., Basarić, N., & Rohand, T. (2020). *Journal of Photochemistry and Photobiology A: Chemistry*, 388, 112206.

[47] Ni, Y., & Wu, J. (2014). *Organic & biomolecular chemistry*, 12(23), 3774-3791.

[48] Li, H., Jia, R., & Wang, Y. (2020). *Spectrochimica Acta Part A: Molecular and Biomolecular Spectroscopy*, 228, 117793.

[49] Buyukcakir, O., Bozdemir, O. A., Kolemen, S., Erbas, S., & Akkaya, E. U. (2009). *Organic letters*, 11(20), 4644-4647.

[50] Neese, F. (2012). *Wiley interdiscip. Rev.: Comput. Mol. Sci*, 2(1), 73-78.

[51] Chen, Y., Wan, L., Zhang, D., Bian, Y., & Jiang, J. (2011). *Photochemical & Photobiological Sciences*, 10(6), 1030-1038.

[52] Kang, H., Si, Y., Liu, Y., Zhang, X., Zhang, W., Zhao, Y., ... & Liu, Z. (2018). *The Journal of Physical Chemistry A*, 122(25), 5574-5579.

[53] Kosower, E. M., & Skorcz, J. A. (1960). *Journal of the American Chemical Society*, 82(9), 2195-2203.

[54] Cakmak, Y., Kolemen, S., Duman, S., Dede, Y., Dolen, Y., Kilic, B., ... & Akkaya, E. U. (2011). *Angewandte Chemie International Edition*, 50(50), 11937-11941.

[55] Żamojć, K., Zdrowowicz, M., Rudnicki-Velasquez, P. B., Krzymiński, K., Zaborowski, B., Niedziałkowski, P., ... & Chmurzyński, L. (2017). *Free radical research*, 51(1), 38-46.

[56] Song, Q., Jiao, Y., Wang, Z., & Zhang, X. (2016). Small, 12(1), 24-31.

[57] Coropceanu, V., Chen, X. K., Wang, T., Zheng, Z., & Brédas, J. L. (2019). Nature Reviews Materials, 4(11), 689-707.

[58] Santra, D.C., Bera, M.K., Sukul, P.K. and Malik, S., 2016. Chemistry–A European Journal, 22(6), pp.2012-2019.

[59] Buwalda, S. J., Vermonden, T., & Hennink, W. E. (2017). Biomacromolecules, 18(2), 316-330.

[60] Prasad, M., Lambe, U. P., Brar, B., Shah, I., Manimegalai, J., Ranjan, K., ... & Prasad, G. (2018). Biomedicine & Pharmacotherapy, 97, 1521-1537.

[61] Re, F., Gregori, M., & Masserini, M. (2012). Maturitas, 73(1), 45-51.

[62] Karg, M., Pich, A., Hellweg, T., Hoare, T., Lyon, L. A., Crassous, J. J., ... & Richtering, W. (2019). Langmuir, 35(19), 6231-6255.

[63] Lee, S. H., Bui, H. T., Vales, T. P., Cho, S., & Kim, H. J. (2017). Dyes and Pigments, 145, 216-221.

[64] Wang, D., Liu, T., Yin, J., & Liu, S. (2011). Macromolecules, 44(7), 2282-2290.

[65] Kajiwara, Y., Nagai, A., & Chujo, Y. (2010). *Journal of Materials Chemistry*, *20*(15), 2985-2992.

[66] Brigger, I., Dubernet, C., & Couvreur, P. (2012). *Advanced drug delivery reviews*, 64, 24-36.

[67] Storm, G., Belliot, S. O., Daemen, T., & Lasic, D. D. (1995). *Advanced drug delivery reviews*, 17(1), 31-48.

[68] Brannon-Peppas, L., & Blanchette, J. O. (2004). *Advanced drug delivery reviews*, 56(11), 1649-1659.

[69] McKinnon, K. M. (2018). *Current protocols in immunology*, 120(1), 5-1.

[70] Logue, S. E., Elgendy, M., & Martin, S. J. (2009). *Nature protocols*, 4(9), 1383-1395.

Acknowledgements

I would like to extend my deepest gratitude to all the people who were directly and indirectly involved in the completion of this work. I am grateful to my supervisor, Prof. Kim Ho-Joong, for his patience, expertise, and invaluable input for this work. Prof. Yang Jaesung and his lab for the photophysical data. Prof. Joomin Lee for the cell imaging and viability data. I also extend my thanks to the review committee. Prof. Gay Balanay for encouraging us to pursue graduate studies. I also thank my colleagues (Temmy Pegarro Vales, Duy Khuong Mai, Moon SeonJoung, Lim Heejung, Lee Eunsu and Jeong Woogyoung) for their help and companionship for the last five years. I thank my best friends for their precious friendship. Lastly, I thank my parents Asterio and Jelita Badon and my whole family for their unfailing support of my endeavors.